

# Interaction of Fluorescent Single-Walled Carbon Nanotubes with Photosynthetic Microbes

Présentée le 7 février 2020

à la Faculté des sciences de base  
Laboratoire de nanobiotechnologie  
Programme doctoral en chimie et génie chimique

pour l'obtention du grade de Docteur ès Sciences

par

**Alessandra ANTONUCCI**

Acceptée sur proposition du jury

Prof. K. Sivula, président du jury  
Prof. A. A. Boghossian, directrice de thèse  
Dr S. Kruss, rapporteur  
Prof. C. Mullineaux, rapporteur  
Prof. B. Fierz, rapporteur



Nothing in life is to be feared,  
it is only to be understood.

Marie Curie

Dedicata ai miei genitori





# Acknowledgements

First and foremost, I am deeply grateful to my research advisor, Prof. **Ardemis A. Boghossian**, for giving me the opportunity of joining her group at EPFL as one of her first PhD students. Ardemis supported and encouraged my various research interests and my scientific curiosity in all stages of my PhD journey. Thank you for guiding me through this important time of my life and inspiring me with your enthusiasm and determination.

I would like to extend my sincere gratitude to my committee members, Prof. **Conrad Mullineaux**, Prof. **Sebastian Kruss**, Prof. **Beat Fierz**, and the jury president, Prof. **Kevin Sivula**, for their invaluable suggestions and helpful feedback. I would especially like to thank my mentor, Prof. **Georges Wagnieres**, for the helpful career advice and many insightful discussions. I also wish to thank him for giving me the opportunity to help with his course and improve my teaching skills.

I would like to thank my funding source, the Swiss National Science Foundation (SNSF) Assistant Professor (AP) Energy grant, for the financial support provided during my PhD. I would also like to acknowledge Prof. **Graham Knott**, **Stephanie Rosset**, and **Anaëlle Dubois** from the BIOEM facility at EPFL, for their valuable help with sample preparation and SEM imaging. I must also extend my sincere thanks to Prof. **Luciana Dini** and Dr. **Elisabetta Carata** from Sapienza Università di Roma and Università del Salento for sharing their expertise in TEM and immunogold labeling. Thank you for your collaboration and great work.

I was lucky to share this incredible adventure with my fellow group members, both past and present. I am grateful to **Nils Schuergers** for guiding me through the first steps of my PhD, sharing his exhaustive experience in cyanobacterial research, and challenging me to always find a new perspective on things. I am indebted to **Melania Reggente** for her untiring support and guidance throughout the darkest and brightest moments of the last two years. Mel is a wonderful and generous friend, with contagious enthusiasm and love for research, and I admire her ability to smile and focus on the positive side despite the situation. Words cannot express my gratitude to **Alice Gillen**. She ALWAYS had time for me when I needed advice or help. Her brilliance, strength, and infinite passion for science will remain an inspiration throughout my life. I am thankful to **Vitalijs Zubkovs** for teaching me everything I know about confocal microscopy and always motivating me to follow my inspirations. Working in the LNB would have not been the same without **Benjamin Lambert**. Thank you for helping and supporting me whenever I've encountered a stall in the progress of my research and always creating a positive atmosphere in the lab. I want to thank **Shang-Jung Wu** for sharing

## Acknowledgements

---

this adventure with me since the very first day, inspiring me with his bright talent and rigor in research. I also want to thank **Mohammed Mouhib** for his helpful suggestions and his contagiously positive mindset.

Other past and present group members that I have had the pleasure to work with are postdocs **Justyna Kupis-Rozmislowicz**, **Mary Wood**, **Amirmostafa Amirjani**, **Liu Xuewen**; PhD student **Daniel Molina**; semester students **Roman Briesse**, **Charlotte Roullier**, **Avip Bastakoti**, and the numerous master, summer students and visiting graduate students who have come through the lab. All the moments spent together in and out of the LNB are life-long memories that will remain always vivid in my mind.

To my entire family in Italy, thank you for encouraging me in all of my pursuits and always inspiring me to follow my dreams. I am especially grateful to my parents, **Angelo and Antonella**, who supported me in every possible way since the very beginning, from when I was a 7-years old girl messing around with the first chemistry set, dreaming about becoming a scientist. They have always been a primary source of motivation, teaching me the importance of persistence and hard work. Thank you for always believing in me. I am also grateful to have a sister like **Caterina** who was always there when I needed an encouraging or reassuring word. I hope to always make her proud of me. I want to thank **Antonella**, **Carmela**, **Ileana**, and **Genny**, my friends of a lifetime, for constantly being by my side despite every distance. I also want to thank **Chiara** for making me feel at home in Lausanne, and helping me during the first months every time I needed. Finally, I want to thank my best friend, **Ono**. Your support has meant more to me than you could possibly realize. Nothing in life makes me happier than sharing my days, my adventures, and my dreams with you. All of this is also yours.

*Lausanne, January 13, 2020*

A. A.

# Abstract

The discovery of carbon-based nanomaterials has impacted a variety of research areas in ways that could not be imagined three decades ago. Their unique combination of structural, optical, and electronic properties has made these nano-sized materials particularly attractive for applications in biotechnology and biomedicine, ranging from sensing, bioimaging, and therapeutics. When appropriately functionalized, nanocarbons (NCs) can overcome the cellular barriers of living organisms, and localize within specific organelles, providing alternative tools for the characterization and manipulation of important processes at a cellular level.

In particular, the fluorescence properties of semiconducting single-walled carbon nanotubes (SWCNTs) provide a practical basis for not only studying cellular dynamics, but also investigating the mechanisms of nanoparticle transport inside cells of living organisms. The internalization of SWCNTs in living cells forms the basis for new technologies in cellular imaging, gene and drug delivery, and other biological and medical whole-cell applications. New areas of research have focused on the targeted integration of engineered SWCNTs into living photosynthetic organisms. The synergistic combination of SWCNTs with plants and algae has the potential to impart photosynthetic organisms with improved capabilities, such as accelerated growth and enhanced photosynthetic activity, expanding their use for novel agricultural or electronic applications.

Although most work has thus far focused on studying the impact of SWCNTs on plants and other eukaryotic organisms, the impact of SWCNTs on prokaryotic species has remained largely unexplored. A study currently lacking in the field is elucidating the physiochemical factors that affect SWCNT transport across the cell wall architecture of prokaryotes, which is crucial for unlocking the variety of applications enabled by SWCNTs.

This thesis will examine the key elements, such as size and surface chemistry, that govern the interaction of fluorescent SWCNTs with photosynthetic microbes. In particular, the work presented herein will explore SWCNT uptake in both unicellular and filamentous strains of cyanobacteria, a well-known model organism for the study of photosynthesis and for use in industrial and biotechnological applications. We demonstrate length-dependent and selective internalization of SWCNTs decorated with small positively charged proteins and discuss SWCNT uptake mechanisms. Furthermore we examine subcellular localization of nanoparticles and the species-dependent impact of SWCNT exposure on cell viability.

The localization of SWCNTs within the internal cell compartments shown in this study, combined with the sustained viability of the cells, opens multiple opportunities for future develop-

## Abstract

---

ments of "green" technologies based on SWCNT integration into photosynthetic microbes. Exemplary applications, highlighting the scope of these technologies, are presented in the final chapter of this thesis. These include investigations on the impact of functionalized-SWCNT incorporation into bio-hybrid devices for improving bio-electricity generation from cyanobacteria, as well as preliminary findings on the suitability of these materials as scaffolds for targeted biomolecule delivery.

**Keywords:** carbon nanotubes, SWCNTs, cyanobacteria, *Synechocystis*, *Nostoc*, near-infrared fluorescence, nanoparticle uptake, bioelectricity, confocal microscopy

# Résumé

La découverte des nanomatériaux à base de carbone a fortement impacté de nombreux domaines de la recherche dans des directions qui ne pouvaient être imaginées il y a trois décennies. La combinaison de leur uniques propriétés structurelles, optiques et électroniques ont rendu ces nanomatériaux particulièrement attrayants pour des applications dans les secteurs de la biotechnologie et la biomédecine, tels que la détection de biomolécules, la bio-imagerie et la thérapie. Lorsqu'ils sont fonctionnalisés de manière appropriée, les nanocarbones (NC) peuvent passer au travers de barrières cellulaires d'organismes vivants et se positionner dans des organelles spécifiques, fournissant de nouveaux outils pour la caractérisation et la manipulation de procédés cellulaires importants.

Plus particulièrement, les propriétés fluorescentes des nanotubes de carbone simple paroi (SWCNTs) semi-conducteurs permettent non seulement l'étude de dynamiques cellulaires, mais aussi l'investigation des mécanismes de transport des nanoparticules au sein d'organismes vivants. L'internalisation des SWCNTs dans des cellules vivantes est l'amorce pour la création de technologies dans les domaines de l'imagerie cellulaire, la distribution de médicaments et de gènes et d'autres applications biologiques et médicales impliquant la cellule entière. De nouveaux domaines de la recherche se sont focalisés sur l'intégration ciblée de SWCNT modifiés à l'intérieur d'organismes photosynthétiques. La combinaison synergique des SWCNTs avec plantes ou algues peut en effet améliorer certaines propriétés de ces organismes, telles qu'une croissance accélérée et une activité photosynthétique accrue, élargissant leur utilisation pour des applications agroalimentaires ou électroniques.

Tandis que la plupart des travaux effectués à ce jour se soient focalisés sur l'impact des SWCNTs sur des plantes et autre organismes eucaryotes, l'impact des SWCNTs sur des espèces procaryotes restent largement peu explorées. Une étude élucidant les facteurs physicochimiques pouvant affecter le transport des SWCNTs à travers l'architecture membranaire des cellules procaryotes manque encore aujourd'hui, bien qu'une telle étude soit cruciale afin de rendre possible de nombreuses applications dépendant sur l'utilisation de SWCNTs.

Cette thèse va examiner les éléments clés, tels que la taille et la chimie de surface, gouvernant l'interaction des SWCNTs fluorescents avec des bactéries photosynthétiques. Plus particulièrement, les travaux présentés ici exploreront l'internalisation des SWCNTs dans des souches unicellulaires et filamenteuses de cyanobactéries, organisme modèle bien connu pour l'étude de la photosynthèse ainsi que pour son usage dans des applications industrielles et biotechnologiques. Nous démontrons une internalisation spécifique de SWCNTs fonctionnalisés

## Résumé

---

par de petites protéines positivement chargées, dépendant de la longueur des nanotubes, et discutons les mécanismes gouvernant l'absorption de SWCNTs. De plus, nous examinons la localisation subcellulaire des nanoparticules et l'impact des SWCNTs sur la viabilité des cellules en fonction du type de souche utilisée.

La localisation des SWCNTs au sein des compartiments internes des cellules montrée dans cette étude, combinée avec la viabilité maintenue des cellules, ouvre la porte à de nombreuses opportunités pour le développement futur de technologies "vertes" basées sur l'intégration de SWCNTs dans des bactéries photosynthétiques. De telles applications, surlignant la portée de ces technologies, sont présentées dans le chapitre final de cette thèse. Celles-ci incluent l'impact de l'incorporation de SWCNTs fonctionnalisés dans des dispositifs bio-hybrides pour la génération d'électricité à partir de cyanobactéries, mais aussi des résultats préliminaires sur l'utilisation de ces systèmes comme plateforme pour la distribution ciblée de biomolécules.

**Mots clés :** nanotubes de carbone, SWCNTs, cyanobactérie, *Synechocystis*, *Nostoc*, fluorescence proche infra-rouge , internalisation de nanoparticule, bioélectricité, microscopie confocale

# Contents

<b>Acknowledgements</b>	<b>v</b>
<b>Abstract (English/Français)</b>	<b>vii</b>
<b>Abbreviations</b>	<b>xiii</b>
<b>List of Figures</b>	<b>xv</b>
<b>List of Tables</b>	<b>xvii</b>
<b>Introduction</b>	<b>1</b>
Background and Context . . . . .	1
Objectives of the thesis . . . . .	5
<b>1 Principles of SWCNT Interaction with Living Cells</b>	<b>9</b>
1.1 Abstract . . . . .	9
1.2 Surface functionalization of SWCNTs to increase biocompatibility . . . . .	10
1.3 Cellular uptake of functionalized SWCNTs by eukaryotic organisms . . . . .	12
1.3.1 Energy-independent mechanisms of SWCNT internalization . . . . .	12
1.3.2 Energy-dependent mechanisms of SWCNT internalization . . . . .	14
1.4 Cellular uptake of functionalized SWCNTs by prokaryotic organisms . . . . .	18
<b>2 Interaction of SWCNTs with Unicellular Cyanobacteria</b>	<b>21</b>
2.1 Abstract . . . . .	21
2.2 Introduction . . . . .	22
2.3 Materials and Methods . . . . .	23
2.4 Results and discussion . . . . .	27
2.4.1 NIR Imaging of Internalized SWCNTs . . . . .	27
2.4.2 Cellular Localization of SWCNTs . . . . .	28
2.4.3 Investigating the Mechanism of SWCNT Internalization . . . . .	31
2.4.4 Impact of SWCNTs on Cell Viability . . . . .	35
2.5 Conclusions . . . . .	36
	<b>xi</b>

## Contents

---

<b>3</b>	<b>Interaction of SWCNTs with Filamentous Cyanobacteria</b>	<b>39</b>
3.1	Abstract . . . . .	39
3.2	Introduction . . . . .	40
3.3	Materials and Methods . . . . .	41
3.4	Results and discussion . . . . .	43
3.4.1	Cell-type dependency of SWCNT-cyanobacteria interaction . . . . .	43
3.4.2	Impact on cell morphology and localization of SWCNTs . . . . .	46
3.4.3	Impact of SWCNTs on Cell Viability . . . . .	47
3.4.4	Influence of the SWCNT wrapping on interaction with <i>Nostoc</i> cells . . . .	48
3.4.5	Positively-charged SWCNTs for targeted cell imaging . . . . .	50
3.5	Conclusions . . . . .	50
<b>4</b>	<b>Real-time monitoring of bacterial growth in the presence of SWCNTs</b>	<b>51</b>
4.1	Abstract . . . . .	51
4.2	Introduction . . . . .	51
4.3	Materials and Methods . . . . .	52
4.4	Results and discussion . . . . .	53
4.4.1	Real-time monitoring of unicellular cyanobacteria . . . . .	53
4.4.2	Real-time monitoring of filamentous cyanobacteria . . . . .	55
4.5	Conclusions . . . . .	57
<b>5</b>	<b>Outlook on Potential Applications of SWCNT-treated Photosynthetic Microbes</b>	<b>59</b>
5.1	Abstract . . . . .	59
5.2	Generation of bio-electricity from cyanobacteria: introduction . . . . .	59
5.2.1	Materials and Methods . . . . .	60
5.2.2	Results and Discussion . . . . .	62
5.3	SWCNTs for gene-delivery applications: introduction . . . . .	64
5.3.1	Materials and Methods . . . . .	65
5.3.2	Results and Discussion . . . . .	67
5.4	Conclusions . . . . .	69
<b>6</b>	<b>General conclusions and perspectives</b>	<b>71</b>
	<b>Appendix</b>	<b>75</b>
<b>A</b>	<b>Interaction of SWCNTs with Unicellular Cyanobacteria</b>	<b>77</b>
<b>B</b>	<b>Interaction of SWCNTs with Filamentous Cyanobacteria</b>	<b>91</b>
<b>C</b>	<b>Real-time monitoring of bacterial growth in the presence of SWCNTs</b>	<b>101</b>
<b>D</b>	<b>Outlook on Potential Applications of SWCNT-treated Photosynthetic Microbes</b>	<b>105</b>
	<b>Bibliography</b>	<b>106</b>
	<b>Curriculum Vitae</b>	<b>127</b>



# Abbreviations

<b>AFM</b>	Atomic Force Microscopy
<b>BSA</b>	Bovine Serum Albumin
<b>BPVs</b>	Biological Photovoltaics
<b>CA</b>	Chronoamperometry
<b>CD</b>	Carbon Dots
<b>CDE</b>	Clatrin-Dependent Endocytosis
<b>CIE</b>	Clatrin-Independent Endocytosis
<b>CMT</b>	Carrier-Mediated vacuolar Transport
<b>CNTs</b>	Carbon Nanotubes
<b>CS-CNTs</b>	Cup-Stacked Carbon Nanotubes
<b>DMF</b>	dimethylformamide
<b>DNA</b>	Deoxyribonucleic Acid
<b>DOC</b>	sodium Deoxycholate
<b>DTT</b>	Dithiothreitol
<b>EDTA</b>	Ethylenediaminetetraacetic acid
<b>FITC</b>	Fluorescein isothiocyanate
<b>GO</b>	Graphene Oxide
<b>HEPES</b>	4-(2-hydroxyethyl)-1-piperazineethanesulfonic acid
<b>Het</b>	Heterocyst
<b>HiPco</b>	High-Pressure carbon monoxide process
<b>HST</b>	Histone
<b>InGaAs</b>	Indium Gallium Arsenide
<b>LSZ</b>	Lysozyme
<b>MWCO</b>	Molecular Weight Cut-Off
<b>NA</b>	Numerical Aperture
<b>NC</b>	Nanocarbon
<b>NIR-II</b>	Second Near-InfraRed Window
<b>PBS</b>	Phosphate-buffered saline
<b>PEG</b>	Polyethylene glycol
<b>PGN</b>	Peptidoglycan
<b>PVA</b>	PolyVinyl Alcohol
<b>RICS</b>	Raster scan Image Correlation Spectroscopy
<b>RGD</b>	Arginine-Glycine-Aspartic acid sequence

## Abbreviations

---

<b>RNA</b>	Ribonucleic Acid
<b>ROS</b>	Reactive Oxygen Species
<b>SC</b>	Sodium Cholate
<b>SDC</b>	Sodium DeoxyCholate
<b>SDCLM</b>	Spinning-Disc Confocal Light Microscopy
<b>SEM</b>	Scanning Electron Microscopy
<b>ssDNA</b>	single-stranded DeoxyriboNucleic Acid
<b>SWCNT</b>	Single-Walled Carbon Nanotube
<b>T4P</b>	Type IV pili
<b>TEM</b>	Transmission Electron Microscopy
<b>UV</b>	UltraViolet
<b>Vis</b>	Visible
<b>VMT</b>	Vesicle-Mediated Transport
<b>WT</b>	Wild Type

# List of Figures

1	Optical properties of SWCNTs. . . . .	2
2	Factors affecting SWCNT-cell interaction. . . . .	3
3	Applications of carbon nanotubes in microbiology. . . . .	5
1.1	SWCNT noncovalent conjugation strategies. . . . .	11
1.2	Energy-independent internalization of SWCNTs. . . . .	14
1.3	Phagocytosis VS Pinocytosis of SWCNTs. . . . .	15
2.1	NIR Imaging of Internalized SWCNTs. . . . .	29
2.2	Localization of Internalized SWCNTs. . . . .	30
2.3	Effect of Surface Charge on SWCNT Uptake. . . . .	32
2.4	SWCNT Internalization by Strains Lacking Pili for DNA Uptake. . . . .	33
2.5	Effect of SWCNT Internalization on Photosynthesis and Cell Viability. . . . .	35
3.1	NIR Imaging Unicellular and Filamentous Cyanobacteria with LSZ-SWCNTs. . . . .	44
3.2	Impact of Whole Cell Zeta-Potential on SWCNT Interaction. . . . .	45
3.3	Impact on cell morphology and localization of SWCNTs. . . . .	47
3.4	NIR Imaging of chitosan-SWCNT Interaction with <i>Nostoc</i> cells. . . . .	49
4.1	Setup for in-situ monitoring of cyanobacterial growth. . . . .	54
4.2	Long-term NIR Imaging of <i>Synechocystis</i> cell growth in presence of LSZ-SWCNTs. . . . .	54
4.3	Comparison of <i>Synechocystis</i> growth in presence and in absence of LSZ-SWCNTs. . . . .	55

## List of Figures

---

4.4	Long-term NIR Imaging of <i>Nostoc</i> cell growth in presence of LSZ-SWCNTs. . . .	56
4.5	NIR Imaging of <i>Nostoc</i> -Het cell growth in presence of LSZ-SWCNTs. . . . .	56
5.1	Light-response from SWCNT-treated <i>Synechocystis</i> cells. . . . .	63
5.2	SWCNTs as scaffolds for DNA immobilization. . . . .	68

## List of Tables

2.1	Effect of LSZ-SWCNTs on the oxygen evolution of unicellular cyanobacteria. . .	36
3.1	Effect of LSZ-SWCNTs on the oxygen evolution of filamentous cyanobacteria. .	48
3.2	Effect of chitosan-SWCNTs on the oxygen evolution of filamentous cyanobacteria.	49
5.1	Primers used in this study. . . . .	66



# Introduction

## Nanocarbons in Cell Biotechnology

Quantum confinement effects, which emerge as a result of changes in the density of the electronic states, give rise to unusual optical and electronic properties in low-dimensional materials that are not attainable in bulk carbons such as diamond or graphite.[1, 2, 3] These exceptional properties make nanocarbons (NCs) particularly interesting for a range of applications, spanning from photonics,[4, 5, 6] electronics,[7, 8, 9] and sensing,[10, 11] to energy and environmental engineering.[12] The last ten years have seen an exponential rise in the use of NCs for biomedical and biotechnological research.[13, 14, 15, 16] The characteristically small dimensions of NCs (from 1 nm to 1  $\mu\text{m}$ ) are very similar in size to most biomolecules involved in vital physiological functions, enabling an effective geometric coupling of nano- and bio-materials. NCs can also traverse cellular barriers and localize within specific organelles, providing alternative tools for the characterization and manipulation of important processes at a cellular level. NCs have thus found further application as molecular scaffolds for facilitating the transport of genetic material, biomolecules, and drugs across cellular barriers.[17, 18, 19] In addition, the distinct optical properties of specific NCs make them ideal candidates for both bioimaging and biosensing technologies. NCs typically employed in biological applications include carbon nanotubes (CNTs), fullerenes, graphene, graphene oxide (GO), carbon quantum dots (CDs), carbon nanohorns, and carbon nanofibers. Furthermore, owing to the significant progress in NC synthesis and functionalization procedures, researchers today have access to an ever-growing set of synthetic nano-probes that can be used to investigate a range of complex molecular dynamics at the nanoscale.

## Properties of Single-Walled Carbon Nanotubes

Graphitic NCs, including graphene and CNTs, consist of a network of  $\text{sp}^2$  hybridized carbon atoms. The resulting electronic structure is characterized by strong optical transitions in a wide range of the electromagnetic spectrum, from visible to near-infrared regions (400-1300 nm).[20] Within the family of synthetic  $\text{sp}^2$  carbon allotropes, single-walled carbon nanotubes (SWCNTs) have attracted great attention over the last decade. SWCNTs can be visually conceptualized as a rolled-up graphene sheet, forming a hollow cylinder in 3D space (**Figure 1a**).[21] The roll-up direction, specified by two vector indices denoted as  $n$  and  $m$ ,

## Introduction

determines the resulting SWCNT optical and electronic properties. Depending on the direction of rolling, a range of nanotube chiralities ( $n,m$ ) can be obtained, with semiconducting or metallic properties. Semiconducting SWCNTs show intrinsic fluorescence emissions in the second near-infrared window (NIR-II), from 1000 to 1350 nm (**Figure 1b,c**). The optical transparency of biological tissue to light in this range substantiates their application in *in vivo* bioimaging.[22, 23, 24] Furthermore, the elevated photostability and single-molecule sensitivity of SWCNT fluorescence make these nanoparticles excellent options for intracellular nanoparticle tracking[25] and sensing applications.[26, 27, 28, 29]

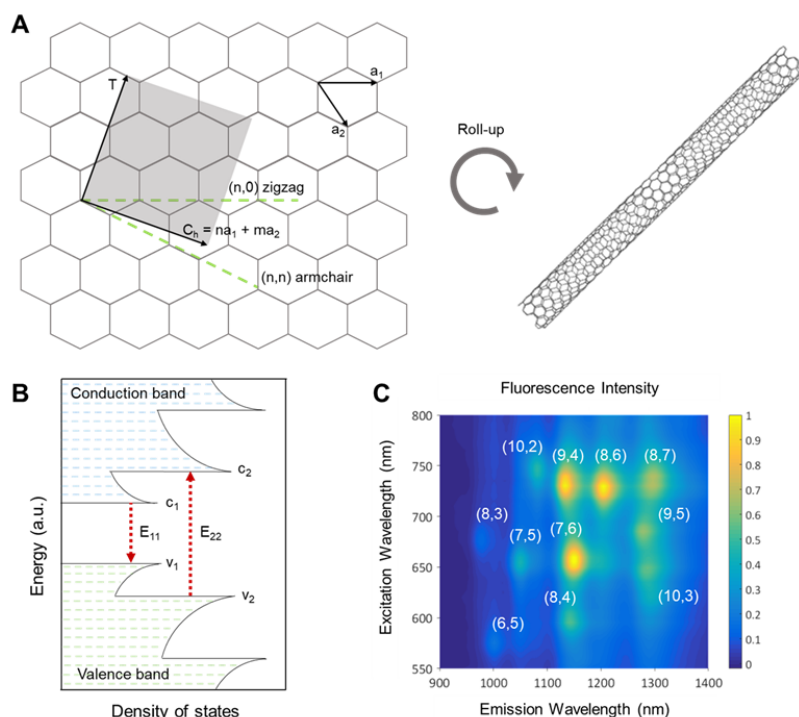


**Figure 1 – Optical properties of SWCNTs.** (A) graphical representation of the roll-up vector of a graphene sheet into a SWCNT. The direction of the rolling vector is denoted by two indices ( $n,m$ ), and determines the resulting optical properties of the SWCNT. (B) Electronic energy diagram of semiconducting SWCNTs showing density of states at the valence and conductive bands. (C) The photoluminescence map of protein-functionalized SWCNTs (HiPco SWCNTs) shows position of the characteristic peaks corresponding to distinct nanotube ( $n,m$ ) chiralities.

## Interfacing SWCNTs with Living Systems

The myriad of potential applications offered by the combination of tunable SWCNT-probes with various biological systems, has led to an expansion of nanobiotechnology research. However, interfacing synthetic SWCNTs with cells of living organisms poses several challenges. These challenges are mainly associated with the poor biocompatibility of pristine nanomaterials and species-dependent cellular responses to nanoparticle exposure. A thorough characterization of the effects and underlying mechanisms of nanoparticle interaction is



therefore needed to take advantage of the multiple opportunities provided by the synergistic combination of SWCNTs and the cells of living species. Several factors, such as environmental conditions (i.e. pH, temperature, ionic strength) or the intrinsic properties of biological membranes (i.e. elasticity, thickness, charge and composition), can have a severe impact on cell interaction with synthetic nanomaterials (**Figure 2**). In addition, many structural properties of SWCNTs, including length, diameter, accessible surface area, surface chemistry, as well as contributions from metal impurities introduced in the manufacturing process, can further influence SWCNT performance when they are interfaced with living organisms.

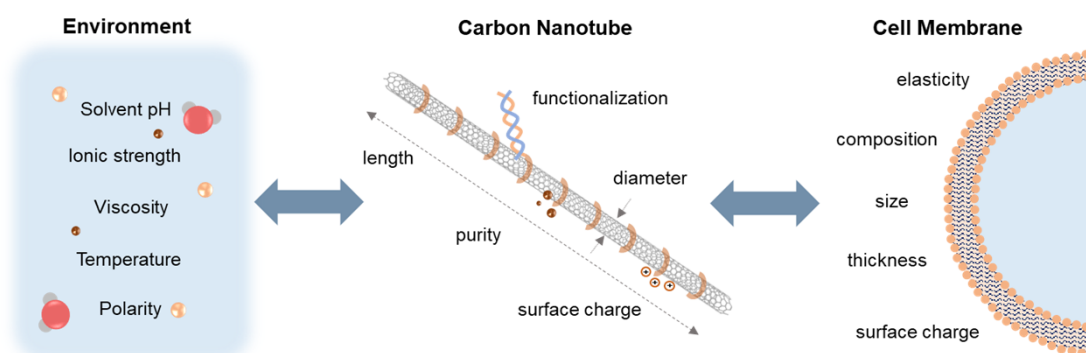


**Figure 2 – Factors affecting SWCNT-cell interaction.** Schematic illustration summarizing the main factors that influence SWCNT-cell interaction.

Suitable functionalizations that improve SWCNT solubility in physiological environments are crucial for enhancing their cellular interaction. In addition to increasing biocompatibility, surface modifications can impart SWCNTs with unique properties, including the capability of crossing cellular membranes and targeting specific subcellular compartments.[30] To date, numerous approaches have been developed to functionalize SWCNTs using a variety of wrapping molecules, including synthetic or bio-polymers. These methods have enabled SWCNT internalization inside cells of different eukaryotic species (i.e. animals, plants), with little to no toxicity.[31, 32] This controlled integration of synthetic SWCNTs into living cells of eukaryotic systems has helped to advance multiple research fields, including theranostics, biosensing, gene-delivery and tissue-engineering.

Within this context, new areas of study aim to employ synthetic nanoparticles to augment and expand the natural functions and capabilities of living species. For example, the emerging field of “plant nanobionics” focuses on improving the native performances of photosynthetic organisms.[33] Plant nanobionics involves the incorporation of synthetic nanoparticles within targeted cellular compartments of plant systems, where the nanoparticle can carry out a diverse range of functions. By broadening the limited light-absorption cross-section of plants and algae, NCs that possess distinct light-harvesting or electron-transfer capabilities have the potential to boost the natural photosynthetic activities of these organisms.[33, 34] Beyond light-harvesting, agronomic applications of SWCNTs can expedite the development of “smart crops”.[35, 36, 37] Synthetic nanoparticles can impart plants with unprecedented capabilities,

such as self-regulation, analyte-monitoring, or an ability to responsively release agrochemicals, thereby revolutionizing agronomy. Furthermore, SWCNTs can also serve as efficient alternatives for targeted biomolecule and gene delivery, as they can be used as vectors to deliver biomolecules into living cells, enabling streamlined genetic modification and regulation of plant or algal metabolism.[32, 38, 39]

### Exploring SWCNT Interaction with Prokaryotic Organisms

Nanomaterials offer a plethora of opportunities for enhancing the natural abilities of many living systems. Several examples of these augmented capabilities have been previously highlighted, such as boosted photosynthetic activity or increased plant germination and crop productivity. Although most work has thus far focused on studying the impact of SWCNTs on plants and other eukaryotic organisms, the impact of SWCNTs on prokaryotic species has remained largely unexplored.

Prokaryotes, including bacteria and archaea, play a key role in multiple life processes involving human health and environmental sustainability. An increased understanding of their microbial metabolisms has led to advancements in numerous industrial applications, such as living microbial factories for the production of commercially important chemicals, proteins, and other metabolites of biomedical interest,[40] as well as the production of bio-fertilizers and pesticides for plant health protection and enhanced crop productivity.[41] Photosynthetic prokaryotes, including cyanobacteria, are also of particular interest for a number of green chemistry applications, such as biophotovoltaics and biofuel productions, as well as high-value microbial chemical synthesis.[42]

The incorporation of SWCNTs into prokaryotes presents new sensing, imaging, enhancing, delivery and antimicrobial applications that are otherwise intractable using conventional approaches (**Figure 3**).[43, 44] Sensing and imaging applications can exploit the NIR-II emissions of the SWCNTs that are distinct from the cell's visible autofluorescence. Owing to their excellent conductivity and elevated electroactive surface area, SWCNTs can potentially improve the native performance of photosynthetic species through augmented photosynthesis and enhanced energy extraction. Furthermore, while some bacteria show “competency”, or a capacity to uptake exogenous genetic material such as DNA from their surroundings, most species often require tedious procedures to become competent, limiting the ability to genetically manipulate these microorganisms. Therefore, SWCNT transport across the cell walls of bacteria represents a first step towards enabling engineered bacterial nanoprobes for targeted and controlled biomolecule delivery into the diverse range of prokaryotic species.[45] In addition, the identification of appropriate surface functionalizations can lead to alternative antibacterial nano-agents for use against drug-resistant species.[46, 47] Hence, SWCNT-based technologies offer accelerated advancements in various microbial-based applications.

Continued developments in the field are contingent on improving SWCNT engineerability for the diverse biological environments of both prokaryotic and eukaryotic species. Consequently,

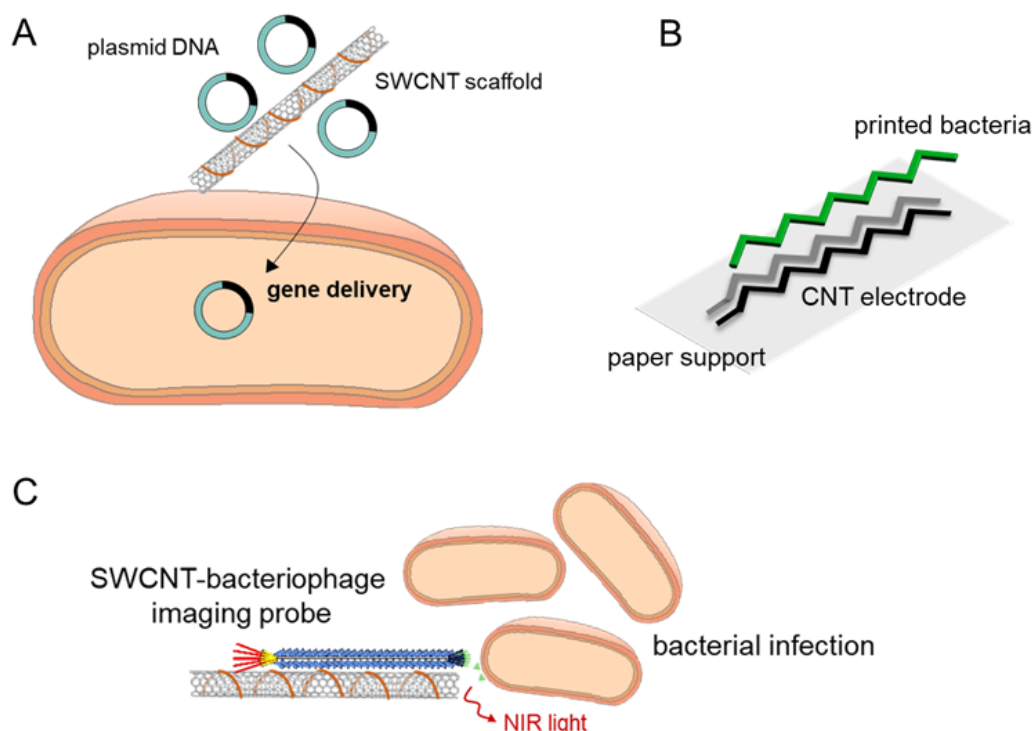


**Figure 3 – Applications of carbon nanotubes in microbiology.** Schematic illustration summarizing the main applications of carbon nanotubes with prokaryotic cells, including (A) gene-delivery, (B) biophotovoltaics, (C) imaging and sensing.

ongoing and future studies are focused on understanding and tuning the biocompatibility of these materials. Although previous studies have already confirmed the benignity of commercially available nanoparticles found in the food and cosmetic industries, such rigorous assessments are lacking in the field of microbial SWCNT applications. Furthermore, to date, the literature contains seemingly conflicting results on the possible side effects associated with nanoparticle uptake and distribution in eukaryotic and prokaryotic ecosystems. The variability in these findings indicates not only a species dependency, but also a strong dependence on the nanoparticle's surface properties, as well as exposure and incubation conditions. In addition, existing studies have largely overlooked the long-term impact of mass-produced SWCNTs into the ecosystem. Therefore, a rigorous delineation of the long-term effects of nanoparticles on the microbial ecosystem, remains imperative for the global implementation of SWCNT-based technologies.

### Objectives of the thesis

The aim of this thesis is to investigate the impact of certain key physical properties of SWCNTs, including size and surface chemistry, on their interaction with prokaryotic cells. The study presented herein is focused on the cells of photosynthetic cyanobacteria, which are a well-known model organism for the study of photosynthesis and for use in multiple industrial and biotechnological applications. Emphasis is directed towards examining the interaction of fluorescent SWCNTs with both unicellular and filamentous strains of cyanobacteria. This thesis also discusses SWCNT uptake mechanisms, as well as their subcellular localization and species-dependent impact of SWCNT exposure on cell viability. SWCNT-cell interaction is examined using a unique, custom-built NIR confocal microscope that benefits from a combination of enhanced NIR resolution and real-time confocal tracking. This technique enables real-time SWCNT monitoring that is used to investigate the fate of internalized nanoparticles upon multiple cellular division events. In summary, this thesis provides an overview of potential applications of SWCNT-based nanoprobe for improved generation of bioelectricity from cyanobacteria and for biomolecule delivery.

The thesis is composed of five chapters that have been or are expected to be published in international peer-reviewed journals and book chapters. The outline for each chapter is summarized below.

#### **Chapter 1:** *Principles of SWCNT Interaction with Living Cells*

The first chapter of this thesis provides an overview of the conjugation strategies that have been employed to increase SWCNT biocompatibility and cellular interaction. Furthermore, it summarizes the fundamental principles governing SWCNT internalization into cells of eukaryotic organisms. Finally, it introduces preliminary studies that focus on exploring SWCNT uptake by prokaryotic cells through covalent SWCNT modification.

#### **Chapter 2:** *Interaction of SWCNTs with Unicellular Cyanobacteria*

The second chapter introduces a fundamentally new mechanism for fluorescent SWCNT uptake by prokaryotes based on non-covalent functionalization strategies that preserve and exploit the SWCNT optoelectronic properties. This chapter investigates the impact of SWCNT physical properties, such as length and surface chemistry, on the interaction with cells of a model unicellular cyanobacterial strain, namely *Synechocystis* sp. PCC 6803. A unique custom-built NIR confocal microscope is employed to investigate the influence of the SWCNT functionalization on nanoparticle internalization. A combination of complementary techniques, including transmission electron microscopy and Raman spectroscopy, are employed to characterize SWCNT subcellular localization. Finally, this chapter concludes with an examination of the impact of SWCNT uptake on cell viability and photosynthetic activity.

#### **Chapter 3:** *Interaction of SWCNTs with Filamentous Cyanobacteria*

The third chapter explores the SWCNT interaction with cells of a filamentous cyanobacterial

strain, *Nostoc* sp. The study presented in this section discusses the contribution of the different cell-wall components on the nanoparticle-cell interaction, illustrating the importance of SWCNT functionalization for preserving long-term cell integrity and activity. This chapter further exploits the cell-type dependency of the internalization mechanism to develop a cell-specific staining and imaging technologies.

### **Chapter 4:** *Real-time monitoring of bacterial growth in the presence of SWCNTs*

The fourth chapter illustrates the application of NIR confocal microscopy to investigate the fate of internalized nanoparticles following multiple cell division events. This is the first time that real-time microscopy is employed to study the effect of SWCNTs on dividing bacterial cells. Furthermore, this chapter explores the use of SWCNTs for real-time tracking and differentiation of living and dead cells based on NIR-II fluorescence.

### **Chapter 5:** *Outlook towards potential applications of SWCNT-treated photosynthetic microbes*

The final chapter of the thesis presents an outlook on ongoing and future developments. Preliminary results are provided to illustrate additional applications based on SWCNT integration in photosynthetic microbes. These applications include the integration of functionalized SWCNTs into bio-hybrid devices for bio-electricity generation from cyanobacteria, in addition to the use of these materials as scaffolds for targeted biomolecule delivery.



# 1 Principles of SWCNT Interaction with Living Cells

*This chapter has been adapted from a review article published in ACS Applied Materials and Interfaces with the title: **Noncovalent Protein and Peptide Functionalization of Single-Walled Carbon Nanotubes for Biodelivery and Optical Sensing Applications** [30] and from a book-chapter submitted from publication with the title: **Biotechnology applications of nanocarbons in plant and algal systems**. The co-authors of the review are: A. Antonucci, Justyna Kupis-Rozmyslowicz and A. A. Boghossian. The co-authors of the book-chapter are A. Antonucci, Alice J. Gillen and A. A. Boghossian.*

## 1.1 Abstract

The unique structural and optical properties of single-walled carbon nanotubes (SWCNTs) have inspired the development of many innovative applications in the field of cell nanobiotechnology, ranging from real-time imaging and sensing, to biomolecule delivery and energy conversion. Key aspects that have to be addressed to exploit the synergism of SWCNT-cells interaction are: (1) designing SWCNT conjugation approaches that preserve cell viability while keeping the near-infrared optical and electronic properties of SWCNTs intact; (2) tuning the SWCNT-membrane interaction, which involves elucidating the mechanisms of SWCNT translocation across cellular barriers. To date, studies have largely focused on promoting cell uptake of SWCNTs by engineering the SWCNT surface through noncovalent functionalization. Noncovalent SWCNT conjugation, using either synthetic- or bio- molecules, has been shown to increase SWCNT solubility and membrane translocation, while enhancing nanoparticle biocompatibility. These functionalizations have facilitated SWCNT uptake in a variety of eukaryotic cells, through both energy dependent (active) and independent (passive) pathways. In this chapter, we illustrate various noncovalent conjugation approaches for immobilizing synthetic polymers, oligonucleotides, peptides, or proteins on SWCNT surfaces, highlighting important factors that affect both the nanoparticle's molecular selectivity and stability in different physiological environments. Furthermore, we discuss the fundamental principles governing the interaction of SWCNTs with cells of eukaryotic organisms, with a particular focus on the SWCNT uptake mechanisms, as well as their localization and functionality post-uptake.

In the final part of the chapter, we highlight more recent studies that also focus on the uptake of SWCNTs by prokaryotic cells. These studies demonstrated the vast potential of SWCNTs in both eukaryotic and prokaryotic systems, and substantiate the importance of elucidating the physiochemical factors that affect SWCNT transport across membranes. However, the presence of the cell wall in prokaryotic organisms increases the complexity of nanoparticle transport, and as a result there is often a need for additional mechanical assistance. This has limited the applicability of SWCNT-based technologies in the field of microbiology and created a need for greater understanding of SWCNT-prokaryotic interaction behaviors.

### 1.2 Surface functionalization of SWCNTs to increase biocompatibility

*In vivo* applications based on CNT-based materials, such as SWCNTs, require nanoparticle biocompatibility with the host cell. Because of their highly hydrophobic nature, pristine SWCNTs are practically insoluble in aqueous cell media and exhibit a very strong tendency to self-associate, forming thick, toxic aggregates.[14] Such aggregates affect nanotube dispersibility in a manner that hinders their interaction with biological components under physiological conditions. The aggregates also demonstrate diminished fluorescence that compromises the use of SWCNTs for optical applications.[48] Because the aggregation is driven by the hydrophobic surface interactions between the SWCNTs, the SWCNT surface chemistry plays a fundamental role in promoting nanoparticle dispersion in physiological environments and improving biocompatibility.[49, 50]

Several bio-conjugation approaches have already been developed to increase SWCNT solubility and facilitate their transport across the cell membranes of various eukaryotic cells. The majority of these approaches rely on noncovalent surface modification, since covalent conjugation is known to perturb and even diminish SWCNT optical properties.[51] Noncovalent functionalization of SWCNTs has been thus far achieved with a variety of wrappings such as synthetic-[52] and bio-polymers (e.g., DNA, RNA oligonucleotides)[53, 54, 55, 27, 56], peptides[57, 58], and proteins[26, 59, 60]. These wrappings can stabilize SWCNT dispersions in water without altering the extended  $\pi$ -conjugated system of the nanotube.[61] In addition to improved dispersivity, noncovalent wrappings can also impart the SWCNT with secondary characteristics such as molecular selectivity. In this regard, protein- and peptide-based conjugation strategies are particularly advantageous for the development of SWCNT materials that require specific molecular recognition capabilities.[14, 62] Optical protein-SWCNT technologies developed using these noncovalent conjugation strategies include, for example, enzyme-based optical biosensors for the label-free intracellular detection of target analytes.[10] In addition to bioanalyte sensing applications, the high surface area-to-volume ratio and uniform structural integrity of the surface, allow the nanotube to behave as a scaffold for protein and peptide immobilization for drug delivery applications.[63]

Most noncovalent immobilization techniques can be broadly categorized into two groups: (i)



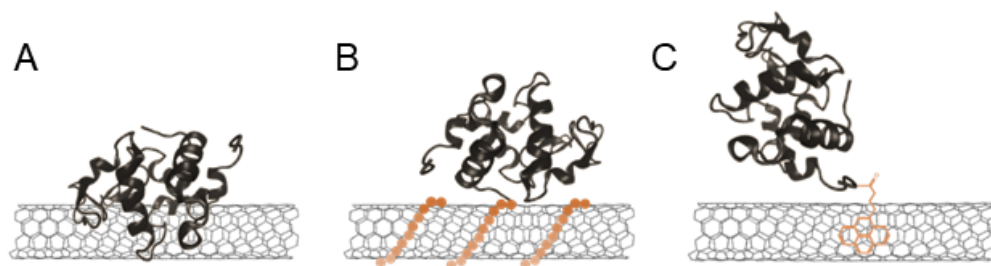


**Figure 1.1 – SWCNT Noncovalent conjugation strategies.** Overview of approaches for noncovalent protein (black) conjugation to a SWCNT (gray): (A) nonspecific physical adsorption of a protein to a SWCNT; (B) hybrid conjugation through covalent attachment to noncovalent wrappings (orange), and (C) protein binding to heterobifunctional linker molecules (orange) adsorbed onto SWCNTs.

purely adsorptive and (ii) hybrid approaches (**Figure 1.1**). Because of its simple and generally applicable procedure, nonspecific adsorption is one of the most commonly used strategies for developing novel nanotube-based technologies. Protocols often consist of an ultrasonication step in which carbon nanotubes are individually debundled in solutions containing the desired coating molecules, followed by ultracentrifugation and filtration to remove remaining aggregates and unbound molecules. However, direct ultrasonication of biomolecules, such as DNA or proteins, may result in denaturation or undesired conformational changes of the biomolecule. Therefore, an alternative approach to conjugating SWCNTs is to suspend the SWCNTs in surfactant and then dialyze the surfactant in the presence of the desired DNA or protein to facilitate biomolecule adsorption upon gradual removal of the detergent.[10, 64, 26]

The enzymatic activity and intrinsic selectivity of most biomolecules, particularly proteins, often require the nearly complete retention of their native fold.[65] Unfortunately, the hydrophobic surface of SWCNTs provides a fundamentally divergent environment that may perturb the structure and functionality of the biomolecule.[66] This drawback may pose serious limitations for sensing or subcellular delivery applications that require specific molecular recognition capabilities. For these applications, hybrid noncovalent/covalent conjugation approaches offer a more versatile, albeit more complex, conjugation strategy for protein immobilization. In one such approach, the SWCNT can be noncovalently covered by a synthetic or biological polymer that can be covalently conjugated to the protein of interest (**Figure 1.1b**).[67, 68] Alternatively, heterobifunctional cross-linking agents may also be used for conjugation (**Figure 1.1c**).[69, 70] The cross-linking agents often contain an aromatic moiety that can interact with the  $\pi$ -network of SWCNTs as well as at least one functional group that selectively binds desired protein residues, such as lysines or cysteines. Site-specific covalent protein functionalization helps to not only control protein orientation, but also increase the degrees of conformational freedom compared to complete adsorption. This increase in the conformational freedom helps to minimize structural perturbation caused by direct adsorption.

Since exogenous environmental factors, such as pH and ionic strength can also affect dispersion stability, the nanotube dispersivity must be specifically tailored with these factors in mind. For example, the strategic selection of SWCNT chirality, in addition to the chemical composition of the coating molecules, become the primary means of tuning dispersivity in environments controlled by cellular pH and ionic strength. Previous studies have shown an overall enhancement in biomolecule binding with increasing SWCNT diameters, and immobilizing the protein or peptide on large diameter SWCNTs may be used to improve stability.[71] Significant advancements in both the experimental and computational fronts over the past several years have helped to elucidate not only the contributions of SWCNT topology, but also factors such as individual amino acid residues of proteins and peptides, on the adsorption process. These principles have been used, for example, to design amphiphilic polypeptides containing cationic groups that can efficiently bind nucleic acids, allowing SWCNTs to behave as efficient gene delivery scaffolds.[72]

### 1.3 Cellular uptake of functionalized SWCNTs by eukaryotic organisms

In addition to affecting the optoelectronic properties, the stability, and the molecular selectivity of SWCNT nanoprobe, surface functionalization plays a key role in controlling the SWCNT's ability to traverse cellular barriers.[25] Although earlier reports have shown that mammalian cellular uptake of covalently functionalized SWCNTs is independent of the nature of the functional groups,[73] more recent results based on real-time *in vitro* and *in vivo* have shown a strong dependence on noncovalent functional groups for uptake by photosynthetic organelles.[25] These studies have revealed that SWCNT surface properties, such as surface patterning and charge, can govern the uptake of synthetic nanoparticles.[74, 25] Furthermore, together with SWCNT size and shape, these factors can ultimately dictate the extent to which SWCNTs can penetrate other tissues and subcellular compartments. The majority of the studies so far have focused on investigating SWCNT uptake into cells of eukaryotic organisms, for which both energy-independent (passive processes) and energy-dependent (active processes) uptake pathways have been reported. The following subsections will illustrate the underlying principles of these two processes and summarize the important factors governing SWCNT internalization into living cells.

#### 1.3.1 Energy-independent mechanisms of SWCNT internalization

Energy-independent mechanisms of SWCNT internalization into eukaryotic cells involve either the enlargement of existing pores or the formation of additional openings within the cell wall and membranes, which can enhance SWCNT penetration without need of any physical, chemical, or mechanical assistance.[75] Theoretical simulations have suggested that the cylindrical shape and high aspect ratio of SWCNTs can enable their spontaneous penetration through lipid bilayers, similarly to a "nano-needle".[76] This mechanism involves two distinct

### 1.3. Cellular uptake of functionalized SWCNTs by eukaryotic organisms

---

steps, namely the adsorption of the SWCNT onto the membrane surface, followed by its reorientation to adopt a transmembrane configuration. These mechanistic models strongly correlate with experimental observations on the interaction between various functionalized SWCNTs with plasma membranes. Indeed, pioneering work from Pantarotto et al. has shown that SWCNTs functionalized with hydrophilic groups can bind to the cell membrane and passively translocate inside HeLa cells as predicted by theoretical studies.[75] In agreement with these results, transmission electron microscopy (TEM) images have revealed that SWCNTs tend to adopt a perpendicular orientation with respect to the cell membrane during internalization.[75]

Based on these mechanisms, nanoparticle length is expected to play an important role for the direct insertion of SWCNTs through lipid bilayers.[77] Indeed, Antonelli and coworkers observed that shortening of SWCNTs (with lengths below 400 nm) promoted passive SWCNT transport across cell envelopes, even in phagocytic cells that are known to take up these nanoparticles mainly through energy-dependent pathways.[78] Similarly, Becker et al. reported that only DNA-wrapped SWCNTs shorter than  $189 \pm 17$  nm were able to access the internal compartments of human fibroblast cells, whereas longer SWCNTs remained in the culture medium.[79] Although numerous studies have reported similar observations, the reported length threshold for SWCNT internalization in these studies appears to vary with cell-type and dispersion conditions.[79, 80, 81]

In addition to SWCNT length, the surface patterning and charge of the SWCNT can also greatly impact internalization.[74] Such surface modulations have been achieved with helical wrappings based on polysaccharides and DNA.[82] Theoretical calculations have shown that certain heterogeneous hydrophobic-hydrophilic molecular arrangements on the SWCNT surface can potentially reduce the energy barrier for direct nanotube transduction through lipid bilayers.[74] Lacerda et al. have reported that the electrostatic forces between hydrophilic and charged functional components on the nanotube surface and the polar headgroups of the lipid molecules within cell membranes are the major contributors to the overall initial interaction.[83] In agreement with theoretical calculations, the introduction of positively-charged groups on the surface of the nanotubes has been shown to promote nanotube binding to negatively charged cell membranes through electrostatic attraction, facilitating their subsequent translocation.[83, 84] Positive charges not only favor SWCNT binding onto cell membranes, but also mediate nanoparticle conjugation with negatively charged polynucleotides such as DNA or RNA,[75, 85] enabling the use of SWCNTs as molecular transporters for efficient gene delivery applications.

Several recent works have demonstrated that the magnitude of the zeta-potential of the nanoparticle wrapping, rather than sign, is critical for triggering energy-independent translocation of SWCNTs through lipid bilayers (**Figure 1.2**).[25] By taking advantage of the SWCNT intrinsic fluorescence properties, Giraldo et al. and Wong et al. have demonstrated that either positively or negatively charged nanotubes could spontaneously accumulate into both isolated plant chloroplasts and subcellular compartments of wall-less plant cells (typically

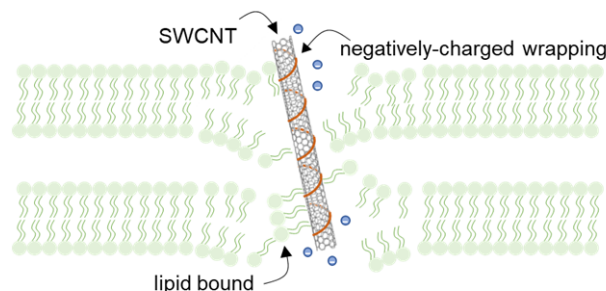


**Figure 1.2 – Energy-independent internalization of SWCNTs.** Glycerolipids wrap around SWCNT coated with negatively charged wrappings as they traverse the membrane. The attraction of lipids in the softened membrane with the nanoparticles acts as driving force for SWCNT translocation.

known as plant protoplasts).[33, 25] More specifically, nanoparticles that were sufficiently charged, either positively or negatively, induced a potential drop across the lipid bilayer, which led to local pore formation inside the membrane that, in turn, promoted nanoparticle entry. SWCNTs that were functionalized with highly charged biopolymers (such as DNA or chitosan with zeta potentials of  $-44.6 \pm 1.9$  mV and  $48.5 \pm 1.0$  mV, respectively) rapidly localized inside plant protoplasts and isolated chloroplasts, while SWCNTs possessing an almost neutral zeta-potential (such as those suspended using poly-vinyl alcohol, PVA, with a zeta potential of  $-6.4 \pm 3.4$  mV) were incapable of penetrating the lipid envelopes.[86, 33] The irreversible adsorption of lipid molecules onto the surface of the nanotube during membrane penetration was hypothesized to act as the driving force for SWCNT translocation in both plant chloroplasts and protoplasts (**Figure 1.2**). This mechanism was believed to prevent nanoparticle escape following internalization. In support of this hypothesis, lipid-coated SWCNTs were found to be unable to penetrate the chloroplast outer envelope, despite their significantly negative zeta potential of  $-35.2 \pm 2.6$  mV. This inability to traverse the chloroplast membrane was attributed to membrane trapping inhibition due to the lipid coating on the SWCNT following internalization.

### 1.3.2 Energy-dependent mechanisms of SWCNT internalization

Energy-dependent internalization processes mainly rely on endocytosis, which involves the formation of membrane invaginations, known as endosomal vesicles, that enable the entrapment of the exogenous nanoparticles and their subsequent transport and release inside the cell.[87] Depending on the cell type and on the size of the ingested particles, endocytic pathways can be typically categorized into one of two broad classes: phagocytosis and pinocytosis.

Phagocytosis is the process by which specialized immune cells such as macrophages, dendritic cells and neutrophils, can ingest particles as large as  $20\ \mu\text{m}$ . Receptor molecules present on the external membrane of these cells can recognize ligands, functional groups or specific

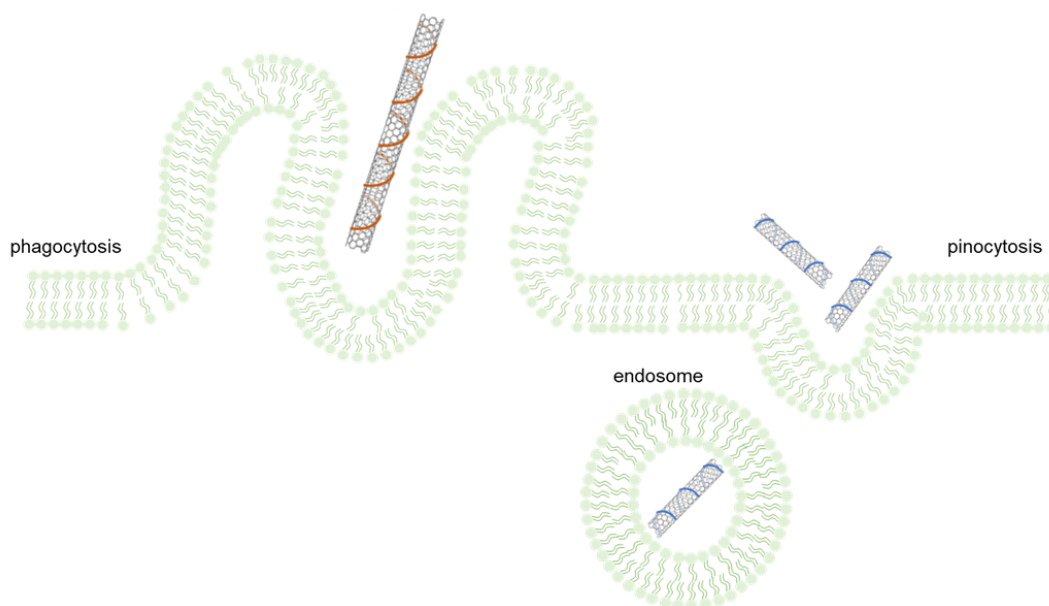


**Figure 1.3 – Phagocytosis VS Pinocytosis of SWCNTs.** Schematic illustration of the main endocytic pathways for SWCNT internalization. Both phagocytosis and pinocytosis involve the formation of membrane invaginations that enable the transport of large and small SWCNT nanoparticles inside the cell respectively.

surface chemistries on the nanoparticle surface that mark these particles for uptake. Owing to their central role in many physiological and pathological conditions, including cancer and inflammation, macrophages have long remained the focus of numerous studies, including recent studies focused on imaging and therapeutic applications.[88, 89] Several of these studies have demonstrated that SWCNTs could accumulate into small phagosomal vesicles within macrophage cells, suggesting active SWCNT ingestion without toxic effects.[81, 90, 78, 89] The ingested nanotubes retained their characteristic fluorescence properties and could be imaged by NIR fluorescence microscopy, enabling diagnostic cell-tracking of macrophages.[91] Other studies observed that the inactivation of phagocytic pathways through specific inhibitors did not affect SWCNT uptake efficiency in macrophages.[78] These findings suggest the co-existence of multiple internalization mechanisms in macrophages that might depend on SWCNT length and size. For example, in contrast to phagocytosis, where preferential internalization is shown for SWCNTs in the  $\mu\text{m}$  range(**Figure 1.3**), energy-independent mechanisms favored the extra-vesicular accumulation of SWCNTs that were shorter than 400 nm.[78] Similarly, Cui et al. reported that the uptake of short SWCNTs inside murine macrophage cells could also take place through pinocytosis.[92]

In contrast to phagocytosis, pinocytosis can be present in almost all different cell types, and it regulates the internalization of smaller nanoparticles that are normally shorter than 1  $\mu\text{m}$  (**Figure 1.3**). The different pinocytic pathways that exist are commonly categorized

according to the type of proteins that are involved in the internalization process. These pathways include (i) clathrin-dependent endocytosis (CDE or receptor-mediated endocytosis), (ii) clathrin-independent endocytosis (CIE) and (iii) macropinocytosis. Multiple pinocytic processes can occur in parallel, and their occurrence depends on the cell type and nanoparticle characteristics. Nanoparticle internalization via CDE can be triggered by SWCNT binding to surface ligands or other receptor molecules located onto most eukaryotic cell membranes.[93] In this process, clathrin proteins assist in the formation of a coated pit on the inner surface of the plasma membrane, which facilitates the transport of the exogenous material inside the cell. One example of active internalization based on ligand-receptor interaction is the targeting of integrins  $\alpha v \beta$ , which are endothelial cell receptors for extracellular matrix proteins possessing a specific RGD sequence (arginine-glycine-aspartic acid). The conjugation of RGD-tagged polypeptides on the surface of the SWCNTs therefore allows for targeted delivery of the nanoparticles inside tumor cells via integrin recognition.[94] Another example involves the immobilization of engineered nuclear proteins, such as the tail domain of lamin B1 (LB1), on SWCNTs to enable targeted nanoparticle penetration across cell nuclear membranes.[31] CDE-based internalization into adherent cell lines can also selectively occur for short SWCNTs (100-200 nm) coated with chitosan molecules.[80] In a similar study, Kam et al. have demonstrated that the disruption of clathrin-coated vesicles under hypertonic treatment can drastically reduce the levels of protein-SWCNT uptake into HeLa cells, indicating CDE as the preferential uptake pathway.[95] In agreement with this observation, the specific inhibition of alternative uptake pathways, such as CIE, results in a retention of cellular uptake, suggesting insignificant contributions from other endocytic routes.

In addition to receptor-mediated interactions, SWCNTs can traverse the cell membrane via alternative energy-dependent pathways. Macropinocytosis for example, involves the encapsulation of the nanoparticles inside a endocyte vesicle, called macropinosome, which is not coated with clathrin or caveolin but encircled by actin. Macropinocytosis provides an efficient process for non-selective uptake of nutrients and solute macromolecules. The integration of SWCNTs inside such vesicles has been reported by several studies, such as the work by Boyer et al., who specifically observed the accumulation of pluronic comopolymer-stabilized SWCNTs within endosomes inside HeLa cells.[89] Interestingly, the pluronic coating was believed to increase the association of SWCNTs with the cell membrane, which could, in turn, enhance SWCNT active uptake. Analogously, Liu et al. reported non-receptor mediated endocytosis of SWCNTs conjugated with a widely used chemotherapy drug, paclitaxel, inside breast carcinoma cells.[96]

As with energy-independent uptake mechanisms, the net charge of the coating molecules can directly influence the active cellular uptake of SWCNTs in energy-dependent uptake mechanisms. Budhathoki-Uprety et al. observed preferential uptake of SWCNTs modified with cationic functionalizations into HeLa cells compared to SWCNTs possessing negatively charged functionalizations.[97] One reason for this distinction has been attributed to differing adsorption/desorption rates of serum proteins present in the cell culture media. Serum proteins can bind to the SWCNT surface through  $\pi - \pi$  interactions or electrostatic attractions,

### 1.3. Cellular uptake of functionalized SWCNTs by eukaryotic organisms

---

forming a protein "corona" that can differentially modulate SWCNT uptake. The intrinsically different affinities of serum proteins for cationic or anionic functional groups on the surface of the SWCNT can, in fact, dictate their internalization fates.

Among the different eukaryotic species, the energy-dependent delivery of SWCNTs into intact plant cells deserves a separate discussion, as it presents many additional challenges over what is observed in their wall-less counterparts. The plant cell wall, whose composition can vary between species, typically consists of a network of cellulose microfibrils cross-linked with hemi-cellulose and interpenetrated by pectin.[98] These thick cellulosic layers provide the cell with increased rigidity and structural support, thereby largely determining the shape. In addition, the cell wall offers increased protection, acting as an additional filtering mechanism and impeding the passage of larger macromolecules to the cell interior due to the small pore sizes (average width ranging between 5-30 nm).[99]

Although a number of reports have documented the possibility of larger nanoparticles traversing the thick plant cell wall, the underlying mechanisms of cell membrane translocation remain largely unclear, with both passive and active mechanisms being reported. Similar to other eukaryotic systems, studies have shown that the entry of SWCNTs inside intact cells of different plant species primarily occurs via energy-dependent mechanisms. Liu and coworkers have been among the first groups to report active internalization of SWCNTs inside the walled cells of *Nicotiana tabacum*. [96] Nanotubes were labelled noncovalently with fluorescein isothiocyanate (FITC), and uptake into the cells over time was monitored using fluorescence microscopy. By examining the temperature-dependence of the SWCNT uptake Liu et al. observed that the amount of SWCNTs was significantly reduced at low temperatures, implying the involvement of endocytosis as an active transport mechanism. In addition, when cells were pretreated using specific inhibitors of cellular endocytosis, a significant decrease in the cellular fluorescence was observed, further suggesting uptake via an energy-dependent pinocytosis mechanism. By studying the uptake of SWCNTs noncovalently functionalized with FITC (SWCNT-FITC) in *Catharanthus roseus*, Serag et al. elucidated that the uptake of SWCNTs can also be associated with various subcellular phenomena, including carrier-mediated vacuolar transport (CMT) and vesicle-mediated transport (VMT). [100] Raster scan image correlation spectroscopy (RICS) showed that the SWCNTs can also elicit autophagy responses in *Catharanthus*. [100] These measurements showed that the distribution of diffusion values inside the cell vacuole were similar to cytoplasmic diffusion values close to the vacuolar membrane (tonoplast). This observation indicates that parts of the cytoplasm are penetrating into the vacuole through autophagy, further revealing that the passage of SWCNTs through the tonoplast occurs at interrupted and localized zones mediated by protein carriers.

One alternative approach for SWCNT internalization into walled plant cells involves the formation of nanopores in the cellulosic wall, which can be mediated by localized enzymatic degradation. Cellulase enzymes are naturally capable of catalyzing cellulolysis, where cellulose is hydrolyzed into shorter chain saccharides. In their study, Serag et al. have demonstrated that the incubation of cellulase immobilized on cup-stacked carbon nanotubes (CS-CNTs) can

induce local lesions in the plant walls, referred to as cellulase-induced nanoholes, allowing CS-CNTs to translocate into the internal compartments of the cell.[101] Compared to previous delivery approaches, this strategy presents an exciting alternative for CNT transport into plant cells, as it also circumvents the need for the complete cell wall removal.

### 1.4 Cellular uptake of functionalized SWCNTs by prokaryotic organisms

In contrast to eukaryotic species, our knowledge on SWCNT uptake inside cells of prokaryotes is remarkably incomplete. With only few exceptions, prokaryotic cells (including archaea and bacteria) are surrounded by rigid walls that impart them with their characteristic shape and provide both structural support and protection against many environmental stresses. The cell walls of most bacteria are categorized into one of two architectures, Gram-positive or Gram-negative, which differ in the architecture of the peptidoglycan backbone. Gram-positive bacteria possess a thick peptidoglycan layer, with average thicknesses usually ranging from 20 to 40 nm. In contrast, Gram-negative cells are characterized by a thinner peptidoglycan layer, enclosed by an outer membrane consisting mainly of lipopolysaccharide. Over the course of evolution, many bacterial species have developed considerably diverse supramolecular architectures, which can include additional layers located on top of the cell wall, such as capsules, sheaths, or S-layers.[102] All together, these structural components largely determine the different properties of the bacterial cell walls in terms of stability, permeability, elasticity and resistance to mechanical or osmotic stress. Such properties also play important roles in dictating cell susceptibility to nanoparticle exposure. The bactericidal activity of different nanomaterials is often associated with their ability to perturb the cell wall architecture by altering its permeability. In this regard, many studies have found that Gram-positive bacteria are more resistant to nanoparticle internalization, due to the presence of a thicker peptidoglycan layer.[103]

Nevertheless, previous investigations have shown that external mechanical or physical forces can favor partial or integral nanoparticle penetration across the cell walls, without toxic effects. The majority of these studies have been largely applied to Gram-negative *Escherichia coli* (*E. coli*) cells for the design of alternative gene-delivery scaffolds. Lee et al. showed that electrosprayed gold nanoparticles could form temporary channels through the cell wall of *E. coli* that facilitated the transport of genetic material inside the cell, while not necessarily resulting in the internalization of the nanoparticles.[104] Similarly, Kumari et al. observed that gold nanoparticles could accumulate inside the bacterial cytoplasm of *E. coli* under vortexing conditions at 50°C.[105] An analogous study from Rojas-Chapana et al. involving the application of microwaves, demonstrated that oxidized, water-dispersible CNTs could transport DNA into *E. coli* cells by opening up temporary nanochannels across the cell envelope.[45] Although TEM analysis showed that CNTs could act as nano-needles that puncture the cell wall upon microwave exposure, no complete internalization of the nanoparticles could be observed. On the other hand, when gold nanoparticles were added to the cell-CNT mixture,



#### 1.4. Cellular uptake of functionalized SWCNTs by prokaryotic organisms

---

local cell membrane disruptions created at the adsorption sites of individual CNTs seemed to favor the transport of the gold nanostructures inside the cytoplasm. Only recently have these principles been applied to develop a nanotube-assisted microwave electroporation technique enabling the genetic manipulation of diverse pathogenic bacteria.[106]

Although these preliminary studies demonstrated the potential of CNTs to function as gene delivery scaffolds for bacterial transformation, the transport of exogenous DNA by SWCNTs, in absence of external mechanical or physical assistance, has yet to be reported. Kostarelos et al. were among the first to observe the spontaneous internalization of shortened SWCNTs bi-functionalized with ammonium groups and FITC inside *E. coli*, even in absence of external mechanical aid.[73] Nevertheless, SWCNT uptake appeared to occur only inside 20% of the treated cells compared to eukaryotic cells incubated with the nanoparticles at similar doses. This difference was attributed to the presence of the cell wall that likely impeded nanoparticle translocation. These preliminary observations substantiate the importance of elucidating the physiochemical factors that affect SWCNT transport across the cell wall architecture of prokaryotes, a study that is currently lacking in the field and crucial for unlocking the variety of applications enabled by SWCNTs.



## 2 Interaction of SWCNTs with Unicellular Cyanobacteria

*This chapter has been adapted from an article submitted for publication with the title: **Inherited Nanobionics Enable Cross-generational Tracking of Bacteria Using Near-infrared Confocal Microscopy**. The co-authors of this article are: A. Antonucci, N. Schuergers, V. Zubkovs, M. Reggente, A.J. Gillen, B. Lambert, E. Carata, L. Dini and A. A. Boghossian.*

**Author contributions:** A.A., N.S., A.J.G., L.D. and A.A.B. participated in experimental design. A.A., M.R, B.L., and E.C. performed the experiments. V.Z. conceived and integrated the NIR confocal microscope. A.A., N.S., and A.A.B. wrote the manuscript. A.A. and A.A.B. conceived and designed the research.

### 2.1 Abstract

The distinctive properties of SWCNTs have inspired the development of novel applications in the field of cell nanobiotechnology. However, studies thus far have yet to explore the effect of SWCNT functionalization on transport across the cell wall of prokaryotes. In this chapter we explore the uptake of SWCNTs in Gram-negative cyanobacteria and demonstrate length-dependent and selective internalization of SWCNTs decorated with small positively charged proteins. The nanoparticles are shown to traverse the cell wall of unicellular strains of cyanobacteria, independent of whether the strain is naturally competent for DNA uptake. We use a custom-built, spinning disc confocal microscope to image near-infrared (NIR) SWCNT fluorescence within cells, which reveals a highly inhomogeneous distribution of SWCNTs that is otherwise overlooked using conventional widefield imaging. Raman spectroscopy and transmission electron microscopy (TEM) confirm internalization of the SWCNTs within the cytosol of the cells. We show that the nanobionic cells exhibit sustained photosynthetic activity and growth.

### 2.2 Introduction

The internalization of carbon nanotubes in living cells forms the basis for new technologies in cellular imaging, gene and drug delivery, and other biological and medical whole-cell applications.[96, 107] Numerous synthetic and biological molecules can be immobilized on the surface of carbon nanotubes which, when appropriately functionalized, are capable of crossing biological barriers and binding specific molecular targets. Single-walled carbon nanotubes (SWCNTs) in particular have optoelectronic properties that are well suited for phototherapy,[108] imaging,[109] and sensing.[11] Unlike conventional fluorescent probes, the electronic bandgap of semiconducting SWCNTs allows these nanostructures to absorb light across a wide range of the electromagnetic spectrum and to re-emit the absorbed energy as near-infrared (NIR) fluorescence. This fluorescence remains photostable even upon continuous exposure to high-intensity excitation.[110, 10] SWCNT fluorescence can optically penetrate biological tissue and biofluids for deep-tissue imaging. Furthermore, the fluorescence provides an optical signal that is distinct from the autofluorescence of biological fluorophores in the visible range. SWCNTs have been used for subcellular targeting to the cell nucleus and peri-nuclear regions,[111, 31] and their semiconducting properties have been exploited for the phototherapeutic treatment of cancer cells.[108] Recently, semiconducting SWCNTs have been shown to enhance the photosynthetic efficiency of light-harvesting organelles extracted from plant cells[33] and enable nitroaromatic detection in living spinach leaves.[36]

The majority of studies to date have focused on interfacing SWCNTs with cells of eukaryotic organisms, for which both active and passive uptake mechanisms of SWCNTs have been reported.[25, 112, 74, 113] Previous studies have shown that SWCNT surface modifications are critical to either promote or hinder nanoparticle penetration through the cell membrane of eukaryotes.[25] By contrast, no work has so far explored the influence of functionalization on SWCNT transport across the complex, multilayered walls that surround bacterial cells. While the interaction of modified nanotubes with *Escherichia coli* cells has been studied[73], bacterial uptake of fluorescent SWCNTs has yet to be reported. A comprehensive study focusing on the physiochemical factors that affect SWCNT transport across the cell wall architecture of prokaryotes, which is currently lacking in the field, is the first step in enabling engineered bacterial nanoprobes for targeted and controlled biomolecule delivery. Beyond delivery, the SWCNT fluorescence allows for spatiotemporal intracellular sensing,[114] NIR cell imaging,[115] and augmented light-harvesting applications[33] in phototrophic strains.

These applications motivate the current study, which focuses on tuning noncovalent surface functionalization to facilitate the uptake of fluorescent SWCNTs in bacterial cells. We focus our investigation on phototrophic cyanobacteria, selected for several reasons. First, cyanobacteria possess a complex cell wall structure that forms a considerable permeability barrier. Like other bacteria, cyanobacteria are surrounded by a rigid peptidoglycan (PGN) cell wall that determines the characteristic cell shape, while protecting it against mechanical stress and rupture. The PGN layer is enclosed by an outer membrane, which is typical of Gram-negative cells. However, compared to other Gram-negative bacteria, the PGN wall found in cyanobac-

teria is considerably thicker (about 10 nm in unicellular strains) and shows a higher degree of cross-linkage, similar to Gram-positive bacteria.[102] Also, the presence of a crystalline surface layer (S-layer) in some species can further limit the translocation of proteins and other high-molecular-weight substances across the outer membrane.[116] Since the transformation of cyanobacteria with foreign DNA often relies on bacterial conjugation based on multiple plasmids and triparental mating strategies, the ability to genetically manipulate these microorganisms can also be limited.[117] SWCNT translocation across cyanobacterial cell walls could therefore facilitate the delivery of larger synthetic or bio-molecules, including genetic material, as previously demonstrated for eukaryotic cells.[32, 39]

In addition to the considerable permeability barrier, cyanobacteria are photosynthetic cells that demonstrate optical properties complementary to those of semiconducting SWCNTs. SWCNTs have been shown to enhance the efficiency of the light reactions of photosynthesis both *in vivo* and *in vitro*, motivating several optical, energy-based applications. Furthermore, the photosynthetic pigments in cyanobacteria autofluoresce at wavelengths overlapping with the fluorescence emissions of visible fluorophores typically used for bioimaging and sensing. Therefore, the NIR emissions of SWCNTs motivate their use in mitigating this spectral overlap for fluorescence imaging and tracking. In the present study, we demonstrate the applicability of internalized SWCNTs as NIR imaging probes for the model cyanobacterium *Synechocystis* sp. PCC 6803 (hereafter *Synechocystis*), using a combination NIR and visible imaging, Raman spectroscopy, and immunogold labeling transmission electron microscopy (TEM). We further characterize the viability of cells incorporating these nanoprobe as we push towards expanding the major advancements achieved with living plant bioelectronics and nanobionics[118] to photosynthetic microbes.

## 2.3 Materials and Methods

**Noncovalent functionalization of SWCNTs.** The SWCNTs used in this study were purified HiPco nanotubes (NanoIntegris, Lot. No. HP26-019) with a diameter of 0.8–1.2 nm and a length of 100–1000 nm. SWCNTs were wrapped with a ((AT)<sub>15</sub>) oligonucleotide (Eurofins Genomics) following a modified protocol from Zheng et al.[53], and with chitosan (Carl Roth) as described in Reuel et al.[119] To summarize, 1 mg of SWCNTs was suspended in either deionized water or, in the case of chitosan, 1% acetic acid to yield a final concentration of 1 mg/mL. Samples were sonicated using a cup-horn sonicator (140 mm, Qsonica, LLC) for 90 minutes at 1% amplitude in an ice bath. The sonicated SWCNT suspension was centrifuged (Eppendorf Centrifuge 5424 R) for 180 minutes at 16500 x g to pellet SWCNT aggregates. The suspensions were dialyzed against 2 L of deionized water using either a 14 kDa MWCO cellulose membrane (Sigma Aldrich), in the case of DNA-SWCNTs, or a 300 kDa MWCO cellulose membrane, in the case of chitosan-SWCNTs. LSZ-, HST- and BSA-SWCNTs were prepared following a similar protocol by suspending 1 mg of HiPco nanotubes and 5 mg of lysozyme from chicken egg white (Sigma Aldrich), 10 mg histone type-III (Sigma Aldrich), or 10 mg of bovine serum albumin (Sigma Aldrich), in 1 mL of 1 mM HEPES buffer (pH 7.4) and sonicating for 90 minutes

at 1% amplitude on ice. Unbound protein was removed through dialysis against 2 L of 1 mM HEPES buffer using a 300 kDa MWCO cellulose membrane. The same protocol was used to suspend SWCNTs with thermally deactivated LSZ. However, prior to dialysis, the LSZ solution was heated to 90°C for 20 minutes, as described by Xie et al.[120] SWCNT concentrations were calculated from absorbance measurements at 632 nm in a UV-Vis-NIR scanning spectrometer (Shimadzu 3600 Plus) using an extinction coefficient of  $0.036 \text{ (mg/L)}^{-1} \text{ cm}^{-1}$ . The concentration of functionalized SWCNT suspensions ranged between 80-100 mg/L, except for BSA- and HST-SWCNT suspensions where concentrations between 35-50 mg/L were obtained.

**Zeta-potential measurements.** All stock solutions of SWCNTs were diluted in 1 mM HEPES buffer (pH 7.4) to yield a final concentration of 10 mg/L. Zeta potential measurements were carried out with a Zetasizer Nano ZS analyzer from Malvern, using folded capillary cells.

**Bacterial strains and growth conditions.** Liquid cultures of wild-type *Synechocystis* and *Nostoc* were grown in BG11 medium (Rippka et al.[121]) supplemented with 10 mM TES buffer (pH 8.0) at 30°C under  $50 \mu\text{mol photons m}^{-2} \text{ s}^{-1}$  of white light with constant shaking. The  $\Delta\text{hfq}$  mutant cells were additionally supplemented with  $7 \mu\text{g/mL}$  of chloramphenicol.[122] At an  $\text{OD}_{750\text{nm}}$  of 0.9-1.2, cells from 2 mL of the culture were harvested by centrifugation at 5000 rpm at room temperature. Pellets were washed three times with 1 mM HEPES buffer (pH 7.4) and then re-suspended in the same buffer to achieve a final  $\text{OD}_{750\text{nm}}$  of 1.4.

**NIR fluorescence imaging.** Cells were fixed onto poly-lysine coated glass-bottom petri dishes by spotting  $30 \mu\text{L}$  of the cell suspension at  $\text{OD}_{750\text{nm}}$  of 1.4 for 10 minutes followed by washing with HEPES. The cells were then covered with  $50 \mu\text{L}$  of 1 mM HEPES buffer (pH 7.4). They were imaged using a custom-built optical setup consisting of an inverted microscope (Eclipse Ti-U, Nikon AG Instruments) with an oil-immersion TIRF 100 x objective (N.A. 1.49, Nikon) coupled to a CREST X-Light spinning-disk confocal imaging system (CREST Optics) ( $60 \mu\text{m}$  pinholes) and an InGaAs camera (NIRvana 640 ST, Princeton Instruments). Samples were illuminated using a TriLine LaserBank system (Cairn Research) at 640 nm and 780 nm, and fluorescence was collected using either an 800 nm (Chroma), 980 nm long-pass filters (Semrock), or a  $1260 \pm 15 \text{ nm}$  band pass filter (Chroma). Images were acquired using the Nikon NIS-Elements software (Nikon Instruments).  $10 \mu\text{L}$  of SWCNT stock solutions were added to a  $50 \mu\text{L}$  droplet of 1 mM HEPES buffer to yield a final concentration of 2 mg/L. Following incubation, the SWCNT solution was replaced by a  $50 \mu\text{L}$  droplet of fresh HEPES buffer. SWCNT fluorescence quenching was monitored by adding ferricyanide to yield a final concentration of 120 mM.

**Length separation of sodium deoxycholate-SWCNTs.** Length separation of SWCNTs was achieved by density gradient centrifugation following a modified protocol from Cognet et al.[123] First, 25 mg of purified HiPCo SWCNTs (NanoIntegris, Lot. No. HP29-064) were dispersed in 25 mL of 1% (w/w) sodium deoxycholate (DOC) solution in deionized water. The dispersion was homogenized for 20 min at 5000 rpm (PT 1300D, Polytron) and sonicated for 1 hour using a probe-tip ultrasonicator (1/4 in. tip. Q700 Sonicator, QSonica) at 10% amplitude in ice bath. The SWCNT suspension was centrifuged at  $164\,000 \times g$  for 4 hours at 25°C (Optima

XPN-80, SW 32 Ti Rotor, Beckman Coulter). The supernatant was collected and stored at room temperature. Density gradient solutions were prepared by stacking four layers of 3 mL of 60 wt%, 10 wt%, 7.5 wt%, and 5 wt% iodixanol solution (OptiPrep, Sigma-Aldrich) from bottom to top in 17 mL polycarbonate centrifugal tubes (Beckman Coulter). A volume of 3 mL stock DOC-SWCNT suspension was added on top of the density-gradient iodixanol solution and centrifuged for 4 hours at 175000 x g and at a temperature of 4°C (SW 32 Ti Rotor, Beckman Coulter). Following centrifugation, SWCNTs with different lengths were found distributed along the density gradient, with shorter nanotubes located closer to the top of the centrifugal tube and longer nanotubes towards the bottom of the tube. Twenty fractions (0.5 mL volume) were extracted by manually pipetting from the top to the bottom of the centrifugal tube.

**AFM imaging.** A small volume (10  $\mu$ L) of length-separated SWCNT fractions was drop-casted on a freshly cleaved mica surface. The sample was rinsed with deionized water several times in order to remove excess surfactant from the surface and dried in air. Morphological characterization was performed using a commercial AFM setup (Cypher, Asylum Research) equipped with a commercial Si cantilever (AC160TSA-R3, Asylum Research). Topography, phase, and amplitude images were acquired in standard tapping mode. SWCNT lengths were evaluated using standard tools (e.g. plane subtraction and profile extraction) featured in the AFM data analysis software (Gwyddion 2.52).

**Protein functionalization of length-separated SWCNTs.** Length-separated DOC-SWCNTs were precipitated according to the literature using methanol.[124] Sedimented SWCNTs were washed using deionized water by centrifugation several times in order to remove unwanted surfactant and iodixanol residues retained from the density gradient ultracentrifugation procedure. Following these washing steps, SWCNTs were mixed with 0.3 mL of lysozyme solution (5 mg/mL) in deionized water and bath sonicated for 15 min. The suspension was then sonicated with a cup horn sonicator for 1.5 hours. The samples were centrifuged at 16500 x g for 3 hours to remove SWCNT aggregates.

**Raman characterization.** Raman spectra were recorded at an excitation wavelength of 532 nm from 200 to 1800  $\text{cm}^{-1}$  using a water-immersion 63x objective (0.90 N.A) on a confocal spectroscopy (inVia Raman Microscope, Renishaw). For automatic confocal Raman mapping, confocal Raman spectra were recorded with a step size < 1  $\mu$ m in X-Y, for a total number of 9x9 spectra. Spectra were automatically acquired along the Z direction, where Z= 0 corresponds to the higher contrast of the cell on a bright-field image. The spectrometer was calibrated before measurements using an internal standard. 3D maps were generated using a Matlab script (Matlab R2015, Mathworks).

**TEM and immunogold labeling.** Following a 1-hour incubation with either 2 mg/L LSZ-SWCNTs (positive control) or with 5 mg/mL lysozyme solution (negative control), *Synechocystis* cells were fixed with 2% paraformaldehyde and 0.2% glutaraldehyde in 0.1 M cacodylate buffer pH 7.2 for 2 h. After washing with 0.1 M cacodylate buffer, pH 7.2, cells were dehydrated with dimethylformamide (DMF) at increasing concentrations (50%, 75%, and 90%). Cells were

embedded in Lowicryl K4M resin (Emsdium, Hatfield, PA, USA), and samples were then placed in gelatin capsules and polymerized at -20°C overnight by UV irradiation at  $\lambda = 360$  nm. Ultrathin sections (60 nm) were subsequently cut with a PT-PC PowerTome ultramicrotome (RMC, Tucson, Arizona USA). The sections were collected on nickel grids and were blocked with PBS with 0.15% glycine for 5 min, followed by 0.4% gelatin in a solution of 0.1% BSA in PBS. Samples were then incubated overnight with the primary antibody, antilysozyme (ab391, Abcam, Cambridge, United Kingdom), at 1:100 dilution in PBS with 1% BSA. After washing with PBS with 0.1% BSA, the grids were incubated with the secondary antibody, gold particle conjugated (10 nm) protein A, in PBS with 4% BSA. After extensive washing, the samples were imaged using a HT7700 TEM (Hitachi, Tokyo, Japan).

**Determination of the chlorophyll a content.** The chlorophyll a content was used to normalize the oxygen evolution and consumption rates. Cells were pelleted for 7 min at 15000 x g and then re-suspended in 1 mL of 99% methanol, pre-cooled at 4°C. The samples were incubated at 4°C for 20 min in the dark and soluble pigments were separated from cell debris by centrifugation for 7 min at 15000 x g at 4°C. Chlorophyll a content was determined according to the equation  $\text{Chla } [\mu\text{g/mL}] = 12.9447 (A_{664\text{nm}} - A_{720\text{nm}})$  as described by Ritchie.[125]

**Measuring net oxygen production and consumption rates under light and dark conditions.** Cells were harvested during the late exponential growth phase ( $\text{OD} > 1$ ) by centrifugation and re-suspended in fresh BG-11 medium to an  $\text{OD}_{750\text{nm}}$  of 1.4. The oxygen concentration under light and dark conditions for whole cells was monitored at 30°C using a Clark-type electrode (Hansatech, OxyLab+, Norfolk). Samples were illuminated at an intensity of 200  $\mu\text{mol photons m}^{-2} \text{ s}^{-1}$  under white light. 10 mM of sodium bicarbonate ( $\text{NaHCO}_3$ ) was added to the cell suspensions in the reaction chamber prior to oxygen measurement to provide the cells with an excess carbon source.

**Computational methods.** Model parameters were determined by fitting numerical solutions of the three differential equations to experimental data. The fit between the model and experimental data was achieved with a Matlab (MathWorks) script by using the OPTI toolbox.[126] A built-in ODE function, ode45, was used for numerical integration. Additional details are provided in **Appendix A** under the section “Computational modeling”.

**Statistical analysis and image processing.** All data points and error bars shown in the figures represent mean values with standard deviations. One-way ANOVA tests were used to evaluate statistically significant differences in oxygen evolution rates. A sample size of  $n=3$  was used for the calculations. Statistical significance was assumed for a  $p\text{-value} < 0.05$ . Z-stacked images of the cells were visualized using a Matlab script. Background subtraction was performed with Fiji-ImageJ for all microscopy images, and an additional median filter (pixel radius = 2) was applied to images shown in Figure A.6 for noise removal.



## 2.4 Results and discussion

### 2.4.1 NIR Imaging of Internalized SWCNTs

SWCNTs were non-covalently functionalized with various coatings shown to preserve SWCNT fluorescence and subsequently screened for their internalization efficiency. We compared uptake by *Synechocystis* cells to uptake by isolated spinach chloroplasts, photosynthetic organelles surrounded by a double membrane lacking a PGN layer. *Synechocystis* cells and chloroplasts were immobilized onto poly-lysine coated glass-bottom dishes and exposed to a 2 mg/L aqueous suspension of SWCNTs functionalized with DNA-, chitosan-, or lysozyme (LSZ) for 10 minutes. After washing with HEPES buffer, the interaction of SWCNTs with the bacterial cells and chloroplasts was probed using NIR fluorescence microscopy (**Figure 2.1a**). Chloroplasts incubated with DNA- or chitosan-wrapped SWCNTs show co-localization of the SWCNT NIR-fluorescence signal and autofluorescence of the chloroplasts' photosynthetic pigments. This observation is in agreement with previous studies that have shown rapid localization of DNA- and chitosan-wrapped SWCNTs within the organelle.[33, 25] By contrast, no NIR fluorescence signal was observed for *Synechocystis* cells (**Figure 2.1**), suggesting that the DNA- and chitosan-wrapped SWCNTs are unable to penetrate the cell wall. Furthermore, varying SWCNT concentration or incubation time did not result in detectable NIR-fluorescence from these conjugates inside or near the cells (data not shown).

Unlike the DNA and chitosan, the LSZ-wrapped SWCNTs (LSZ-SWCNTs) show NIR fluorescence that co-localizes with the autofluorescence of both the photosynthetic organelles and *Synechocystis* cells. Containing only 129 residues, LSZ serves as a small model protein whose folding kinetics and interaction with SWCNTs has been well-studied.[127, 128, 120] This enzyme is known to disrupt the PGN layer of bacteria through muramidase activity and has been shown to retain its tertiary structure when immobilized on SWCNTs.[129] The resulting nano-biohybrid complexes retain enzymatic activity both in solution and in solid assemblies. As such, LSZ-SWCNTs have been used to produce high strength, antimicrobial fibers and films.[130, 131, 132] The cellular uptake of LSZ-SWCNTs has only been investigated in eukaryotes: while LSZ-stabilized gold nanoparticles were internalized by mouse embryonic fibroblasts through receptor-mediated endocytosis,[133] internalization of LSZ-SWCNTs in the same cells was not observed.[134] This inability to internalize has been attributed to the poor stability of the LSZ-SWCNT dispersions in cell culture media. Conversely, no measurable flocculation of LSZ-SWCNTs was observed in the 1 mM HEPES buffer used in this study (**Figure A.1**).

To establish the precise distribution of LSZ-SWCNTs within cells, we used a custom-built confocal microscope for NIR detection. This unique setup, schematically represented in **Figure 2.1c**, consists of a customized spinning-disc unit with a NIR anti-reflection coating on the lenses, enabling unrivaled real-time monitoring of SWCNT NIR fluorescence.[22] In contrast to the widefield NIR measurements, the increased spatial resolution of the confocal mode clearly revealed a heterogeneous distribution of SWCNT fluorescence inside the cells (**Figure**

**2.1b and 2.1d**). The overlay of the confocal SWCNT fluorescence and bright-field images of *Synechocystis* shows enhanced SWCNT fluorescence overlapping with the peripheral regions of the cells (**Figure 2.1b** and **Figure A.2**), an observation that is consistent with previous nanoparticle uptake studies.[73] These findings suggest that the majority of the LSZ-SWCNTs lie within the periplasmic region. Significantly less SWCNT fluorescence is observed in both the cytoplasmic space and the autofluorescent thylakoid membranes that accommodate the light-harvesting complexes of the photosynthetic apparatus.

The contribution of length to the nanoparticle localization within *Synechocystis* cells was studied using length-fractionated LSZ-SWCNTs. Figure 1e presents atomic force microscopy (AFM) images of two fractions of length-separated SWCNTs, containing short ( $210 \pm 83$  nm) and long ( $836 \pm 362$  nm) SWCNTs. A fluorescence comparison of the two fractions confirm that the longer SWCNTs exhibit higher fluorescence intensity (at 780 nm excitation) than the shorter SWCNTs at the same nanotube concentration (**Figure A.3**), in agreement with previous reports.[135, 136, 137] Despite the lower quantum yield, cells incubated with the shorter LSZ-SWCNTs showed significantly higher NIR fluorescence (**Figure 2.1e**) compared to those incubated with the longer LSZ-SWCNTs. The elevated fluorescence levels suggest a preferential accumulation of short LSZ-SWCNTs inside *Synechocystis*. These observations are in agreement with Boyer et al. and Kang et al.[137, 80], who reported a length dependence of nanoparticle uptake inside mammalian cells. Becker and co-workers have similarly observed that only DNA-wrapped SWCNTs shorter than  $189 \pm 17$  nm were able to access the internal cellular compartments, whereas longer SWCNTs remained in the culture medium.[79]

### 2.4.2 Cellular Localization of SWCNTs

Although the nanobionic cells showed significant NIR fluorescence at the cell center, the enhanced fluorescence signal in the cytoplasmic space could arguably originate from out-of-focus periplasmic SWCNT fluorescence, rather than from SWCNTs that crossed the cytoplasmic membrane into the central cell volume. To explore this possibility, we monitored the LSZ-SWCNT interaction with *Synechocystis* cells in real-time during a 1 h incubation with a 2 mg/L LSZ-SWCNT suspension. We separately analyzed SWCNT fluorescence intensity change either near the cell envelope or in the inner compartments of the cell including the thylakoid membranes and cytosolic space (**Figure 2.2a**). Following the addition of the SWCNTs, we observe a rapid increase in fluorescence at 200 seconds along both the periphery and the central part of the cell (**Figure 2.2b**). At the cell periphery, the sharp initial increase is followed by a more gradual increase of fluorescence that levels off during the course of the measurement. By contrast, although SWCNT fluorescence in the cell center increases slowly following the initial jump, the rate of this enhancement accelerates over time. This spatiotemporal difference in NIR localization suggests that the fluorescence signal at the cell center originates, at least partially, from SWCNTs slowly accumulating inside the cell, and it therefore cannot entirely be attributed to contaminating fluorescence from the substantially brighter cell periphery.

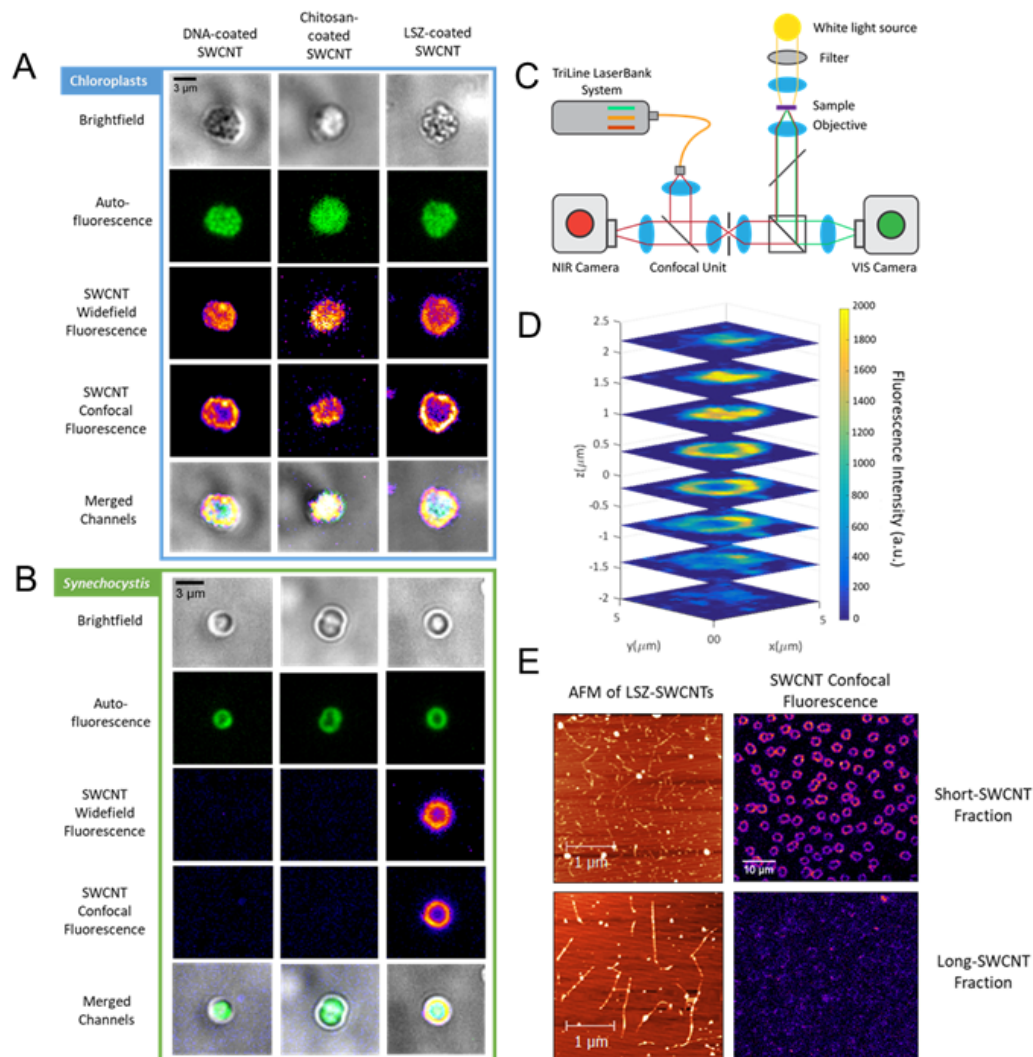


**Figure 2.1 – NIR Imaging of Internalized SWCNTs.** Representative images of (A) chloroplasts and (B) *Synechocystis* cells after incubation with DNA-, chitosan-, or LSZ-wrapped SWCNTs. Fluorescence intensity was recorded for cell autofluorescence (excitation at 640 nm, emission above 800 nm), SWCNTs in widefield mode (excitation at 780 nm, emission above 800 nm, at 1.8 mW/cm<sup>2</sup>), and SWCNTs in confocal mode (excitation at 780 nm, emission above 800 nm, at 3.7 mW/cm<sup>2</sup>). (C) The custom-built, NIR confocal setup used to image internalized SWCNTs consists of a 500 mW laser coupled to an inverted microscope body. The spinning-disc confocal head contains transmission lenses with an anti-reflective NIR coating. An indium gallium arsenide (InGaAs) camera is used for imaging. (D) Z-stacked confocal images of *Synechocystis* show the SWCNT distribution throughout the cell. (E) AFM images of short and long fractions of length-separated SWCNTs (top and bottom respectively). Confocal fluorescence images of wild-type *Synechocystis* cells incubated with 2 mg/L of short (top) and long (bottom) LSZ-SWCNT fractions.

The penetration of SWCNTs into the cytoplasm was further studied by monitoring their fluorescence response following the addition of ferricyanide. Ferricyanide is a redox active molecule capable of SWCNT fluorescence quenching.[138] Although this anionic compound

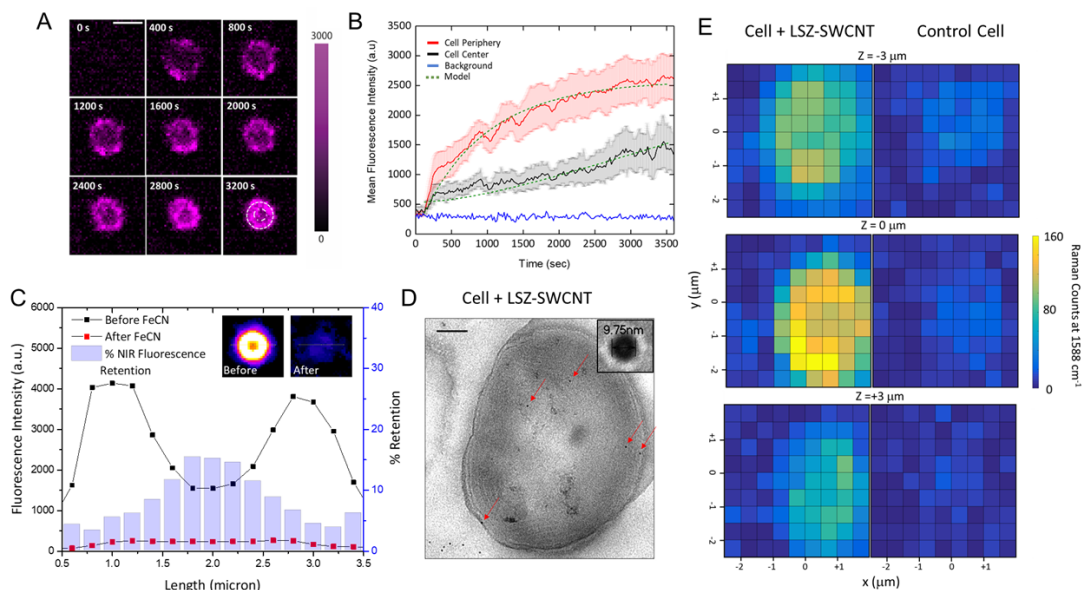


**Figure 2.2 – Localization of Internalized SWCNTs.** (A) Time-lapse NIR confocal images of SWCNT fluorescence inside the cell. The concentric dashed circles in the last frame indicate the cell periphery and center of the cell. Scale bar = 3  $\mu\text{m}$ . (B) Corresponding mean fluorescence variations over time measured along the periphery (red) and center (black) of *Synechocystis* cells compared to background (blue) during internalization. Quantitative measurements are averaged among  $n=12$  cells. The results of the fitted kinetic model at the periphery and at the center of the cell is shown in green ( $R^2 = 0.97$ ). (C) SWCNT fluorescence along the cell diameter traced from a representative *Synechocystis* cell (inset) is reported before (black line) and after (red line) addition of 120 mM ferricyanide. The ratio between the fluorescence intensities after and before the addition of ferricyanide is represented with a blue histogram, as percentage of fluorescence retention inside the cell. (D) TEM sections of *Synechocystis* cells treated with 2 mg/L LSZ-SWCNTs labeled with anti-lysozyme antibody and 10 nm gold-labeled secondary antibody. Gold nanoparticles inside *Synechocystis* cells are indicated with red arrows. Scale bar = 500 nm. (E) Representative confocal 3D Raman mapping of the characteristic SWCNT G'-band (at 1580  $\text{cm}^{-1}$ ) under 532 nm laser excitation, used to explore the spatial distribution of LSZ-SWCNTs within *Synechocystis* cells. Scans were performed at different heights Z within the cells, with Z=0  $\mu\text{m}$  corresponding to the focal plane of the cell exhibiting the highest image contrast in the bright-field imaging mode. The images show the comparison of a LSZ-SWCNT-treated cell with a non-treated cell at different heights along the z-axis. The Raman signal at 1580  $\text{cm}^{-1}$  can be attributed to SWCNTs that accumulated within the cell.

is unable to penetrate the plasma membranes of eukaryotes, studies have shown that it can access the periplasmic space of intact cyanobacterial cells without penetrating their inner membrane.[139, 140] The addition of ferricyanide (**Figure 2.2c**) resulted in significantly higher quenching of LSZ-SWCNT fluorescence at the cell periphery compared to the cell center. Calculating the ratio of NIR fluorescence pre- and post-addition (**Figure 2.2c**) showed that while only 3-5% of the initial SWCNT fluorescence at the cell periphery was preserved, a significantly higher amount of 15% was retained at the cell center. Furthermore, even the addition of excess ferricyanide did not reduce intracellular NIR fluorescence emissions to background levels (data not shown). Since *Synechocystis* cells do not exhibit significant

autofluorescence in absence of SWCNTs at the same imaging conditions (**Figure A.4b** and **Figure A.5c**), these results further suggest that the retained NIR signal at cell center originates from a fraction of SWCNTs reaching the inner compartments of the cells.

As an additional method to validate the ability of LSZ-SWCNTs to access the inner compartments of *Synechocystis*, we probed the presence of intracellular lysozyme proteins by immunogold labeling and TEM. A representative image of a section of a *Synechocystis* cell treated with 2 mg/L LSZ-SWCNTs confirmed the localization of the gold nanoparticles within the cell (**Figure 2.2d**). The majority of gold nanoparticles were observed to preferentially localize within the cell wall and over the thylakoid membranes of cells treated with LSZ-SWCNTs, whereas the cytoplasmic space contained significantly fewer particles (**Figure A.6**). In contrast to the cells incubated with the labelled LSZ-SWCNTs, cells treated with excess LSZ showed no internalized gold nanoparticles within the cells (**Figure A.6**), indicating both an absence of unspecific labeling and the inability of the protein alone to penetrate intact cells of *Synechocystis*. These findings are in agreement with previous reports that have demonstrated the inefficacy of LSZ on *Synechocystis* cells in the absence of additives such as ethylenediaminetetraacetic acid (EDTA), dithiothreitol (DTT), or spermine.[141, 142] This resistivity to lysis is attributed to the protective S-layer surrounding the outer membrane as well as to the robust PGN layers discussed above.[143] Additional control experiments, where the anti-LSZ antibody was omitted, also lacked gold nanoparticles within the cell sections (**Figure A.6**).

The intracellular distribution of LSZ-SWCNTs inside *Synechocystis* cells was further confirmed using confocal Raman spectroscopy (**Figure 2.2e**). Confocal Z-scan maps of the characteristic G-band at  $1588\text{ cm}^{-1}$  showed that the SWCNT signal was distributed throughout the volume of the cell, with elevated intensity located at the cell periphery (**Figure 2.2b** and **Figure A.7a**), supporting our observations from confocal fluorescence images. We further noted an increase in the D to G band ratio of the nano-biohybrid particles upon internalization, in agreement with other cell studies,[144] suggesting possible modification of the LSZ-SWCNTs following internalization.

### 2.4.3 Investigating the Mechanism of SWCNT Internalization

The underlying mechanism for LSZ-SWCNT internalization was studied by evaluating the influence of the enzymatic muramidase activity on SWCNT uptake. *Synechocystis* cells were incubated with SWCNTs functionalized with thermally inactivated LSZ (**Figure 2.3**), which is unable to hydrolyze the PGN network. Interestingly, as shown in the top panel of **Figure 2.3a**, the inactive LSZ-SWCNTs (LSZ\*-SWCNTs) localized within *Synechocystis* cells to a similar extent as LSZ-SWCNTs. This observation suggests that the inherent physiochemical protein characteristics, such as charge, rather than enzymatic activity, are likely responsible for nanoparticle internalization.

In agreement with this hypothesis, previous reports have shown that the hydrophobic and cationic properties of inactive LSZ as well as engineered peptides can still interact with bac-

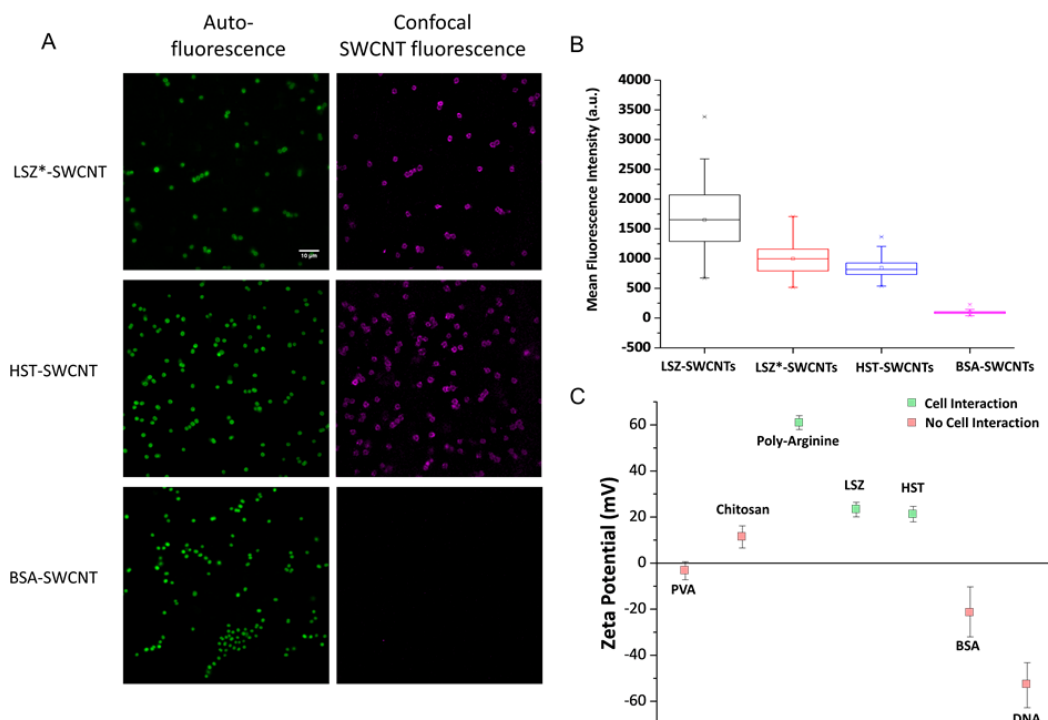


**Figure 2.3 – Effect of Surface Charge on SWCNT Uptake.** (A) Comparison of widefield autofluorescence (excitation at 640 nm, emission above 800 nm) (left) and NIR confocal images (excitation at 780 nm, emission above 800 nm) (right) of *Synechocystis* cells incubated with LSZ\*- (inactive LSZ), HST-, and BSA- SWCNTs. (B) The corresponding mean NIR fluorescence intensity determined from n=51 (LSZ), n=37 (LSZ\*), n=67 (HST), and n=121 (BSA) individual cells. (C) Zeta-potential of SWCNTs functionalized with PVA, chitosan, poly-arginine, LSZ, HST, BSA and DNA in 1 mM HEPES buffer at pH 7.4. Nanoparticles that interact with *Synechocystis* cells are shown in green whereas those that do not are shown in red. Measurements were performed in triplicates.

terial membranes.[145, 146] This hypothesis was tested by comparing the localization of SWCNTs functionalized with bovine serum albumin (BSA) and histone H1 from *bos taurus* (HST), which demonstrate distinct physiochemical characteristics. BSA is a medium-sized protein ( $MW_{BSA} = 66.5$  kDa) present in blood serum. This protein has been previously conjugated to SWCNTs for intracellular nanoparticle delivery in eukaryotic cells.[115] On the other hand, HST is a small protein ( $MW_{HST} = 21.5$  kDa) that is structurally similar to LSZ. It contains a high content of basic residues, which assist in cation-interactions on the nanotube surface, and it possesses an overall positive charge at physiological pH.[59] NIR confocal images (**Figure 2.3a**) showed uptake of HST-SWCNTs that was comparable to both LSZ-SWCNTs and LSZ\*-SWCNTs. In contrast to HST-SWCNTs, no NIR fluorescence was detected within cells incubated with BSA-SWCNTs. A quantitative comparison of the mean NIR fluorescence intensities of LSZ-, LSZ\*-, HST-, and BSA-SWCNTs in individual cells confirmed minimal uptake for BSA-SWCNTs (**Figure 2.3b**). Zeta-potential measurements of the functionalized SWCNTs (**Figure 2.3c**) revealed that wrappings that facilitate cellular uptake possess positive surface potentials above 20 mV at pH 7.4. Additional experiments with functionalized-SWCNTs possessing even



higher zeta-potentials, such as poly-arginine SWCNTs (61 mV), confirmed this observation (Figure A.8). These measurements suggest that the considerable positive surface charge of the protein corona drives the electrostatic interaction between the SWCNT conjugates and the negatively charged cell envelope, which, in turn, facilitates the penetration of the nanoparticles inside the cell. This mechanism is consistent with the results of Pedersen et al., who have shown that positively charged nanoparticles are prone to interact with negatively-charged lipopolysaccharide-containing leaflets of Gram-negative bacterial cell walls.[147]

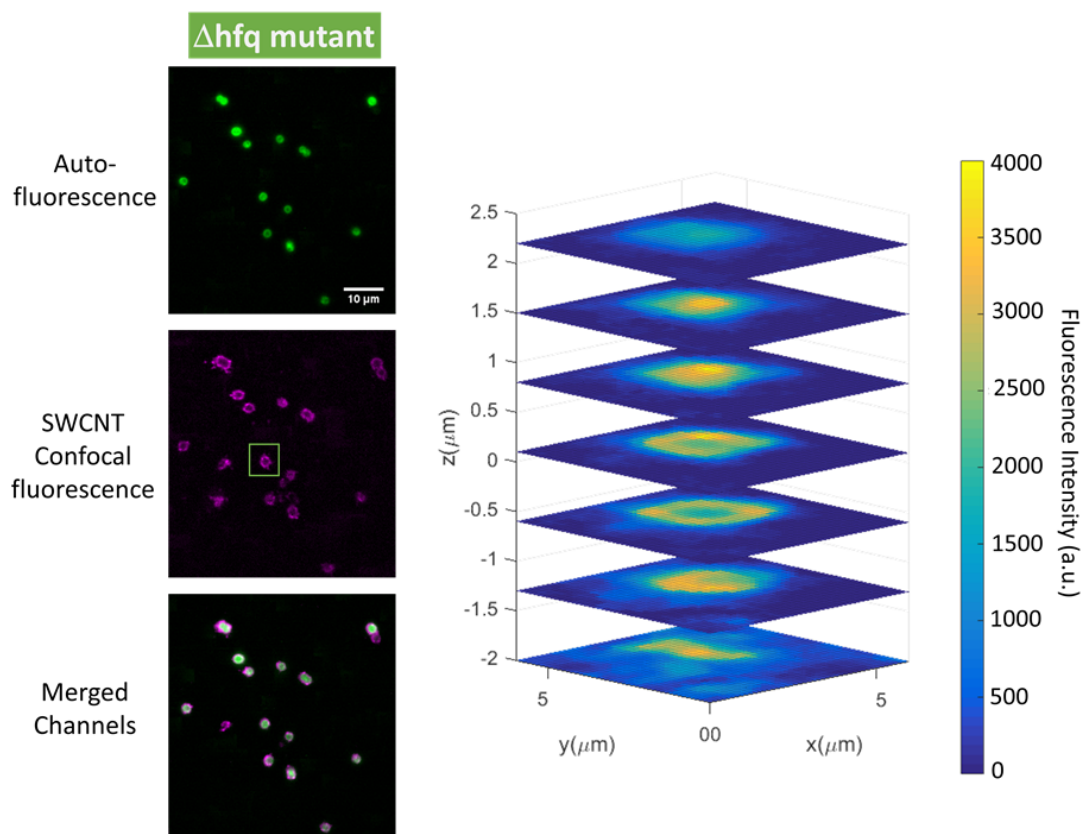


**Figure 2.4 – SWCNT Internalization by Strains Lacking Pili for DNA Uptake.** Representative images of cyanobacteria lacking natural competence, namely *Synechocystis*  $\Delta$ hfq. Cells incubated with LSZ-SWCNT show cell autofluorescence (excitation at 640 nm, emission above 800 nm) (top), and confocal SWCNT fluorescence (excitation at 780 nm, emission above 800 nm) obtained after complete photobleaching of the cell (middle). An overlay of the fluorescence emissions is shown on the bottom, alongside stacked confocal images of the boxed cell in the axial direction.

Nanoparticle accumulation within the plasma membrane before internalization has been previously observed in eukaryotic cells.[148] Shang et al. suggest that a strong localized interaction between the nanoparticles and cell envelope is required to trigger subsequent permeation into the cytosol via energy-dependent endocytosis. Although bacterial cells are generally capable of both active and passive membrane transport, no known active mechanisms exist for the uptake of supramolecular complexes, such as conjugated SWCNTs, in cyanobacteria. One means of uptake could occur via type IV pili (T4P), retractable appendages that are not

only involved in cell motility, but are also crucial for the uptake of exogenous DNA in some bacteria, including *Synechocystis*. [149]

To evaluate if T4P facilitate SWCNT uptake, a mutant strain of *Synechocystis*, lacking T4P ( $\Delta hfq$ ) [150] was incubated with LSZ-SWCNTs. Fluorescence images (**Figure 2.4a**) show that uptake by  $\Delta hfq$  cells was comparable to wild type *Synechocystis* cells, demonstrating that T4P are not required for internalization. The uniform uptake of SWCNTs by non-piliated cells suggests that uptake likely proceeds through a passive membrane penetration mechanism based on charge-dependent binding of SWCNTs to the negatively-charged cell wall prior to internalization. Based on this proposed mechanism, SWCNT uptake in cyanobacterial cells can be modeled as a two-step internalization mechanism:



where  $SWCNT_{buffer}$  represents free SWCNTs in solution,  $SWCNT_{bound}$  represents SWCNTs that have adsorbed to the cell wall, and  $SWCNT_{in}$  represents SWCNTs that have been internalized by the cell. The adsorption and internalization rate constants are  $k_{ads}$  and  $k_{in}$ , respectively. In this model, detachment of the nanoparticles from the cell wall is neglected, as it was not observed under the tested conditions. The corresponding variation in SWCNT concentration,  $[SWCNT]$ , can be modeled with the following system of equations:

$$\frac{\partial [SWCNT]_{buffer}}{\partial t} = -k_{ads}[SWCNT]_{buffer}([SWCNT]_{max} - [SWCNT]_{bound}) \quad (2.2)$$

$$\begin{aligned} \frac{\partial [SWCNT]_{bound}}{\partial t} = & k_{ads}[SWCNT]_{buffer}([SWCNT]_{max} - [SWCNT]_{bound}) \\ & - k_{in}[SWCNT]_{bound} \end{aligned} \quad (2.3)$$

$$\frac{\partial [SWCNT]_{in}}{\partial t} = k_{in}[SWCNT]_{bound} \quad (2.4)$$

where  $[SWCNT]_{max}$  is the maximum concentration of SWCNTs that can be accommodated by the surface of the cells. The kinetic parameters in Equations 2-4 were determined by fitting the model to the time-traces of SWCNT NIR-fluorescence shown in **Figure 2.2b** (see “Computational modeling” section in Appendix A for model details). The calculated best-fit rate constants for SWCNT adsorption and internalization in cyanobacteria were compared to the values obtained by Au et al., who applied an analogous two-step model to describe



nanoparticle transport in tumor cells.[151] The resulting best-fit internalization rate constant,  $k_{in} = (1.466 \pm 0.011) \times 10^{-4} \text{ s}^{-1}$  was in close agreement to what had previously reported for nanoparticle internalization,  $(1.7 \pm 0.1) \times 10^{-4} \text{ s}^{-1}$ . The best-fit rate constant for SWCNT-adsorption is  $k_{ads} = (9.08 \pm 0.16) \times 10^{-8} \text{ s}^{-1} [\text{fluorescence counts}]^{-1}$ . Considering that the LSZ-SWCNT concentration used ranges between 2-30 nM (which corresponds to  $10^5$  fluorescence counts), the resulting  $k_{ads}$  ranges in the order of  $10^6 \text{ s}^{-1} [\text{M}]^{-1}$ , that is higher than what previously reported for nanoparticle adsorption on tumor cells,  $(1.1 \pm 0.3) \times 10^4 \text{ s}^{-1} [\text{M}]^{-1}$ .

#### 2.4.4 Impact of SWCNTs on Cell Viability

Following internalization, we examined the effects of the SWCNTs on cell viability by comparing the oxygen evolution of cells in the presence and absence of LSZ-SWCNTs (**Figure 2.5**). Photosynthesis and respiration, which are, respectively, oxygen-evolving and -consuming processes, occur simultaneously when photosynthetic cells are illuminated.

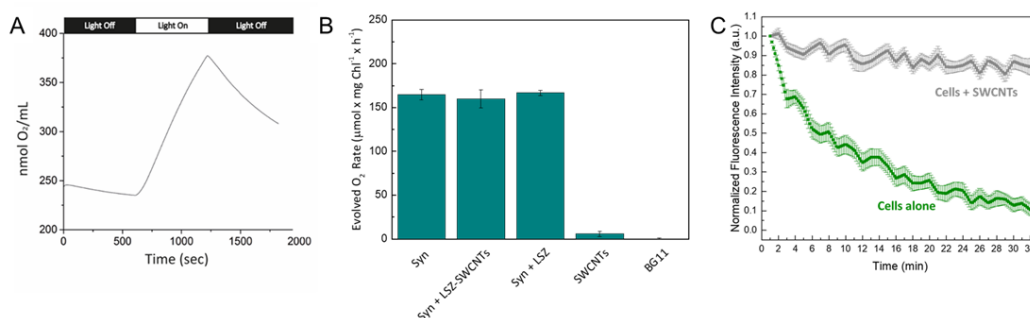


**Figure 2.5 – Effect of SWCNT Internalization on Photosynthesis and Cell Viability.** (A) A representative plot of dissolved oxygen concentration in a *Synechocystis* culture in the presence of 10 mg/L LSZ-SWCNTs. Samples were illuminated with white light at  $200 \mu\text{mol photons m}^{-2} \text{ s}^{-1}$ . (B) Net oxygen production rate of illuminated *Synechocystis* cells in the absence and presence of LSZ-SWCNTs. Control measurements were taken for LSZ-SWCNTs in BG11 medium and medium only. Measurements were normalized by chlorophyll content and are based on three independent experiments. (C) Average NIR fluorescence emission of cells with (grey line, 980 nm long-pass emission filter) and without LSZ-SWCNTs (green line, 800 nm long-pass emission filter) over time upon continuous illumination at 780 nm with  $31 \text{ mW/cm}^2$  power.

Photosynthetic activity of *Synechocystis* cells incubated with LSZ-SWCNTs was confirmed by continuous, light-dependent oxygen evolution over a 10-minute interval (**Figure 2.5a**). Cells incubated in the presence of LSZ-SWCNTs showed no significant difference in the oxygen evolution rate compared to control cells (in the absence of LSZ-SWCNTs) under the conditions tested (**Figure 2.5b** and **Table 2.1**).

Cell viability over ten days was further verified by growth experiments, where the majority of cells treated with LSZ-SWCNTs (ca 75%) were shown to retain normal growth characteristics (**Figure A.9-10**). We further examined the effects of SWCNT properties across the accelerated lifespan of cells undergoing photobleaching. Compared to autofluorescent cell pigments,

Oxygen evolution rates ( $\mu\text{mol O}_2/(\text{mgChl} \times \text{h})$ )				
BG11	Syn	Syn + LSZ-SWCNTs	LSZ-SWCNTs	Syn + LSZ
$0 \pm 1$	$165 \pm 6$	$160 \pm 10$	$6 \pm 3$	$167 \pm 3$

**Table 2.1** – Rates of oxygen evolution under illumination for treated and untreated cells as well as for LSZ-SWCNTs in media and BG11 media only. Values are based on independent measurements obtained from three replicates and normalized by chlorophyll pigment content. The oxygen evolution rate of illuminated *Synechocystis* cells incubated with 2 mg/L LSZ-SWCNTs was not significantly different from non-treated cells ( $F < F$  crit. in Table A.2).

which undergo rapid photobleaching upon continuous exposure to high-power 780 nm excitation (**Figure 2.5c**), the nanobionic cells incubated with LSZ-SWCNTs show enhanced NIR photostability under continuous illumination, sustaining over 95% of the initial NIR fluorescence intensity over 30 minutes.

## 2.5 Conclusions

Nanobionic SWCNT applications thus far have largely focused on augmenting light-harvesting or biochemical detection capabilities of extracted organelles or leaf lamina from plants. The study presented herein offers an uncharted exploration of nanobionic applications based on living prokaryotic cells. These nanobionic cells show a persisting, augmented fluorescence that extends beyond the visible fluorescence limits of the cell, enabling long-term, optical imaging in autofluorescent living systems. In contrast to previously studied systems, where internalization was observed in the presence of functionalized SWCNTs with both positive or negative zeta potentials, cyanobacterial cells demand more stringent engineering design rules, requiring SWCNTs to possess strongly positive zeta potentials in order to traverse the surrounding wall of the cell. Though the successful conjugative methods demonstrated herein are restricted to protein-functionalized SWCNTs, the internalization of both active and inactive protein conjugates suggests that synthetic functionalization with suitable charge distributions may also be used for nanoparticle uptake.

The NIR setup used in this analysis, which benefits from a combination of enhanced NIR resolution and real-time confocal tracking, provides a previously inaccessible tool for exploring phenomena otherwise intractable with existing NIR imaging platforms. The enhanced resolution allows us to monitor living cells in real-time for the length-dependent, heterogeneous accumulation of SWCNTs that is unobservable with conventional widefield NIR microscopy. Furthermore, real-time tracking capabilities of the spinning-disc setup unveils a two-step microbial uptake mechanism consisting of adsorption and internalization steps. A comparison of the corresponding rate constants,  $k_{\text{ads}}$  and  $k_{\text{in}}$ , suggests an adsorption step that is distinct from that previously reported for mammalian cells.

Beyond the fundamental insight into the mechanisms of prokaryotic nanoparticle uptake, SWCNT-based nanobionics provides an advantageous basis for imaging, sensing, and light-

harvesting applications in photosynthetic systems.[33] Furthermore, SWCNTs, which have previously shown uptake by plant tissue and isolated chloroplasts,[33, 25] have recently demonstrated use as gene delivery vehicles in living plants.[32] The localization of SWCNTs within the internal cell compartments shown in this study, where chromosomal and plasmid DNA are accessible, combined with the sustained viability of the cells, now discloses the opportunity to deliver genes into prokaryotic cells. This demonstration is advantageous for cyanobacteria cells in particular, for which the majority strains are not readily capable of active DNA uptake and require complex, specialized procedures for DNA transformation.



## 3 Interaction of SWCNTs with Filamentous Cyanobacteria

### 3.1 Abstract

The internalization of fluorescent SWCNTs in cells of photosynthetic microbes can be exploited for applications ranging from energy conversion to biomolecule delivery. However, the intrinsic, species-dependent properties of microbial cell walls, including their surface charge density, composition, thickness, and elasticity, can severely impact nanoparticle uptake and affect the cellular response following SWCNT exposure. Therefore, a careful examination of the interaction of SWCNTs in various species, and the impact of this on cell viability, is imperative for the future development of SWCNT-based microbial applications. In this chapter, we extend the technology we developed for internalizing SWCNTs in unicellular cells to filamentous cells. We specifically investigate the interaction of SWCNTs with cells of a filamentous cyanobacterial strain, *Nostoc* sp. and compare our findings to the previous observations for unicellular *Synechocystis*. This filamentous strain poses additional, and previously unmet challenges for nanoparticle internalization, as it can differentiate in response to nitrogen starvation to form heterocysts, specialized compartments within the filament that are capable of nitrogen fixation. Heterocysts possess distinct cell wall components, compared to vegetative cells, which confer reduced permeability and increased resistance to mechanical and osmotic stress. In this work, using a combination of NIR fluorescence, scanning electron microscopy, and Raman spectroscopy, we investigate the contribution of the different cell-wall components on SWCNT-cell interaction. We demonstrate that the careful selection of appropriate SWCNT functionalizations preserves long-term cell integrity, activity, and viability. We further show that local variations in membrane structure within the filament can dictate the extent of SWCNT association and uptake in *Nostoc* cells. In particular, SWCNTs functionalized with positively charged wrappings are found to preferentially localize within the heterocyst compartments. The cell-type dependency of nanoparticle internalization mechanism can be exploited for the development of alternative cell-specific staining and imaging technologies.

### 3.2 Introduction

Semiconducting single-walled carbon nanotubes (SWCNTs) have enabled the development of several whole-cell technologies, including intracellular imaging and sensing[109, 23], gene-delivery[152], and cancer treatment[108]. In particular, the fluorescence properties of SWCNTs provide a practical basis for not only studying cellular dynamics, but also investigating nanoparticle transport in such technologies. SWCNT fluorescence emissions have been used for spatiotemporal mapping of intra- and extra-cellular fluxes.[67, 44] In addition, techniques such as real-time fluorescence tracking, allow monitoring of SWCNT translocation across cellular membranes both *in vitro* and *in vivo*. [33, 124, 153]

The success of these applications is contingent on a clear understanding of the underlying nanoparticle interaction with living cells, and this is critical for the design of novel nanoprobes with improved biocompatibility and specificity. Studies thus far have largely focused on SWCNT translocation across the cell membranes of various eukaryotic cells.[25] They have shown that SWCNT translocation depends on a range of factors, including diverse physical and chemical properties of SWCNTs such as length, diameter, surface functionalization, and charge density, along with dispersion quality. Although early studies have shown SWCNT uptake to be independent of cell type [73], more recent studies that have focused on a wider range of incubation and functionalization conditions have reported cell-specific interaction and uptake mechanisms.[154, 78] Moreover, intrinsic cell membrane properties, including surface charge, composition, thickness and elasticity, are known to affect the extent by which nanoparticles are ultimately able to penetrate cell compartments and tissues.[155] For example, SWCNT binding to ligands, or other receptor molecules located on the outer surface of eukaryotic cells, can trigger nanoparticle internalization via receptor-mediated interactions.[94] Beyond regulating nanoparticle transport, Roxbury *et al.* have reported that cell surface electrostatic potentials (mediated by cell-specific membrane proteins) can also modulate the optical response of fluorescent SWCNTs.[156]

Like eukaryotic cells, prokaryotic cells are surrounded by outer membranes that play a central role in mediating the cell-nanoparticle interaction. Notably, the surface charge of bacterial cell walls, which govern important phenomena such as cell aggregation or biofilm formation, can dictate the efficiency of nanoparticle-cell association and subsequent internalization.[157] Most bacterial walls exhibit a net negative charge, due to the presence of specific anionic components such as lipopolysaccharides. Jacobson *et al.* have shown that the structure and density of the lipopolysaccharides can govern the extent and the distance of nanoparticle interaction with the outer membranes of Gram-negative bacteria.[147] This interaction is largely dominated by electrostatic forces, with cationic nanoparticles prevailing over anionic materials with respect to binding to the negatively-charged cell leaflets. In agreement with these observations, our previous study on SWCNT interaction with cells of unicellular, Gram negative cyanobacteria, namely *Synechocystis* sp. PCC 6803, has shown that the zeta-potential of functionalized SWCNTs is a critical factor for facilitating nanoparticle uptake. In contrast to SWCNTs modified with negatively charged or neutral wrappings, SWCNTs wrapped with

small, positively charged proteins, such as lysozyme, could penetrate the negative cell wall of *Synechocystis* without toxic effects.

Similar to *Synechocystis*, *Nostoc* sp. cells are photosynthetic cells that are surrounded by a negatively charged cell wall. This is composed of inner and outer membranes separated by a large periplasmic space and a thick peptidoglycan layer.[158] Despite common features, *Nostoc* cells lack DNA competence and external surface layers, such as S-layers, which provide *Synechocystis* cells with increased resistance against mechanical and osmotic stress.[102] The *Nostoc* furthermore assemble into multicellular filaments that are distinct from the unicellular *Synechocystis* cultures. Under nitrogen deprivation conditions, 5-10% of the vegetative cells that comprise these filaments differentiate to heterocysts, which are specialized compartments for N<sub>2</sub> fixation.[159] Compared to vegetative cells, heterocysts are characterized by a distinct pigmentation and are enclosed by an additional cell envelope composed of two chemically different layers deposited on top of the outer membrane. [160] This bilayered structure limits the permeation of gas and the transport of ions or other hydrophylic solutes inside the heterocyst, establishing a microoxic environment that is needed for the expression and function of enzymes devoted to nitrogen fixation.[159]

In this study, we explore the interaction of SWCNTs with the filamentous *Nostoc* sp. strain. The distinct cell wall architecture, along with the lack of DNA uptake mechanism and heterogeneity of its cell types, motivates the need to explore nanoparticle delivery for filamentous strains, which have yet to be studied. The successful characterization of SWCNT translocation across a variety of cell architectures allows a more complete understanding of nanoparticle delivery that is needed for unlocking the variety of SWCNT applications for an even broader range of cells.

### 3.3 Materials and Methods

**Functionalization of SWCNTs.** The SWCNTs used in this study were purified HiPco nanotubes (NanoIntegris, Lot. No. HP26-019) with a diameter of 0.8–1.2 nm and a length of 100-1000 nm. LSZ-SWCNTs were prepared by suspending 1 mg of HiPco nanotubes and 5 mg of lysozyme from chicken egg white (Sigma Aldrich) in 1 mL of 1 mM HEPES buffer (pH 7.4) and sonicating using a cup-horn sonicator (140 mm, Qsonica, LLC) for 90 minutes at 1% amplitude on ice. Chitosan-SWCNTs were prepared as described in Reuel et al.[119]. Briefly, 1 mg of HiPco nanotubes were suspended in 1 mL of 2.5 mg/mL chitosan (Carl Roth) solution in 1 mM HEPES buffer with 1% acetic acid. The sample was sonicated for 90 minutes at 1% amplitude on ice using cup-horn sonication. The sonicated SWCNT suspensions were centrifuged (Eppendorf Centrifuge 5424 R) for 180 minutes at 16500 x g to pellet SWCNT aggregates. Unbound proteins and polymers were removed through dialysis against 2 L of 1 mM HEPES buffer using a 300 kDa MWCO cellulose membrane. SWCNT concentrations were calculated from absorbance measurements at 632 nm in a UV-Vis-NIR scanning spectrometer (Shimadzu 3600 Plus) using an extinction coefficient of 0.036 L/(mg cm).

**Bacterial strains and growth conditions.** Liquid cultures of wild-type *Synechocystis* strain PCC 6803 and *Nostoc* sp. were grown in BG11 medium (containing  $\text{NaNO}_3$  as the nitrogen source according to Rippka et al.) or BG11<sub>0</sub> (without addition of combined nitrogen) supplemented with 10 mM TES buffer (pH 8.0) at 30°C under 50  $\mu\text{mol photons m}^{-2} \text{ s}^{-1}$  of white light with constant shaking.

**NIR fluorescence imaging.** Cells were harvested during the late exponential growth phase ( $\text{OD}_{750\text{nm}}$  between 1-1.5) by centrifugation, washed twice with 1 mM HEPES buffer (pH 7.4), and re-suspended in the same buffer to an  $\text{OD}_{750\text{nm}} = 0.9$ . Cells were fixed onto poly-lysine coated glass-bottom petri dishes by spotting 30  $\mu\text{L}$  of the cell-SWCNT suspensions for 10 minutes followed by washing with HEPES. The cells were treated with 50  $\mu\text{L}$  LSZ-SWCNTs at final concentration of 2 mg/L. The cells and SWCNTs were incubated at room temperature for 10 minutes in the dark, followed by washing with HEPES. They were imaged using a custom-built optical setup consisting of an inverted microscope (Eclipse Ti-U, Nikon AG Instruments) with an oil-immersion TIRF 100 x objective (N.A. 1.49, Nikon) coupled to a CREST X-Light spinning-disk confocal imaging system (CREST Optics) (60  $\mu\text{m}$  pinholes) and an InGaAs camera (NIRvana 640 ST, Princeton Instruments). Samples were illuminated using a TriLine LaserBank system (Cairn Research) at 640 nm and 780 nm, and fluorescence was collected using either an 800 nm (Chroma) or a 980 nm long-pass filters (Semrock). Images were acquired using the Nikon NIS-Elements software (Nikon Instruments).

**Zeta-potential measurements.** All stock solutions of SWCNTs were diluted in 1 mM HEPES buffer (pH 7.4) to yield a final concentration of 10 mg/L. Cell suspensions were diluted to an  $\text{OD}_{750\text{nm}} = 0.9$ . Zeta potential measurements were carried out with a Zetasizer Nano ZS analyzer from Malvern, using folded capillary cells.

**Raman characterization.** Raman spectra were recorded at an excitation wavelength of 532 nm from 200 to 1800  $\text{cm}^{-1}$  using a water-immersion 63x objective (0.90 N.A) on a confocal spectroscope (inVia Raman Microscope, Renishaw). For automatic confocal Raman mapping, confocal Raman spectra were recorded with a step size < 1  $\mu\text{m}$  in X-Y, for a total number of 9x9 spectra. Spectra were automatically acquired along the Z direction, where Z= 0 corresponds to the higher contrast of the cell on a bright-field image. The spectrometer was calibrated before measurements using an internal standard. 3D maps were generated using a Matlab script (Matlab R2015, Mathworks).

**Scanning electron microscopy (SEM) experiments.** Cells were harvested during late exponential growth phase by centrifugation, washed twice with 1 mM HEPES buffer (pH 7.4), and re-suspended in the same buffer to an  $\text{OD}_{750\text{nm}} = 0.9$ . The cells were fixed onto poly-lysine coated glass slides (#1, 15 x 15 mm) by spotting 30  $\mu\text{L}$  of the cell-SWCNT suspension for 10 minutes followed by washing with HEPES. The cells were then incubated with LSZ-SWCNTs at a concentration of 2 mg/L for 1 hour, followed by washing with HEPES. Control samples were also prepared in the absence of LSZ-SWCNTs. All samples were immersed in a 1.25% glutaraldehyde solution made in 0.1 M phosphate buffer (pH 7.4), and incubated for 2 hours.



Following incubation, the samples were washed three times in 0.1 M cacodylate buffer (pH 7.4). Post-fixation was performed by immersing the samples into 0.2% osmium tetroxide in 0.1 M cacodylate buffer, followed by two washing steps with deionized water. Samples were immersed in 30%, 50%, 70%, 90%, 96% and 100% alcohol-water gradients for three minutes each for dehydration. The samples were critical-point dried and covered with a 4 nm osmium coating. The samples were subsequently analysed with a ultra-high resolution microscope (Field Emission SEM, Zeiss Merlin), using an extra-high tension (EHT) voltage of 1.5 kV.

**Measuring net oxygen evolution.** Cells were harvested during the late exponential growth phase ( $OD_{750nm}$  between 1-1.5) by centrifugation, washed with 1 mM HEPES buffer, and re-suspended in the same buffer to an  $OD_{750nm} = 0.9$ . Cell suspensions were mixed with SWCNT suspension at final concentration of 2 mg/L for 1 hour in the dark. The oxygen concentration under light and dark conditions for whole cells was monitored at room temperature using a Clark-type electrode (Hansatech, OxyLab+, Norfolk). Samples were illuminated at an intensity of  $100 \mu\text{mol photons m}^{-2} \text{s}^{-1}$  under white light. 10 mM sodium bicarbonate ( $\text{NaHCO}_3$ ) was added to the cell suspensions prior to oxygen measurement to provide the cells with an excess carbon source.

## 3.4 Results and discussion

### 3.4.1 Cell-type dependency of SWCNT-cyanobacteria interaction

**Figure 3.1** shows representative near-infrared confocal images of unicellular *Synechocystis* cells, filamentous *Nostoc* cells grown in standard BG11, and *Nostoc* cells grown in nitrogen-free medium (hereafter *Nostoc*-Het) following incubation with LSZ-SWCNTs. The overlay of the confocal SWCNT fluorescence and bright-field images of *Synechocystis* cells shows preferential SWCNT localization along the peripheral regions of the cells, suggesting heterogeneous nanoparticle accumulation within the peripheral region of the cells, in agreement with previous results (**Chapter 2**). On the other hand, *Nostoc* cells showed an overall diminished SWCNT uptake, with preferential localization within the septal regions between adjacent vegetative cells in the filament (red arrow, **Figure 3.1b** and **Figure B.1 and B.3**).

In contrast to both *Synechocystis* and *Nostoc* cells, the *Nostoc*-Het cells showed significant SWCNT fluorescence within the peripheral regions of only select cells interspersed within the filament (**Figure 3.1b**). These cells, which showed diminished autofluorescence compared to their neighboring cells, were identified as nitrogen-fixing heterocysts, which lack the autofluorescent photosynthetic pigments found in their neighboring vegetative cells. Interestingly, the SWCNT fluorescence also appeared to localize at the neck-shaped ends of some heterocysts, within the septal regions connecting the nitrogen-fixing compartments with adjacent vegetative cells (red arrows, **Figure 3.1c**). This observation further suggested possible nanoparticle accumulation inside the contiguous periplasmic regions of the filament. A comparison of the near-infrared fluorescence of isolated heterocysts and of spheroplasts

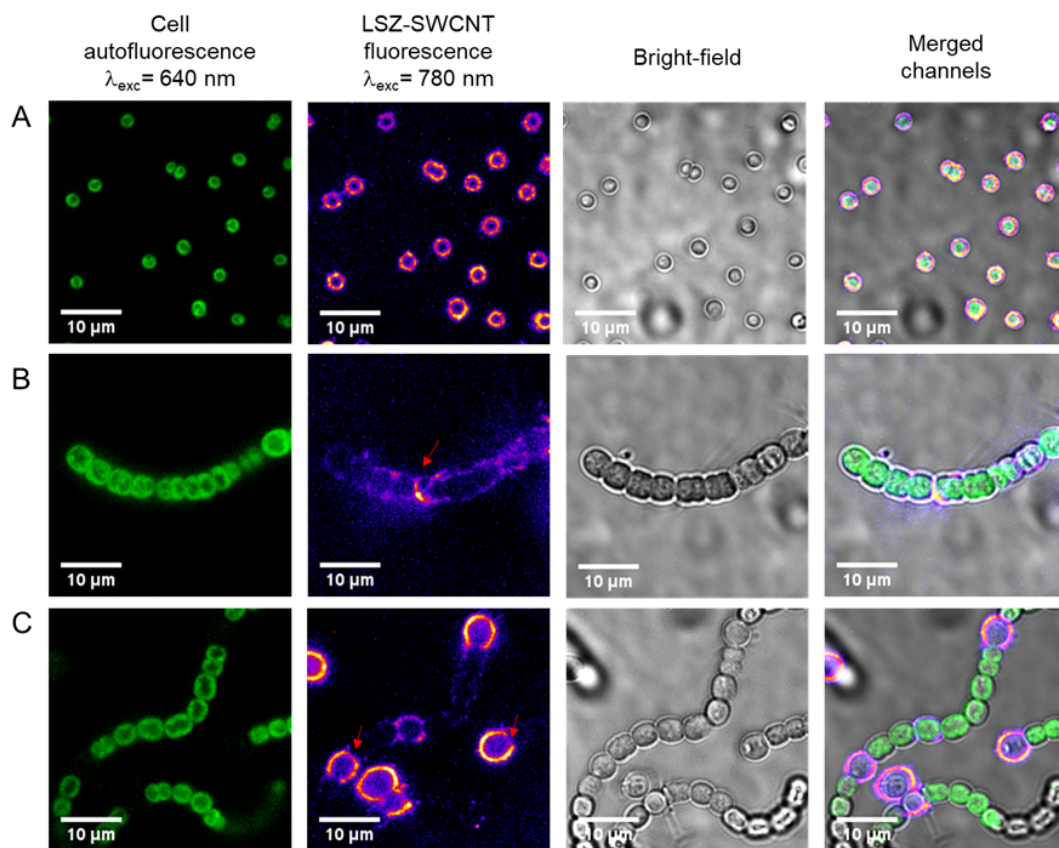


**Figure 3.1 – NIR Imaging Unicellular and Filamentous Cyanobacteria with LSZ-SWCNTs.** Representative images of (A) *Synechocystis* cells, (B) *Nostoc* cells, and (C) *Nostoc*-Het cells after incubation with LSZ-SWCNTs. Fluorescence emissions were used to image cell autofluorescence (excitation at 640 nm, emission above 800 nm) and SWCNT fluorescence in confocal mode (excitation at 780 nm, emission above 980 nm, at 3.7 mW/cm<sup>2</sup>). Red arrows indicate significant SWCNT fluorescence signals localizing at septal regions between adjacent cells.

from vegetative cells further confirmed preferential SWCNT accumulation within the nitrogen-fixing heterocysts (**Figure B.2**). The cell-specific localization of the SWCNTs is attributed to different cell wall architectures found in *Synechocystis*, vegetative *Nostoc* cells, and heterocysts (**Figure 3.2**).

Unlike vegetative *Nostoc* cells and heterocysts, the *Synechocystis* cells are surrounded by external surface layers, called S-layers, which are two-dimensional crystalline arrays of proteinaceous subunits that cover the entire surface of the cells (**Figure 3.2a**). These units are composed of weekly acidic glyco-proteins that contain 40-60% hydrophobic amino acids and possess an average isoelectric point of 4-6 that contributes to the overall negative charge of the cells.[116] The cell wall of the nitrogen-fixing heterocysts, on the other hand, contains an additional bi-layered structure on top of the outer membrane. This bilayer consists of an inner layer of hydroxylated glycolipids and an outer layer of polysaccharides (**Figure 3.2a**). In contrast to *Synechocystis* cells and hetetocysts, current studies suggest that vegetative *Nostoc*

cells lack either an additional S-layer or an additional bilayer.[158, 161]

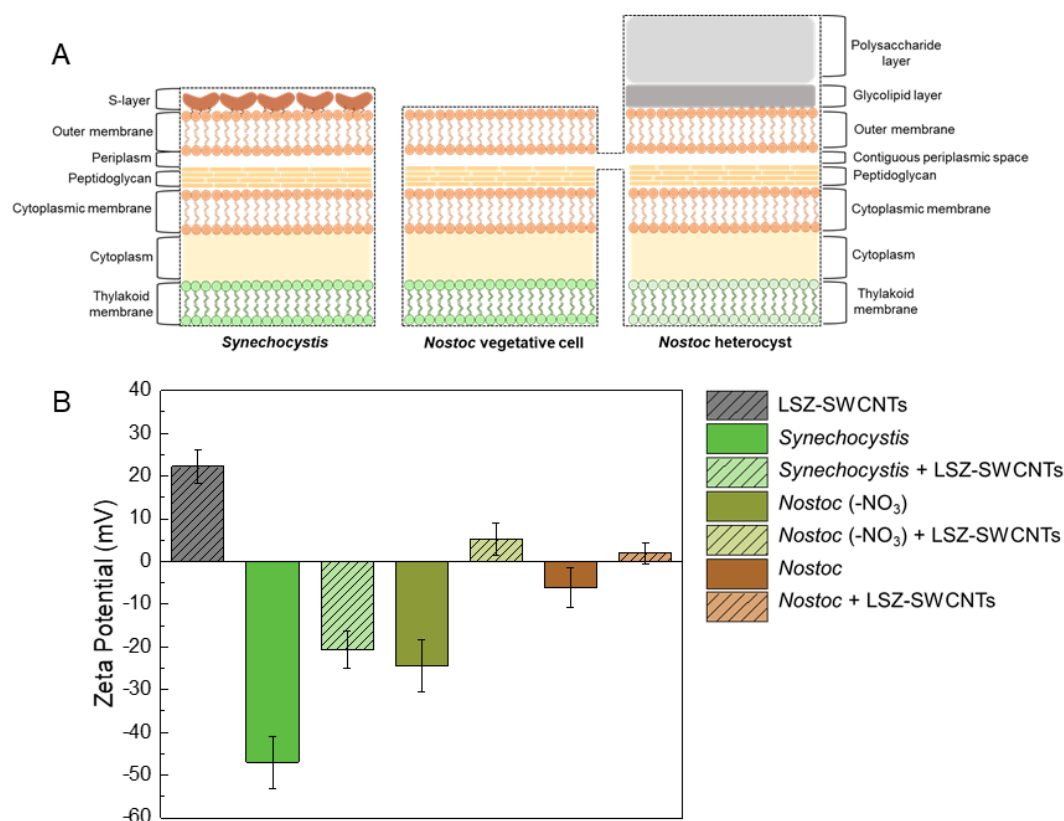


**Figure 3.2 – Impact of Whole Cell Zeta-Potential on SWCNT Interaction.** (A) Schematic illustration of the cell wall architecture of *Synechocystis*, vegetative *Nostoc* and *Nostoc* heterocysts, respectively. (B) Zeta-potentials of LSZ-SWCNTs, *Synechocystis* cells, *Nostoc* cells grown in nitrogen-free medium (*Nostoc* -NO<sub>3</sub>), and *Nostoc* cells grown in normal medium, before and after the addition of 2 mg/L of LSZ-SWCNTs. All samples are suspended into 1 mM HEPES buffer at pH 7.4. Error bars represent the standard deviation of three replicates.

Such variations in the cell wall composition and density of negatively charged macromolecules, have been shown to strongly impact cell-nanoparticle interactions. For example, Jacobson et al. demonstrated a 70% decrease in the number of Gram-negative bacterial cells with associated positively-charged gold nanoparticles following the removal of 50% of the cell lipopolysaccharide content.[147] Nanoparticle interactions also strongly depend on the whole-cell zeta-potential.[162, 163] These potentials correlate with the total amount of polysaccharide on the surface of the cell and the associated density of ionic surface charges produced by cyanobacteria.[164]

In agreement with these previous reports, the zeta potentials of the *Synechocystis*, *Nostoc* and *Nostoc*-Het cells also appear to be correlated with LSZ-SWCNT association. As shown in **Figure 3.2d**, all three cells show an overall negative charge at pH 7.4, with magnitudes of  $-47.0 \pm 6.2$  mV,  $-24.4 \pm 6.1$  mV, and  $-6.1 \pm 4.7$  mV for *Synechocystis*, *Nostoc*-Het and *Nostoc*,

respectively. The more strongly negative zeta-potentials of *Synechocystis* and *Nostoc*-Het cells may be attributed to the higher density of negatively charged glycoproteins or polysaccharides, respectively, on the outer cell surface. The magnitudes of these negative charges all decrease following incubation with LSZ-SWCNTs. Indeed, the LSZ-SWCNTs show an overall positive zeta-potential (**Figure 3.2d**), which may favor charge-charge interactions with a negatively charged cell surface.

Consequently, we observed an overall decrease in the magnitudes of the negatively charged cells upon incubation with LSZ-SWCNTs. In particular, cells with the more negative zeta potentials showed the largest change in their zeta-potentials upon incubation with the LSZ-SWCNTs. These trends are in agreement with fluorescence images shown in Figure 3.1, which suggest increased nanoparticle localization, and therefore a larger change in surface charge, for the more negatively charged cells. These observations thus confirm our hypothesis that the targeted accumulation of LSZ-SWCNTs within the *Nostoc* heterocysts, could be at least partially attributed to higher surface charge density in the cell wall.

#### 3.4.2 Impact on cell morphology and localization of SWCNTs

The intracellular distribution of LSZ-SWCNTs inside *Nostoc* heterocysts was further studied using confocal Raman spectroscopy. Confocal Z-scan maps of the characteristic G-band at  $1588\text{ cm}^{-1}$  showed that the SWCNT signal was heterogeneously distributed throughout the volume of the nitrogen-fixing cell, with higher intensities found at the cell periphery, supporting previous observations using confocal fluorescence (**Figure 3.3a** and **Figures B.4-5**). Conversely, a weak SWCNT Raman signal was detected within the vegetative cells along the same filament, further indicating preferential accumulation of the nanoparticle within the nitrogen-fixing compartment (Figures B.4-5).

In addition to the inner cellular distribution, we also studied the extracellular distribution of the LSZ-SWCNTs using scanning electron microscopy (SEM). Representative SEM images (**Figure 3.3a-b**) showed that untreated vegetative and heterocyst cells of *Nostoc* possessed undisrupted, smooth outer membrane surfaces in the absence of nanotubes. Following nanoparticle exposure, the heterocyst cell wall appeared to become covered by an extracellular, nano-filamentous network (**Figure 3.3e-g** and **Figure B.6**). This is likely composed of polysaccharide membrane fragments as well as possible membrane-associated protein-coated nanotubes. Control SEM images of individual LSZ-SWCNTs immobilized onto poly-lysine coated glass coverslips, showed tubular structures that resembled those observed at the exterior of the heterocyst (**Figure B.7**), further suggesting a protrusion of the nanotube structures from the cell surface. Notably, significant distortions in the cell wall structures of vegetative cells along the treated filaments were observed, indicating a possible disruptive interaction in terms of cell viability (**Figure B.6**).

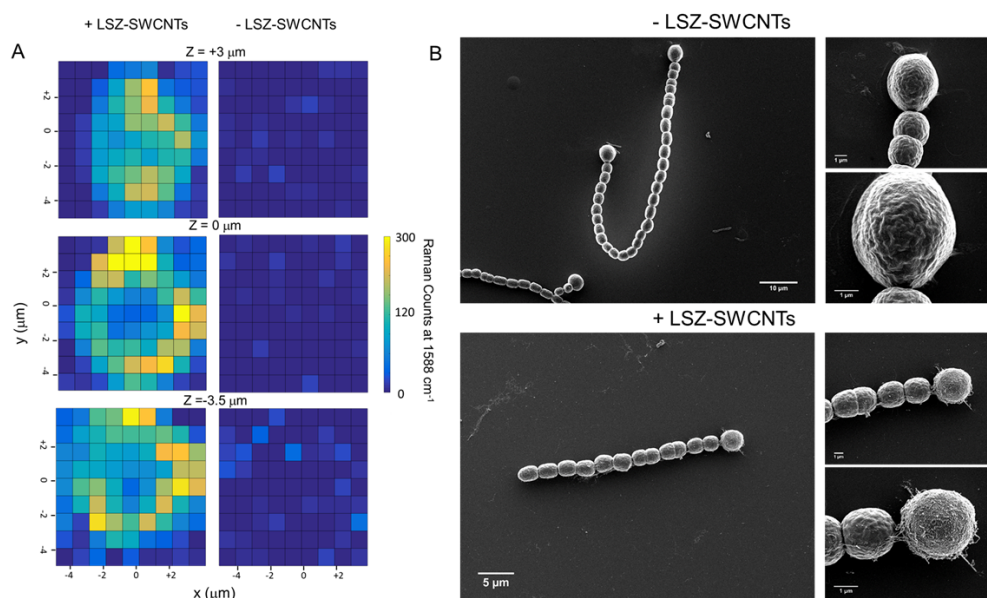


**Figure 3.3 – Impact on cell morphology and localization of SWCNTs.** (A) Representative confocal 3D Raman mapping of the characteristic SWCNT G'-band (at  $1580\text{ cm}^{-1}$ ) under  $532\text{ nm}$  laser excitation, used to explore the spatial distribution of LSZ-SWCNTs within *Nostoc* heterocysts. Scans were performed at different heights  $Z$  within the cells, with  $Z=0\text{ }\mu\text{m}$  corresponding to the focal plane of the cell exhibiting the highest image contrast in the bright-field imaging mode. The images show the comparison of a terminal heterocyst from a *Nostoc* filament treated with LSZ-SWCNTs with a non-treated heterocyst at different heights along the  $z$ -axis. The Raman signal at  $1580\text{ cm}^{-1}$  can be attributed to SWCNTs that accumulated within the cell. (B) Typical SEM (scanning electron microscopy) images of *Nostoc* cells containing heterocysts, before and after treatment with LSZ-SWCNTs at  $2\text{ mg/L}$  concentration.

### 3.4.3 Impact of SWCNTs on Cell Viability

To examine the impact of the LSZ-SWCNTs on cell viability, we used oxygen evolution measurements to compare the photosynthetic activity of cells in the presence and absence of functionalized-SWCNTs. As shown in **Table 3.1**, *Synechocystis* cells incubated in the presence of LSZ-SWCNTs exhibited similar oxygen evolution rates compared to control cells (those in the absence of LSZ-SWCNTs) under the conditions tested. These observations are in agreement with our previous work (Chapter 2).

However, both *Nostoc* and *Nostoc*-Het cells showed a remarkable decrease of the oxygen evolution rates on exposure to LSZ-SWCNTs, indicating a severe loss in cell viability. Since structural destabilization of the outer membrane is known as one primary mechanism of toxicity caused by cationic nanomaterials in prokaryotic cells[165], we first hypothesized that the interaction with positively-charged LSZ-SWCNTs could dramatically alter the permeability of *Nostoc* vegetative cells compared to *Synechocystis*. On the other hand, the enzymatic activity of lysozyme proteins, which can be preserved on the nanotube surface, could also play an active role in creating local disruptions of the bacterial cell wall, thereby affecting

Oxygen evolution rates ( $\mu\text{mol O}_2/(\text{mgChl} \times \text{h})$ )		
Strain	Control	+ LSZ-SWCNTs
<i>Synechocystis</i>	$142 \pm 6$	$140.2 \pm 10$
<i>Nostoc</i>	$81.2 \pm 4.0$	$-0.6 \pm 2.2$
<i>Nostoc</i> -Het	$60.1 \pm 7.8$	$2.4 \pm 4.0$

**Table 3.1** – Rates of oxygen evolution under illumination ( $100 \mu\text{mol photons m}^{-2} \text{ s}^{-1}$ ) for treated and untreated cells of *Synechocystis*, *Nostoc* and *Nostoc*-Het. Values are based on independent measurements obtained from three replicates and normalized by chlorophyll pigment content. The oxygen evolution rates of illuminated *Nostoc* and *Nostoc*-Het cells incubated with 2 mg/L LSZ-SWCNTs were significantly different from non-treated cells.

long-term cell viability. Treatment of *Synechocystis* cells with lysozyme is known to have a little effect due to the protective role of the S-layer that might limit diffusion of the lysozyme proteins to the peptidoglycan layer.[143] On the contrary, the absence of additional exopolysaccharides on the surface of *Nostoc* vegetative cells might facilitate the access of lysozyme proteins to the peptidoglycan layer, leading to higher susceptibility towards LSZ-SWCNT treatment. In agreement with this hypothesis, bright-field imaging of *Nostoc* cells following 1 hour incubation with LSZ-SWCNTs revealed almost complete rupture of the filaments into individual cells (**Figure B.8**).

#### 3.4.4 Influence of the SWCNT wrapping on interaction with *Nostoc* cells

In order to further discern the role of the SWCNT wrapping on cell viability, we also investigated the interaction of *Nostoc* and *Nostoc*-Het cells with positively charged chitosan-coated SWCNTs. Chitosan is a positively charged bio-polymer, soluble in weakly acidic solutions, with a charge density that is dependent on the pH and the degree of deacetylation.

Previous studies have shown that chitosan-coated SWCNTs can cross the lipid bilayer of isolated chloroplasts, and can be used as molecular scaffolds for the delivery of genetic material into plant cells.[39] Since chitosan-SWCNTs exhibit lower fluorescence intensities compared to LSZ-SWCNTs (**Figure B.9**), cell-nanoparticle interactions were monitored by NIR widefield fluorescence microscopy instead of confocal. **Figure 3.4** reports the NIR widefield images of *Nostoc* and *Nostoc*-Het cells incubated with chitosan-SWCNTs (concentration = 2 mg/L, zeta-potential =  $25 \pm 5$  mV). Similarly to LSZ-SWCNTs, the fluorescence signals of chitosan-SWCNTs were found to preferentially localize within the peripheral regions of heterocysts within *Nostoc*-Het filaments. In absence of the heterocysts, fluorescence was found to distribute more evenly throughout the volume of *Nostoc* filaments, suggesting possible internalization of the nanoparticle within the cell cytoplasm. Measurements of oxygen evolution rates of *Nostoc* and *Nostoc*-Het cells following 1 hour incubation with chitosan-SWCNTs, showed retained photosynthetic activity of both strains under tested conditions. Retained cell viability upon exposure to chitosan-SWCNTs confirmed the previous hypothesis that the activity of the lysozyme proteins, more so than the charge characteristics of the wrapping molecules, com-



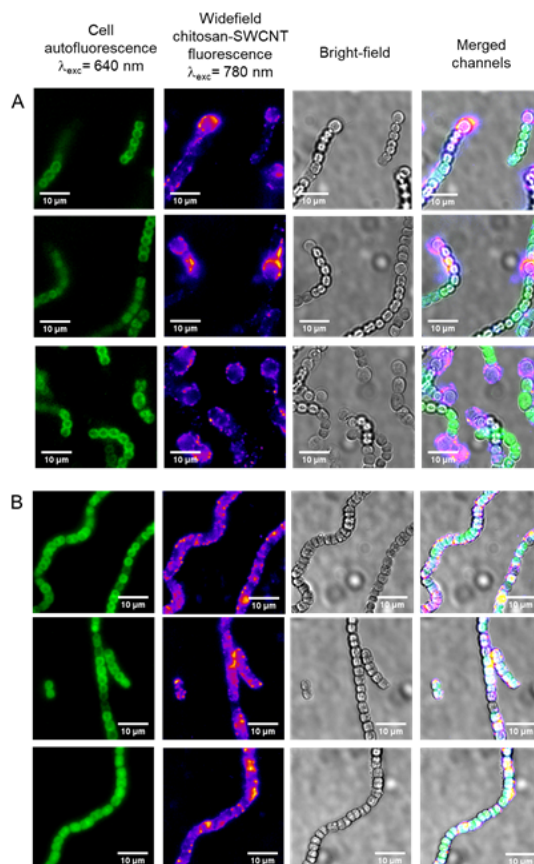


**Figure 3.4 – NIR Imaging of chitosan-SWCNT Interaction with *Nostoc* cells.** Representative images of (A) *Nostoc*-Het cells and (B) *Nostoc* cells after incubation with chitosan-wrapped SWCNTs at 2 mg/L concentration. Fluorescence intensity was recorded for cell autofluorescence (excitation at 640 nm, emission above 800 nm), and SWCNTs in widefield mode (excitation at 780 nm, emission above 980 nm).

promised the long-term viability of filamentous cells treated with LSZ-SWCNTs.

Oxygen evolution rates ( $\mu\text{mol O}_2/(\text{mgChl} \times \text{h})$ )	
Strain	+ chitosan-SWCNTs
<i>Nostoc</i>	$49.1 \pm 19.2$
<i>Nostoc</i> -Het	$49.2 \pm 13.3$

**Table 3.2 – Rates of oxygen evolution under illumination ( $100 \mu\text{mol photons m}^{-2} \text{ s}^{-1}$ ) for *Nostoc* and *Nostoc*-Het cells incubated with 2 mg/L chitosan-SWCNTs.** Values are based on independent measurements obtained from three replicates and normalized by chlorophyll pigment content.

### 3.4.5 Positively-charged SWCNTs for targeted cell imaging

As shown, the selection of an appropriate SWCNT coating, which must consider the unique cell wall characteristics of distinct bacterial species, is imperative for developing SWCNT-based bio-imaging or bio-delivery applications that can preserve long-term cellular integrity for many species. Due to the preferential uptake by heterocysts of positively charged nano-complexes, such as LSZ-SWCNTs and chitosan-SWCNTs, these hybrids present an alternative method to conventional poly-cationic dyes (Alcian blue) for distinguishing between vegetative and non-vegetative cells in *Nostoc* (see **Figure B.10-11**). Furthermore, due to increased photostability and intrinsic near-infrared fluorescence of SWCNTs, these are attractive probes for long-term imaging where visible dyes are not applicable. Moreover, the unique ability to selectively functionalize the surface of the nanotubes, and thereby control the surface charge, presents a tunable approach to create imaging probes for a larger variety of organisms. The properties of these probes can be tuned while considering the the membrane composition and charge of the organism in question, to create dyes that exhibit increased affinities for the cells, while simultaneously minimising cytotoxic effects.

## 3.5 Conclusions

In this study, we used confocal fluorescence microscopy, alongside other complementary techniques, to study the interaction of functionalized SWCNTs with cells of different cyanobacterial strains. We observed that the structure and composition of the cell wall have a profound impact on the cellular response to nanoparticle exposure. In particular, the presence of additional negatively-charged layers on the outer membrane of cyanobacterial cells, such as those found in *Synechocystis* cells or in *Nostoc* heterocysts, increases cell association with positively charged SWCNTs and their resistance to cytotoxic effects. These distinct behaviors upon nanoparticle exposure can find application for long-term tracking of cyanobacterial cells or for monitoring of specific cell differentiation processes. The varying susceptibility of different microbial strains to nanoparticle treatment exemplifies the complexity of these systems, and motivates a systematic exploration of these strains under a wider range of control tested conditions.



## **4 Real-time monitoring of bacterial growth in the presence of SWCNTs**

### **4.1 Abstract**

The ability to understand and predict the fate of SWCNT accumulation within living organisms is important for many applications in the field of cell nanobiotechnology. Long-term subcellular reorganization of SWCNTs, including intracellular agglomeration phenomena, has been shown to induce deleterious changes in many important cell physiological processes. A better understanding of the intracellular fate of SWCNT accumulation within cells of living organisms and their impact on cell behavior over multiple division cycles is therefore required. The study presented in this chapter illustrates the application of NIR confocal fluorescence microscopy for the investigation of the fate of internalized nanoparticles upon multiple cell division events in photosynthetic microbes. Although both unicellular and filamentous cyanobacteria can sustain growth and continued cell division following exposure to nanoparticles, we observed a reduced doubling rate compared to unexposed cells. In addition, the nanoparticle distribution to daughter cells was observed to follow the formation of membranes within the new cells. Conversely, we noticed that SWCNTs remained entrapped inside non-dividing unicellular bacteria, which in turn exhibited substantially higher levels of NIR fluorescence after 48 hours. Similarly, heterocysts, which are incapable of cell division, showed increased levels of SWCNT fluorescence compared to vegetative cells within the filament. These findings indicate that NIR fluorescence can be used to identify non-dividing cells and also track membrane formation in newly formed cells. This represents the first time that real-time microscopy is employed to study the effect of SWCNTs on dividing bacterial cells and presents a new direction for future studies of long-term fates of SWCNT-cell interaction.

### **4.2 Introduction**

The reactive stability of SWCNTs, combined with their tendency to aggregate in solutions over times, motivates the need for long-term intracellular nanoparticle tracking. The intracellular fate of SWCNTs has been studied via time-lapse live cell microscopy and micro-Raman

spectroscopy.[166, 167, 168, 169]

These studies have helped elucidate the possible effects of SWCNTs on many critical cellular processes. For example, several studies have shown a preservation of cell viability when SWCNTs are functionalized with wrappings that increase their solubility and stability in complex cellular environments.[124, 170] Cheng and coworkers have similarly observed that the uptake of polyethylene glycol-SWCNTs (PEG-SWCNTs) into the cell nucleus had no effects on the growth kinetics and cell cycle for up to five days.[169] These tracking studies have also lead to the discovery of excretion mechanisms found in many eukaryotic cells that are responsible for expelling internalized SWCNTs via exocytosis, which is mediated by cell-released microvesicles.[124]

Other studies, however, have shown that the long-term subcellular reorganization of SWCNTs, including intracellular agglomeration, can induce deleterious changes in many important cell physiological processes.[171, 88] These processes include altered cellular adhesion,[172] compromised cell shape and morphology,[173] as well as perturbed cell differentiation and proliferation.[174, 168] For example, Holt et al. demonstrated that SWCNTs can induce actin bundling in cells, which could lead to reduced cell proliferation. These alterations resulted in actin-related division defects such as the formation of giant cells, the appearance of multinucleated cells, and incomplete cytokinesis.[175] These findings suggested that SWCNT-treated cells were unable to continue cell division, and therefore the intracellular fate of SWCNTs following cell division has thusfar remained largely unexplored.

A rigorous understanding of the intracellular fate of SWCNTs is critical for assessing the viability of SWCNT-based technologies for both medical and environmental applications. In this work, we employ NIR confocal fluorescence microscopy to investigate the long-term impacts of SWCNTs inside photosynthetic microbes. In particular, we investigate the effects of SWCNTs on cell division for both unicellular and multicellular microbes, as well as the propensity of daughter cells to inherit the nanotube's optoelectronic properties.

### 4.3 Materials and Methods

**Functionalization of SWCNTs.** The SWCNTs used in this study were purified HiPco nanotubes (NanoIntegris, Lot. No. HP26-019) with a diameter of 0.8–1.2 nm. LSZ-SWCNTs were prepared by suspending 1 mg of HiPco nanotubes and 5 mg of lysozyme from chicken egg white (Sigma Aldrich) in 1 mL of 1 mM HEPES buffer (pH 7.4) and sonicating using a cup-horn sonicator (140 mm, Qsonica, LLC) for 90 minutes at 1% amplitude on ice. The sonicated SWCNT suspension was centrifuged (Eppendorf Centrifuge 5424 R) for 180 minutes at 16500 x g to pellet SWCNT aggregates. Unbound protein was removed through dialysis against 2 L of 1 mM HEPES buffer using a 300 kDa MWCO cellulose membrane. SWCNT concentrations were calculated from absorbance measurements at 632 nm in a UV-Vis-NIR scanning spectrometer (Shimadzu 3600 Plus) using an extinction coefficient of 0.036 L/(mg cm).

**Bacterial strains and growth conditions.** Liquid cultures of wild-type *Synechocystis* sp. PCC 6803 and *Nostoc* sp. were grown in BG11 medium supplemented with 10 mM TES buffer (pH 8.0) at 30°C under 50  $\mu\text{mol photons m}^{-2} \text{s}^{-1}$  of white light with constant shaking.

**NIR Fluorescence Imaging.** Cells were fixed onto poly-lysine coated glass-bottom Petri dishes by spotting 30  $\mu\text{L}$  of the cell suspension at  $\text{OD}_{750\text{nm}}$  of 1.4 for 10 minutes followed by washing with HEPES. The cells were then covered with 50  $\mu\text{L}$  of 1 mM HEPES buffer (pH 7.4). 10  $\mu\text{L}$  of SWCNT stock solutions were added to a 50  $\mu\text{L}$  droplet of 1 mM HEPES buffer to yield a final concentration of 2 mg/L. Following incubation, the SWCNT solution was replaced by a 50  $\mu\text{L}$  droplet of fresh HEPES buffer. For the long-term imaging measurements, the cells were covered with 5 mL of warm 1% agar in BG11 after washing with HEPES buffer to eliminate the excess of nanoparticles. Following solidification of the agar the plate was sealed to minimize evaporation and transferred onto the microscope stage (Eclipse Ti-U, Nikon AG Instruments). The cells were kept under 20  $\mu\text{mol photons m}^{-2} \text{s}^{-1}$  of white light and bright-field images were recorded every 20 min for the duration of the experiment with a visible camera (Andor). After one day of growth, SWCNT fluorescence was monitored with 780 nm excitation (2.5 mW/cm<sup>2</sup>) (Cairn Research) and a 980 nm long-pass emission filter (Semrock). Images were acquired with the Nikon NIS-Elements software (Nikon Instruments), using a custom-built optical setup consisting of an inverted microscope (Eclipse Ti-U, Nikon AG Instruments) with an oil-immersion TIRF 100 x objective (N.A. 1.49, Nikon) coupled to a CREST X-Light spinning-disk confocal imaging system (CREST Optics) (60  $\mu\text{m}$  pinholes) and an InGaAs camera (NIRvana 640 ST, Princeton Instruments).

## 4.4 Results and discussion

### 4.4.1 Real-time monitoring of unicellular cyanobacteria

The distribution of LSZ-SWCNTs was studied in dividing *Synechocystis* cells using time-lapse NIR confocal imaging based on the setup shown in **Figure 4.1**.

Time-lapse confocal fluorescence microscopy showed that the majority (ca 70%) of the *Synechocystis* cells exhibited sustained growth and cell division for more than 100 hours following exposure to LSZ-SWCNTs (**Figure 4.2**). A closer look at the nanoparticle distribution following division revealed that a portion of the SWCNTs originally incorporated within the mother cells are transferred to the daughter cells (see merged images in **Figure 4.2**). We observed no differences in the localization of the SWCNT fluorescence for control cells maintained in dark or low light-intensity conditions (**Figure C.2**). However, we noticed a heterogeneity in the NIR fluorescence distribution over time on the single-cell level; cells that did not undergo division displayed higher levels of NIR fluorescence over the course of the experiment. We attributed the observed higher fluorescence intensities to entrapped SWCNTs that could not migrate to newly formed daughter cells, as well as to a trace increase in NIR autofluorescence that arises from dying photosynthetic cells (see also **Figure A.5**). The distinctive intensities can therefore

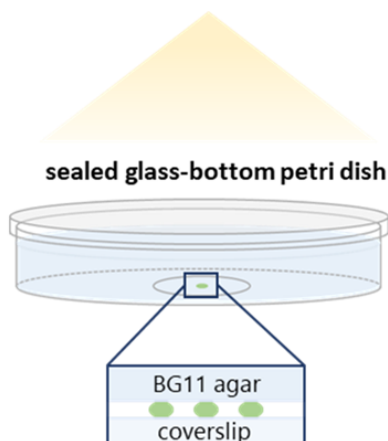


**Figure 4.1 – Setup for in-situ monitoring of cyanobacterial growth.** Schematic of the glass-bottom Petri dish used to monitor cyanobacterial growth on the microscope stage. Cells are immobilized onto a poly-lysine-coated coverslip and covered by a thick layer of warm 1% agar in BG11. Following agar solidification, dishes were sealed to minimize evaporation.

optically distinguish dividing and non-dividing cells through NIR imaging.

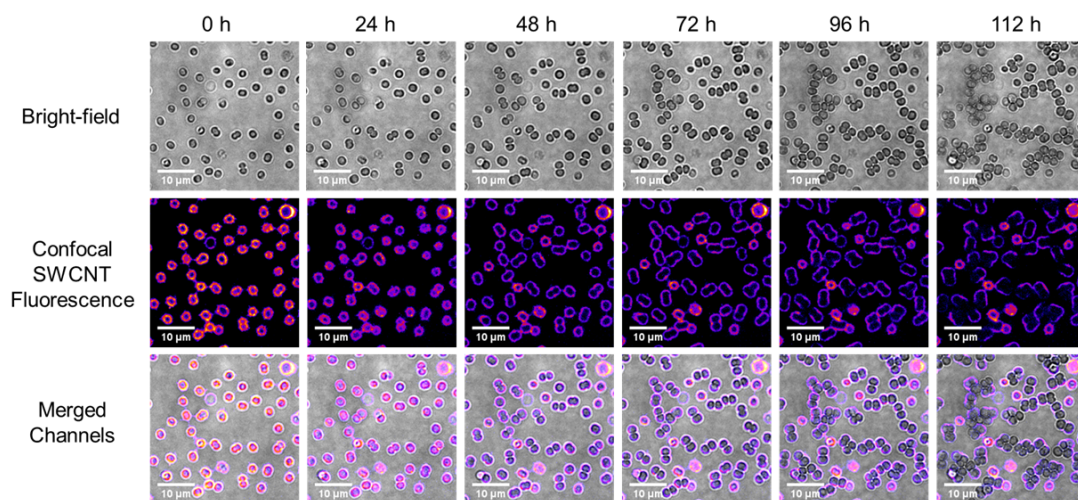


**Figure 4.2 – Long-term NIR Imaging of *Synechocystis* cell growth in presence of LSZ-SWCNTs.** NIR confocal fluorescence and bright-field images of *Synechocystis* cells treated with LSZ-SWCNTs and grown on 1% agar in BG11. Fluorescence intensity was recorded every 24 hours for SWCNTs in confocal mode (excitation at 780 nm, emission above 980 nm, at 2.5 mW/cm<sup>2</sup>). Cell growth was monitored for more than 100 hours.

Although the prokaryotic cells treated with LSZ- SWCNTs showed sustained cell growth, their growth rate appears lower than those of cells treated with only 1 mM HEPES buffer in the absence of SWCNTs (**Figure 4.3**). Based on cell-counting of cells in bright-field mode, we estimated growth rates of 0.02 h<sup>-1</sup> (doubling time of 33 hours) and 0.015 h<sup>-1</sup> (doubling time

of 47 hours) for cells treated in absence and presence of LSZ-SWCNTs, respectively (**Figure C.4**). These measurements lie within the range of reported doubling times of 20 – 40 hours for diurnally cultured *Synechocystis*, [176] and are in agreement with previous reports that have reported slowed doubling times for eukaryotic cells treated with SWCNTs. [167]

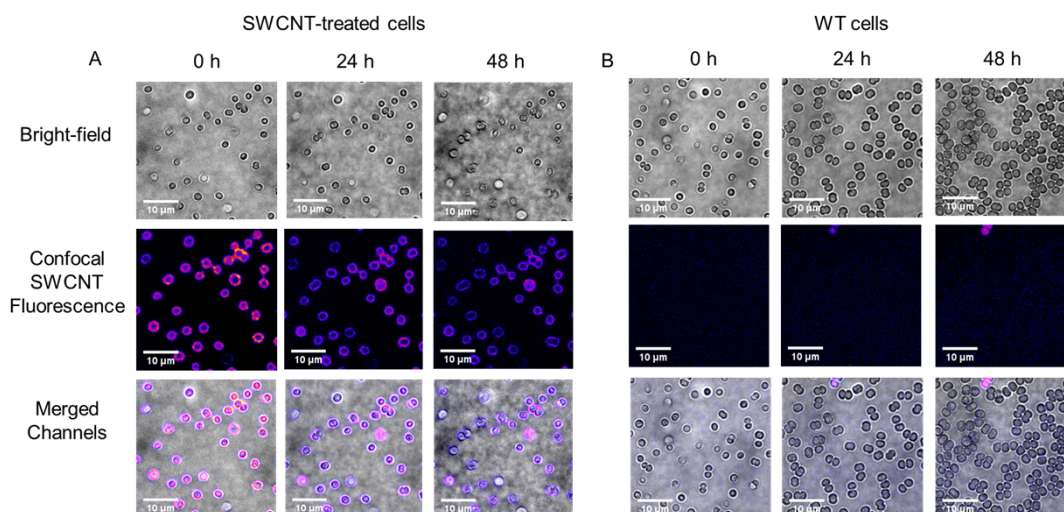


**Figure 4.3 – Comparison of *Synechocystis* growth in presence and in absence of LSZ-SWCNTs.** NIR confocal fluorescence and bright-field images of *Synechocystis* cells treated with LSZ-SWCNTs (A) or with 1 mM HEPES buffer only for control (B). Cells were grown on 1% agar in BG11 for 48 hours. Fluorescence intensity was recorded every 24 hours for SWCNTs in confocal mode (excitation at 780 nm, emission above 980 nm, at 2.5 mW/cm<sup>2</sup>).

#### 4.4.2 Real-time monitoring of filamentous cyanobacteria

The setup shown in **Figure 4.1**, was similarly used to monitor the effects of LSZ-SWCNTs on the growth of both *Nostoc* and *Nostoc*-Het filaments.

As shown in **Figure 4.4** and in **Figure 4.5**, both *Nostoc* and *Nostoc*-Het cells treated with LSZ-SWCNTs show sustained growth and division over 48 hours that is similar to that of the control filaments in the absence of LSZ-SWCNTs. Moreover, the intracellular LSZ-SWCNT fluorescence appeared to distribute between the mother and the newly formed vegetative cells in the filaments, as indicated by the even distribution of SWCNT fluorescence observed within the filament after 24 and 48 hours (**Figure 4.4a** and **Figure 4.5a**). Conversely, non-dividing heterocyst cells exhibited higher levels of SWCNT fluorescence over the course of the experiment. These observations suggested that the internalized SWCNTs were entrapped within the nitrogen-fixing compartment, without compromising the growth of adjacent vegetative cells (**Figure 4.5a**).

The ability of both *Nostoc* and *Nostoc*-Het cells to sustain growth and division on agar plates when treated with LSZ-SWCNTs, seemed to contradict previous observations of suppressed



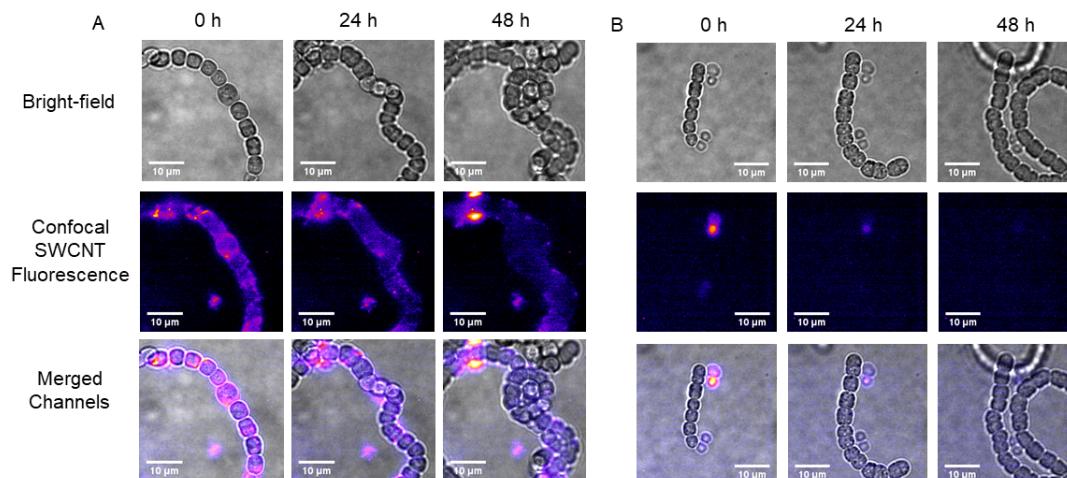


**Figure 4.4 – Long-term NIR Imaging of *Nostoc* cell growth in presence of LSZ-SWCNTs.** Representative images of *Nostoc* cells in presence (A) or in absence (B) of LSZ-SWCNTs and grown on 1% agar in BG11. Fluorescence intensity was recorded every 24 hours for SWCNTs in widefield mode (excitation at 780 nm, emission above 980 nm). Cell growth was monitored for 48 hours.

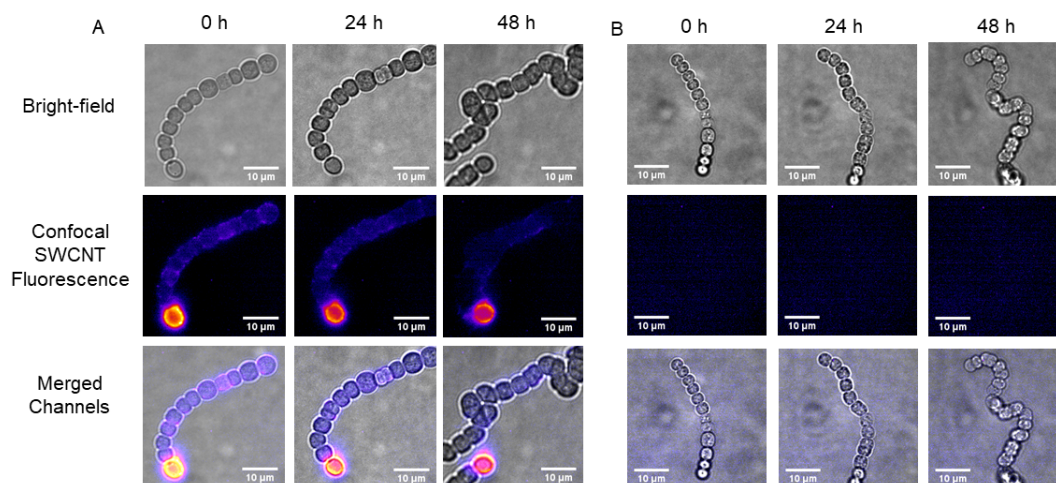


**Figure 4.5 – NIR Imaging of *Nostoc*-Het cells growth in presence of LSZ-SWCNTs.** Representative images of *Nostoc*-Het cells in presence (A) or in absence (B) of LSZ-SWCNTs and grown on 1% agar in BG11. Fluorescence intensity was recorded every 24 hours for SWCNTs in widefield mode (excitation at 780 nm, emission above 980 nm). Cell growth was monitored for 48 hours.

photosynthetic activity upon exposure of LSZ-SWCNTs. In particular, compared to the unicellular *Synechocystis* cells, which showed sustained photosynthetic activity upon LSZ-SWCNT exposure, the filamentous *Nostoc* cells showed an overall decrease in photosynthetic activity when exposed to LSZ-SWCNTs (Chapter 3). We attribute these distinct responses to differences

in the experimental conditions. In this study, the cells were first immobilized onto poly-lysine coated Petri dishes and then incubated with LSZ-SWCNTs. The study presented in Chapter 3 kept the cells suspended in a buffered solution in the presence of LSZ-SWCNTs under mixing conditions. The immobilization of the cells on the glass substrate and the absence of mixing may inhibit cell susceptibility due to differences in nanoparticle accessibility and hence uptake mechanism. This important aspect is the focus of ongoing studies.

## 4.5 Conclusions

To our knowledge, this is the first time that NIR confocal fluorescence microscopy has been employed to investigate the effect of SWCNTs on living microbial cells growing on the microscope stage, as well as their cellular distribution following division events. In this study we observed that both *Synechocystis* and *Nostoc* show sustained growth and division following treatment with LSZ-SWCNTs, and that SWCNTs could be transferred to daughter cells over the course of cell division. The *in situ* single-cell tracking of SWCNTs first reported in this study shows that nanobionic capabilities can be inherited by living cells without genetic manipulation, and the inherited NIR fluorescence can be used in cross-generational cell tracking. The heterogeneity in individual fluorescence can further distinguish between dividing and non-dividing cells. However, reduced doubling rates were observed compared to untreated cells, opening additional questions on the role of SWCNTs in the cell division process. To further elucidate this aspect, studying the impact of different SWCNT wrapping molecules on cell division is required. Extending the use of SWCNTs for the long-term monitoring of cell differentiation processes is one potential downstream application of our technique, and could be used to obtain valuable information on local variations of membrane structure within specific cell compartments.





## **5 Outlook on Potential Applications of SWCNT-treated Photosynthetic Microbes**

### **5.1 Abstract**

The integration of synthetic nanomaterials in cells of photosynthetic organisms, such as plants and microalgae, has shown to improve their native performance, by broadening the range of solar light absorption and scavenging reactive oxygen species (ROS). Notably, the integration of carbon nanotube materials into biophotovoltaic devices has been shown to improve energy extraction from living photosynthetic microbes, boosting device efficiencies through more efficient electrical communication between the cells and the electrode substrates. Beyond enhanced charge transfer, the capability of SWCNTs to traverse the multilayered wall of plant cells can be exploited to transport biomolecules and genetic material into living cells, enabling streamlined genetic modification and regulation of plant or algal metabolism.

The localization of SWCNTs within the internal cell compartments of photosynthetic microbes, combined with the sustained cell viability demonstrated in the previous chapters of this thesis, opens multiple opportunities for future developments of these "green" technologies. Exemplary applications, highlighting the scope of these technologies, are presented in this final chapter. These applications include investigations on the impact of SWCNT incorporation into bio-hybrid devices for improving bio-electricity generation from cyanobacteria, as well as preliminary findings on the suitability of these materials as platforms for targeted biomolecule delivery.

### **5.2 Generation of bio-electricity from cyanobacteria: introduction**

The application of nanotechnology in the field of photosynthesis research is still in its infancy. Synthetic NCs in particular hold the promise to enhance or even expand the native capabilities of photosynthetic systems, enabling the development of cost-effective, "green" technologies that are based on abundant living organisms with improved performance.[42] Owing to their excellent conductivity and elevated electroactive surface area, together with their unique optical properties, carbon nanotubes (CNTs) have shown to potentially improve the native

## Chapter 5. Outlook on Potential Applications of SWCNT-treated Photosynthetic Microbes

performance of photosynthetic systems through augmented photosynthesis and enhanced energy extraction. The incorporation of semiconducting single-walled carbon nanotubes (SWCNTs) inside *Arabidopsis* leaves and in isolated chloroplasts has shown to contribute to an increase in photosynthetic electron transport rates, by broadening the range of solar light absorption and scavenging reactive oxygen species (ROS).[33]

More recent works have demonstrated the ability to combine synthetic CNTs with photosynthetic microorganisms into biological photovoltaics (BPVs). Within a BPV, the high-energy electrons generated either during photosynthesis (under illumination) or by oxidation of internal carbon stocks (in the dark) are transferred from the microbial cells to an external electrode. The integration of CNTs onto the electrode surface, which can promote more intimate contact between the substrate and the living cells, has been shown to boost device efficiencies through more efficient charge extraction from the microbes.[177] By combining multi-walled carbon nanotube (MWCNT) anodes with a filamentous cyanobacterium, *Nostoc* sp., Sekar et al. successfully produced BPVs with average power densities of  $35 \text{ mW m}^{-2}$  under light illumination.[177] More recent work by Sawa et al. fabricated thin-film, paper-based BPVs by printing a layer of cyanobacterial cells on top of MWCNT-coated substrates.[178] The cells remained viable after printing, retaining their photosynthetic activity, and bio-generated currents were sustained for over 100 hours.

These aforementioned approaches employed similar electrode fabrication strategies, whereby a solid layer of cyanobacterial cells was deposited, or printed, on top of a conductive CNT substrate. However, alternative studies have reported increased electron transfer using three-dimensional cell networks, which are believed to promote more intimate contact between synthetic nanoparticles and cell membranes.[42, 179, 180, 181] These inter-penetrated microbial-nanomaterial composites could also be applied to bacterial strains that do not possess the ability to form thick biofilms, bringing new opportunities for enhancing BPV performance.

Our previous study on the interaction of SWCNTs and *Synechocystis* cells has shown that the functionalization of SWCNTs with positively charged wrappings can favor SWCNT accumulation within the peripheral regions of the cells. Furthermore, this incorporation can preserve cell photosynthetic activity and growth. The direct coupling of conductive nanotube structures with the insulating wall of *Synechocystis* cells has the potential to improve bacteria-electrode interactions by providing a highly conductive network for charge transfer. This network could overcome the limited ability of *Synechocystis* cells to form biofilms that can attach to the electrode's surface.[182, 183] In this work, we exploit the inter-penetrating CNT technology developed in this thesis to present a new approach towards achieving improved electron transfer in BPVs.

### 5.2.1 Materials and Methods

**Functionalization of SWCNTs.** The SWCNTs used in this study were purified HiPco nanotubes (NanoIntegris, Lot. No. HP26-019) with a diameter of 0.8–1.2 nm. LSZ-SWCNTs were prepared

## 5.2. Generation of bio-electricity from cyanobacteria: introduction

by suspending 1 mg of HiPco nanotubes and 5 mg of lysozyme from chicken egg white (Sigma Aldrich) in 1 mL of 1 mM HEPES buffer (pH 7.4) and sonicating using a cup-horn sonicator (140 mm, Qsonica, LLC) for 90 minutes at 1% amplitude on ice. The sonicated SWCNT suspension was centrifuged (Eppendorf Centrifuge 5424 R) for 180 minutes at 16500 x g to pellet SWCNT aggregates. Unbound protein was removed through dialysis against 2 L of 1 mM HEPES buffer using a 300 kDa MWCO cellulose membrane. SWCNT concentrations were calculated from absorbance measurements at 632 nm in a UV-Vis-NIR scanning spectrometer (Shimadzu 3600 Plus) using an extinction coefficient of 0.036 L/(mg cm).

**Bacterial strains and growth conditions.** Liquid cultures of wild-type *Synechocystis* sp. PCC 6803 were grown in BG11 medium supplemented with 10 mM TES buffer (pH 8.0) at 30°C under 50  $\mu\text{mol photons m}^{-2} \text{ s}^{-1}$  of white light with constant shaking.

**Preparation of the electrodes.** Graphite rods (3.05 mm diameter, AlfaAesar) were sonicated in ethanol and deionized water (10 min each) at room temperature to remove possible impurities. *Synechocystis* cells were drop-casted onto the graphite electrodes according to the method used by Hasan et al.[184] Briefly, wildtype *Synechocystis* cells were grown in BG11 medium to an OD<sub>750nm</sub> of 3. The cells were then pelleted by centrifugation at 5000 rpm for 5 minutes and re-suspended in 1 mM HEPES buffer (pH 7.4) to yield a solution with an OD<sub>750nm</sub> of 2. This washing step was repeated, and the double-washed pellet was finally re-suspended in 10  $\mu\text{L}$  of 1 mM HEPES buffer (concentration of 1mg/mL), drop-casted on the top surface of a PEDOT electrode, and mixed with 10  $\mu\text{L}$  of LSZ-SWCNTs at a concentration of 60 mg/L. The cell-SWCNT suspension was left to dry for 1 hour. After drying, a 14 kDa MWCO dialysis membrane (Sigma-Aldrich), which was previously soaked in HEPES for at least 1 hour, was pressed onto the electrode and tightly fixed with a rubber O-ring and parafilm. The control *Synechocystis*- and LSZ-SWCNT-modified graphite electrodes were prepared in an analogous manner.

**Photo-response measurements.** The *Synechocystis* electrodes were inserted in a conventional three-electrode electrochemical cell containing HEPES with a Pt wire counter-electrode and a standard Ag/AgCl (sat. KCl) reference electrode. The cell was connected to a PalmSens4 potentiostat (PalmSens BV) equipped with PStace software. Measurements were conducted in the presence of 1 mM K<sub>3</sub>Fe(CN)<sub>6</sub>. The CA measurements were performed at an applied potential of 300 mV, corresponding to the oxidation potential of the K<sub>3</sub>Fe(CN)<sub>6</sub>/K<sub>4</sub>Fe(CN)<sub>6</sub> redox couple. The current was continuously monitored during dark-light cycles for 3 hours. In particular, the system was stabilized in the dark for 30 minutes, followed by 1 hour illumination with an LED light at 100  $\mu\text{mol photons m}^{-2} \text{ s}^{-1}$ , followed by 30 minutes of incubation in the dark and another 1 hour incubation in the light. Corresponding measurements were taken for *Synechocysts*-, SWCNT/*Synechocysts*- and SWCNT-modified graphite electrodes.

### 5.2.2 Results and Discussion

**Figure 5.1a** and **Figure 5.1b** show a diagram of the experimental setup used for the electrode preparation and the corresponding the electrochemical setup, respectively. The electrochemical setup was used to perform chronoamperometry (CA) measurements in the presence of  $\text{K}_3\text{Fe}(\text{CN})_6$ , which is known to cross the outer cell membrane, to overcome limited current densities that are achieved with direct electron transfer.[177]

In this mediated system, accessible membrane redox complexes reduce  $\text{Fe}(\text{CN})_6^{3-}$  to  $\text{Fe}(\text{CN})_6^{4-}$ . The  $\text{Fe}(\text{CN})_6^{4-}$  can be subsequently oxidized at the electrode by applying a potential exceeding the oxidation potential of the reduced mediator. Prior to illumination, all electrodes exhibited an initial drop in current that was attributed to diffusion-limited extraction of capacitive charge (**Figure 5.1c**). Upon cyclic light-dark periods, we observed a reversible photoresponse of the electrodes in the presence of *Synechocystis* cells. Notably, within the first illumination cycle, the electrode composed of SWCNT-treated *Synechocystis* cells exhibited up to a three-fold enhancement of the collected photocurrent density, reaching current densities of  $0.45 \mu\text{A}/\text{cm}^2$  under  $100 \mu\text{mol photons m}^{-2} \text{s}^{-1}$  illumination, compared to  $0.15 \mu\text{A}/\text{cm}^2$  for untreated cells under the same conditions. Furthermore, the steady-state current reached during the second illumination cycle by untreated *Synechocystis* cells, was still lower compared to the one collected from SWCNT-treated cells. Increases in current output were visible only in samples containing the cyanobacterial cells, while no photoresponse was observed when the electrode surface was modified with LSZ-SWCNTs alone. This observation suggests that the observed increase was associated with enhanced photosynthetic charge extraction from the microbes, rather than a photoresponse from the LSZ-SWCNTs or the  $\text{K}_4\text{Fe}(\text{CN})_6$  mediator. However, the time taken to reach the steady-state regime for photocurrent output was increased for SWCNT-treated cells, suggesting a higher capacitive behavior and increased charge accumulation within the hybrid systems.

Though the precise mechanism of charge extraction remains an area of ongoing study, we hypothesize that the metallic SWCNTs may contribute to enhancing the membrane conductivity of the cell. This hypothesis is supported by the detailed SWCNT-microbe characterization reported in **Chapter 2**, which showed preferential nanoparticle accumulation within the peripheral regions of the cells. In addition to membrane conductivity, the semiconducting SWCNTs may also contribute to enhanced light absorption and energy transfer processes. Both enhanced membrane conductivity from metallic nanotubes and improved light harvesting by semiconducting nanotubes may result in the observed increase in photocurrent.

Independent of the precise electron transfer mechanism and means of enhancement, these findings demonstrate an unexplored avenue for using inter-penetrating SWCNTs for cell/electrode design in BPVs. Future research on the integration of SWCNTs into BPVs will focus on exploring alternative electrode configurations to further improve the optical transparency and increase long-term stability of generated photo-currents in these systems. Promising approaches for this include the use of indium-tin-oxide electrode substrates for the immobi-

## 5.2. Generation of bio-electricity from cyanobacteria: introduction

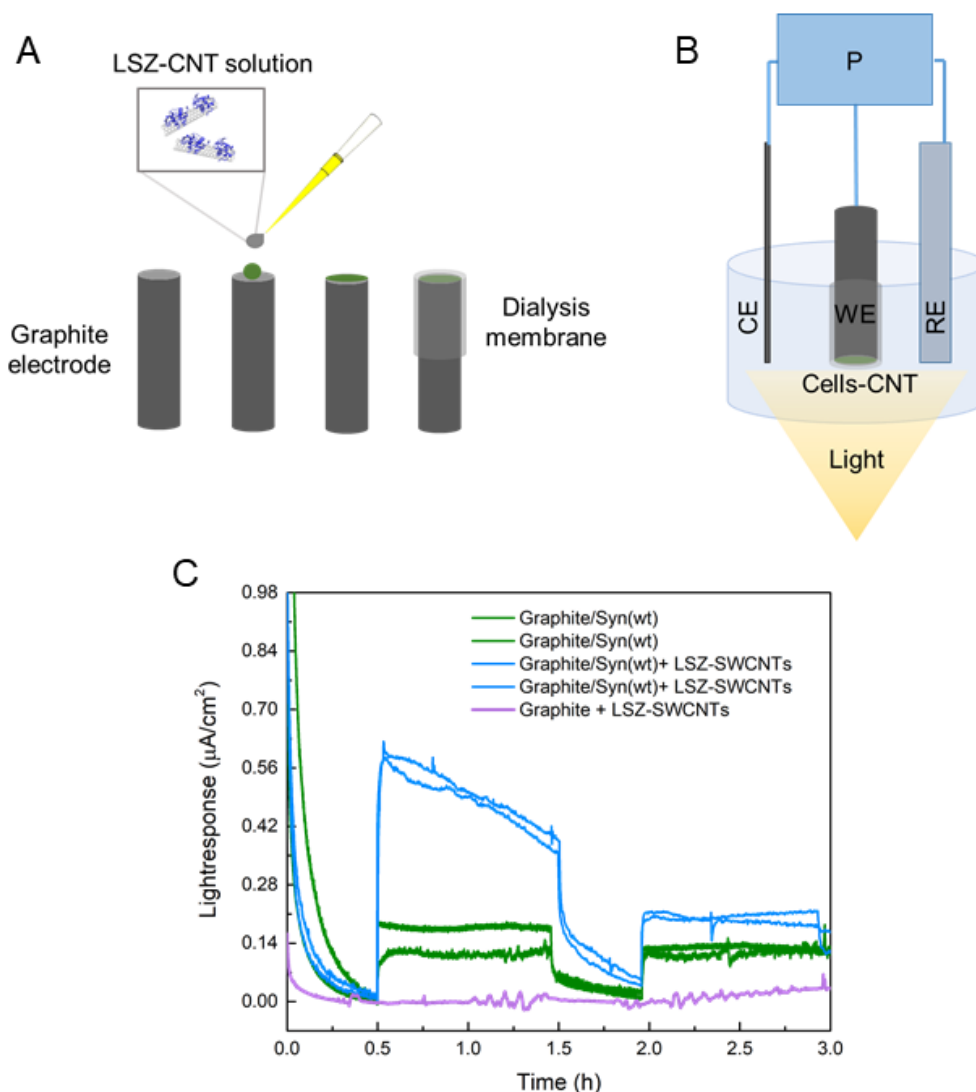


**Figure 5.1 – Light-response from SWCNT-treated *Synechocystis* cells.** (A) Schematic illustration showing the preparation of the composite SWCNT-microbe electrodes. *Synechocystis* cells were drop-casted on the surface of a graphite rod and mixed with a suspension of LSZ-SWCNTs. The mixture was dried and covered with a dialysis membrane. (B) Schematic representation of the electrochemical cell used to test the electrode performance. (CE, counter electrode; WE, working electrode; RE, reference electrode; P, potentiostat). (C) Mediated photo-response of *Synechocystis* (green) and *Synechocystis*-LSZ-SWCNT composite (blue) on graphite electrodes measured in HEPES medium supplemented with  $K_3Fe(CN)_6$ . The purple curve represents the light-response of LSZ-SWCNT modified graphite in the absence of *Synechocystis* cells.

lization of SWCNT-treated photosynthetic cells, as well as the use of purified metallic SWCNTs, which would offer greater electrical conductivity.

### 5.3 SWCNTs for gene-delivery applications: introduction

In addition to BPVs, inter-penetrating SWCNTs also hold strong promise for biomolecule delivery applications. Most eukaryotes to date benefit from a range of technologies for biomolecule delivery that typically rely on either mechanical, chemical, or biological approaches. While some prokaryotes demonstrate a natural capacity to uptake foreign genetic material from their surroundings, also known as "competency", without the need for these invasive technologies, most prokaryotes require tedious procedures to become competent, limiting the ability to genetically manipulate these microorganisms.[117] In particular, most cyanobacteria require complex bacterial conjugation methods based on multiple plasmids and triparental mating strategies for delivery of exogenous DNA. Furthermore the success rate of transformation/conjugation using such techniques is significantly low.[185]

The absence of a versatile and straightforward genetic modification protocol hinders many bioengineers from accessing these microbes.[186] Hence, the development of new materials and tools that facilitate genetic manipulation of these species has the potential to accelerate future advancements in microbial-based applications.

The ability of nanomaterials, such as SWCNTs to interact with the multilayered cell walls of both eukaryotes and prokaryotes offers a promising avenue for versatile gene delivery. SWCNTs further benefit from elevated surface area-to-volume ratios and flexible functionalization, allowing for significant DNA carrying capacity and targeted cellular and sub-cellular specificity. Combined with the NIR tracking abilities demonstrated in the previous chapters of this thesis and the propensity of SWCNT to protect conjugated DNA from nuclease degradation [152], these characteristics are particularly suited for DNA transformations of photosynthetic cells that are otherwise difficult to transform. Only this year have these advantageous properties been used to develop highly-efficient, species-independent DNA delivery in plant cells.[96, 32, 39] However, the exploitation of SWCNTs in prokaryotes has yet to be achieved.

The transport of SWCNTs across the multilayered cell walls of bacteria might facilitate the delivery of larger synthetic or bio-molecules, including genetic material, into otherwise non-competent strains. Although previous investigations on CNT-mediated bacterial transformation have shown that external mechanical or physical forces can favor partial or integral CNT penetration across the cell walls, the transport of genetic material via CNT in absence of mechanical or physical assistance has not been reported.[45, 106]

Our previous studies with *Synechocystis* sp. PCC 6803 and *Nostoc* cells, used SWCNTs as delivery vehicles for internalizing positively-charged proteins, such as lysozyme (LSZ). In addition to improving the interaction of the SWCNTs with the negatively-charged cell membrane, the strongly positive charge carried by LSZ makes this protein suitable for binding negatively-charged nucleic acids. The electrostatic complexation of DNA represents a common strategy for the fabrication of SWCNT-based gene delivery scaffolds in eukaryotic systems.[39] The ability of LSZ to condense DNA molecules has been exploited so far for the development

### 5.3. SWCNTs for gene-delivery applications: introduction

---

of DNA-based electrochemical sensors for LSZ detection, as well as for the fabrication of DNA-LSZ-SWCNT fibrillar structures with antimicrobial activity.[131, 187]

In this section, we propose the use of LSZ-SWCNTs for immobilizing DNA vectors for the genetic transformation of cyanobacteria. Preliminary results demonstrate the possibility to form stable DNA-LSZ-SWCNTs complexes that can accumulate within the peripheral regions of unicellular cyanobacteria.

Future studies will investigate SWCNT-mediated gene delivery into *Synechocystis* sp. PCC 6803 mutants (namely  $\Delta$ hfr strain)[150] that lack the type IV pili (T4P) needed for DNA uptake, as well as wild-type *Nostoc*, which lacks natural DNA competence. This powerful demonstration may enable alternative opportunities for gene manipulation and biomolecule delivery into an even broader range of cyanobacterial species.

#### 5.3.1 Materials and Methods

**Bacterial strains and growth conditions.** All cloning procedures were carried out in *Escherichia coli* DH5 $\alpha$  grown in liquid LB medium at 37°C in a shaking incubator at 200 rpm or on solidified LB plates containing 1.5% agar. When appropriate, media were supplemented with antibiotics needed for propagation of a specific plasmid. Liquid cultures of wild-type *Synechocystis* sp. PCC 6803 were grown in BG11 medium (Rippka et al.[121]) supplemented with 10 mM TES buffer (pH 8.0) at 30°C under 50  $\mu$ mol photons m<sup>-2</sup> s<sup>-1</sup> of white light with constant shaking.

**Design of the integration vector.** Isolated genomic DNA of *Synechocystis* was amplified using the primers Hom1-F, Hom1-R and Hom2-F, Hom2-R (Table 1) to create the flanking homologous regions in the plasmid used for insertion of antibiotic-resistance cassette into the cyanobacterial genome, via homologous recombination. The two selected homologous regions (Hom1 and Hom2) target *slr0168*, a neutral site in the *Synechocystis* genome. The kanamycin resistance cassette was amplified from I5023 plasmid[188, 189] using primers Km-F and Km-R. The final linear vector was obtained by multiple-overlap-extension PCR. This vector was cloned into the pJET1.2 vector (Thermo-Scientific) to create pJET-Syn-Hom12 plasmid. Plasmids used for cloning and for transformation of *Synechocystis* were constructed using standard cloning techniques. All primers were purchased from Microsynth.

**Transformation of *Synechocystis*.** Cells were harvested from a 5 mL *Synechocystis* suspension in exponential growth phase by centrifugation, and they were resuspended in 100  $\mu$ L of modified BG11. 25 ng of plasmid DNA per transformation were added to the cell mixture, followed by a 5 hours incubation under illumination. Cells were plated onto 1.5% BG-11 agar supplemented with sodium thiosulfate (0.15%) and 2  $\mu$ g/mL kanamycin. After isolation of individual colonies, colonies were sequentially transferred onto agar plates containing increasing concentrations of kanamycin, to segregate the resistance-cassette in the cyanobacterial genome. Complete segregation was achieved at 25  $\mu$ g/mL kanamycin. Recombinant Taq

## Chapter 5. Outlook on Potential Applications of SWCNT-treated Photosynthetic Microbes

**Table 5.1** – Primers used in this study.

Primer name	Primer sequence (5' to 3')	Size (bp)
Hom1-F	CAG ATT GCC TTT GAC AAC AAT GTG G	25
Hom1-R	TCC ATA TAA ATC CCC GCC ACT G	22
Hom2-F	GAC CAA GCC CAA TTT CGT TTG	21
Hom2-R	ACC GCT AAA CCC ACC TCT TG	20
Km-F	CAA ACG AAA TTG GGC TTG GTC att tca ggt ggc act ttt cg	41
Km-R	CAG TGG CGG GGA TTT ATA TGG A ggt cat gaa caa taa aac tgt ctg c	47

DNA polymerase was used for nonpreparative PCR, such as colony PCR, to verify the correct incorporation of the DNA fragments into the *Synechocystis* genome.

**Preparation of LSZ-SWCNTs.** LSZ-SWCNTs were prepared by suspending 1 mg of HiPco nanotubes and 5 mg of lysozyme from chicken egg white (Sigma Aldrich) in 1 mL of 1 mM HEPES buffer (pH 7.4) and sonicating using a cup-horn sonicator (140 mm, Qsonica, LLC) for 90 minutes at 1% amplitude on ice. The sonicated SWCNT suspension was centrifuged (Eppendorf Centrifuge 5424 R) for 180 minutes at 16500 x g to pellet SWCNT aggregates. Unbound protein was removed through dialysis against 2 L of 1 mM HEPES buffer using a 300 kDa MWCO cellulose membrane. SWCNT concentrations were calculated from absorbance measurements at 632 nm in a UV-Vis-NIR scanning spectrometer (Shimadzu 3600 Plus) using an extinction coefficient of 0.036 L/(mg cm).

**Electrostatic grafting of DNA onto LSZ-SWCNTs.** The linear DNA vector was mixed with LSZ-SWCNTs in a 1:14 ratio (i.e. 100 ng DNA mixed with 1.4  $\mu$ g of LSZ-SWCNTs), and the solution was incubated at room temperature for 30 minutes. DNA incubation could be scaled up or down by keeping the DNA-to-LSZ-CNT mass ratio constant. The mixture was centrifuged at 16000 x g at room temperature for 10 minutes to remove possible aggregates.

**Characterization of DNA-LSZ-SWCNT complexes.** Following centrifugation of the DNA-LSZ-SWCNT mixtures, the pellet containing DNA-LSZ-SWCNT aggregates was resuspended in 1 mM HEPES buffer. 30  $\mu$ L of pellet and supernatant were loaded onto 1.25% agarose gel in 1X Tris-acetate-EDTA (TAE) buffer at 100 V for 45 minutes. DNA-LSZ-SWCNT complexes were recovered from the wells of the agarose gel for DNA purification. DNA was purified from the SWCNT suspension through phenol–chloroform alcohol extraction, by adding an equal volume of phenol-chloroform to the suspension. After centrifugation for 5 min at 16 000 x g at room temperature, the aqueous phase was collected, and the DNA was precipitated according to literature using ethanol supplemented with glycogen (Carl Roth) and sodium acetate (0.3 M).[190] The pellet was washed with 70% ethanol and resuspended in 1 mM HEPES. Recovered DNA vectors were amplified by PCR over 20 cycles. The amplified fragments were analysed by 0.75% agarose gel electrophoresis in TAE buffer, conducted at 90 V for 35 minutes. The DNA was stained with SYBR Gold (Thermo Fisher) for around 25 minutes and visualized on a blue-light imager.



**NIR imaging of DNA-LSZ-SWCNT interaction with *Synechocystis* cells.** Cells were harvested during the late exponential growth phase ( $OD_{750nm}$  between 1-1.5) by centrifugation, washed twice with 1 mM HEPES buffer (pH 7.4), and re-suspended in the same buffer to an  $OD_{750nm} = 0.9$ . Cells were fixed onto poly-lysine coated glass-bottom petri dishes by spotting 30  $\mu$ L of the cell suspensions for 10 minutes followed by washing with HEPES. The cells were then covered with 50  $\mu$ L of 1 mM HEPES buffer. DNA-LSZ-SWCNTs were added to the cells to reach a final concentration of 2 mg(SWCNT)/L. They were imaged using a custom-built optical setup consisting of an inverted microscope (Eclipse Ti-U, Nikon AG Instruments) with an oil-immersion TIRF 100 x objective (N.A. 1.49, Nikon) coupled to a CREST X-Light spinning-disk confocal imaging system (CREST Optics) (60  $\mu$ m pinholes) and an InGaAs camera (NIRvana 640 ST, Princeton Instruments). Samples were illuminated using a TriLine LaserBank system (Cairn Research) at 780 nm, and fluorescence was collected in wide-field mode using an 800 nm (Chroma) long-pass filter. Images were acquired using the Nikon NIS-Elements software (Nikon Instruments).

#### 5.3.2 Results and Discussion

The scheme in **Figure 5.2a** represents a simple integration DNA vector that was designed to achieve stable chromosomal incorporation of a kanamycin resistance marker within the *slr0168* neutral site in *Synechocystis*, via homologous recombination. Control transformation of naturally competent *Synechocystis* cells, followed by repeated plating on BG11-agar plates with increasing antibiotic concentrations (**Figure 5.2b**), allowed isolation of fully segregated transformants in which the kanamycin resistance marker was stably incorporated in the targeted site. The segregation process was monitored by colony PCR.

The proposed method for DNA immobilization on SWCNTs involved electrostatic grafting, in which SWCNTs were initially functionalized with LSZ to acquire a positive surface charge, and then incubated with negatively-charged linear or circular DNA vectors (**Figure 5.2c**). Following incubation (step 1), the DNA-LSZ-SWCNTs mixture was centrifuged to allow sedimentation of possible nanoparticle-DNA aggregates (step 2), and the supernatant was collected for further characterization (step 3). The adsorption of linear DNA on the surface of LSZ-SWCNTs was studied by agarose gel electrophoresis (step 4 and **Figure D.1**). The DNA-LSZ-SWCNT fractions were not able to migrate within the gel under the conditions tested, and remained entrapped within the top wells (**Figure D.1a**).

Previous studies have shown that, in contrast to free (uncomplexed) DNA, the condensation of nucleic acids by CNTs impede the intercalation of staining dyes, such as ethidium bromide, and quenches the fluorescence signal.[191] Similarly, we observed no fluorescent bands in the lanes corresponding to DNA-LSZ-SWCNTs from neither the supernatant nor the pellet fractions obtained after incubation of the complexes in step 1 (**Figure D.1b**). The absence of fluorescent bands within the gel suggested either the absence of free DNA in the fractions, or that the immobilization of DNA on the surface of LSZ-SWCNTs might hinder the binding

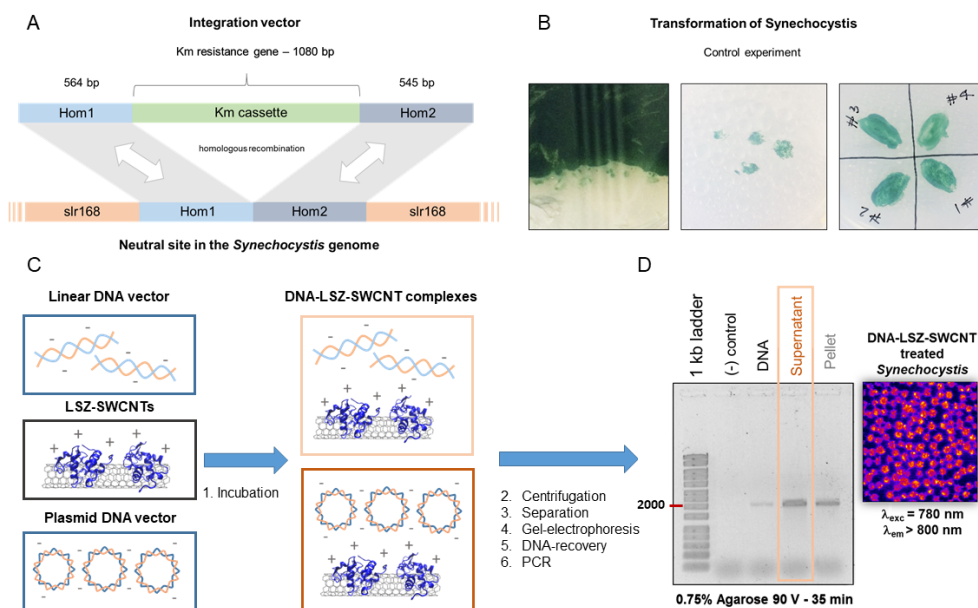


**Figure 5.2 – SWCNTs as scaffolds for DNA immobilization.** (A) Schematic representation of the vector construction scheme for the integration of a kanamycin resistance cassette (Km cassette) into the neutral docking site, *slr0168*, of *Synechocystis* sp. PCC 6803, resulting in disruption of the open reading frame of *slr0168*. (B) Control transformation of *Synechocystis* cells with the designed vector. Transformed colonies were transferred on agar plates at increasing kanamycin concentration. (C) DNA grafting onto LSZ-SWCNTs through electrostatic attachment. Following incubation (step 1), DNA-LSZ-SWCNT complexes are centrifuged (step 2). The supernatant is collected (step 3) for further characterization via agarose gel-electrophoresis (step 4). (D) Verification by PCR (step 6) of immobilized linear DNA vector on the surface of LSZ-SWCNTs, following DNA recovery (step 5) from the DNA-LSZ-SWCNT supernatant (i.e. stable DNA-LSZ-SWCNT fraction), and from the DNA-LSZ-SWCNT pellet (i.e. aggregated DNA-LSZ-SWCNT fraction). On the right, a widefield NIR image of *Synechocystis* cells incubated with stable DNA-LSZ-SWCNTs shows the localization of SWCNT fluorescence within the cells.

of SYBR Gold to DNA, similar to observations in previous works.[191] Hence, in order to confirm the association of DNA on the surface of LSZ-SWCNTs, and simultaneously verify the integrity of the vector, we collected the DNA-LSZ-SWCNT fractions from the gel wells and recovered the DNA from the nanotube surface through phenol-chloroform extraction and ethanol precipitation (step 5). The recovered DNA fragments were amplified by PCR and run on 0.75% agarose gel. The gel shown in **Figure 5.2d** (and in **Figure D.1c**) showed a stronger fluorescent band in the lane corresponding to the DNA extracted from the supernatant fraction of DNA-LSZ-SWCNTs. This observation confirmed that DNA could be absorbed on the surface of LSZ-SWCNTs, without compromising DNA integrity. Furthermore, stable DNA-LSZ-SWCNT complexes could accumulate within *Synechocystis* cells as demonstrated by NIR imaging of SWCNT fluorescence within the cells (**Figure 5.2d**).

## 5.4 Conclusions

Preliminary results presented in this chapter demonstrate the potential application of SWCNTs for improved bioelectricity generation from cells of cyanobacteria, as well as their suitability as scaffolds for targeted gene delivery. The SWCNT/*Synechocystis*-based electrodes presented herein are capable of capturing photosynthetically derived current under multiple light-dark cycles when incorporated in a BPV system. These electrodes show up to three-fold enhancement over conventional graphite electrodes under ferricyanide-mediated conditions. Future experiments in this area will focus on discerning the role of SWCNTs in the electron transfer process, by testing the effect of both metallic or semiconducting SWCNTs on photocurrents. Furthermore, future research on SWCNT integration into BPVs will focus on exploring alternative electrode configurations to further increase the optical transparency and improve long-term stability of generated photo-currents in these systems. Promising approaches for this purpose include the use of indium-tin-oxide electrode substrates for the immobilization of SWCNT-treated photosynthetic cells.

In addition to the advancements in bioelectricity generation, the SWCNTs also show a promising prospect for DNA delivery. We demonstrate the development of DNA-loaded LSZ-SWCNT hybrids that are able to localize in *Synechocystis* cells. Future developments will focus on demonstrating DNA uptake in non-competent cyanobacterial mutants ( $\Delta hfq$ ) and naturally incompetent strains such as *Nostoc*.



## 6 General conclusions and perspectives

Understanding and predicting the impacts of nanoparticle exposure on cells of living organisms is imperative for the continued development of SWCNT-based applications in the field of cell biotechnology. To this end, a rigorous assessment of key factors governing SWCNT interaction, across various species, and the long-term responses of these organisms to nanoparticle treatment, is necessary. Extended work is especially needed to further understand the exact interactions that can lead to long-term changes in cytotoxicity, compromising the survival of living systems to prolonged exposure to specific nano-probes. Although several studies thus far have elucidated many important aspects of SWCNT uptake mechanisms, function in, and impact on cells of eukaryotic species, as discussed in **Chapter 1**, our knowledge of the interaction of SWCNTs with cells of prokaryotic species has remained largely incomplete.

The studies presented herein investigated the impact of certain key physical properties of SWCNTs, such as size and surface chemistry, on their interaction capabilities with prokaryotic cells. In particular, this work focused on examining the interaction of fluorescent SWCNTs with both unicellular and filamentous strains of a photosynthetic microbe, cyanobacteria. This is a well-known model organism for the study of photosynthesis, and have been applied industrially for multiple "green" applications, including the production of high-value chemicals and the generation of bioelectricity.

In **Chapter 2**, we employed NIR fluorescence confocal microscopy, in combination with Raman spectroscopy and TEM, to explore the internalization of SWCNTs in unicellular *Synechocystis* sp. PCC 6803. These results showed that surface coatings possessing highly positive zeta-potentials can enable the accumulation of SWCNTs within the cells, without the need for any external mechanical assistance. Furthermore, this approach does not compromise the morphological integrity of the cell nor its photosynthetic performance. Similarly to previous observations of SWCNT uptake in eukaryotic systems, our studies showed that the internalization process is dependent on the SWCNT length, and that short SWCNTs, with lengths between 130 and 300 nm, preferentially translocate the membrane. By characterizing the SWCNT-cell interaction using TEM, we further discovered that SWCNTs can promote the transport of small proteins across cell membranes.

In *Chapter 3*, we extend this study to determine the species-dependency of nanoparticle uptake by examining the interaction of fluorescent SWCNTs with cells of filamentous cyanobacteria, *Nostoc* sp. Based on these findings, we conclude that the careful selection of appropriate SWCNT functionalizations can help to preserve long-term cell integrity, viability, and activity, and that this must be optimized for different cell membrane architectures. Notably, SWCNTs functionalized with positively charged wrappings were found to preferentially localize within the heterocyst compartments of *Nostoc* filaments, a feature that could be exploited for the development of alternative cell-specific staining and imaging technologies.

Our work has also uncovered important information on the long-term impacts of SWCNT interaction with prokaryotic systems that had yet to be addressed in the literature. For instance, the long-term SWCNT imaging studies presented in **Chapter 4** showed continued cell division following exposure to nanoparticles. This demonstrates that the growth of both unicellular and filamentous cyanobacteria can be sustained, indicating there are limited cytotoxic effects upon nanoparticle exposure. However, reduced doubling rates were observed compared to untreated cells, opening additional questions on the role of SWCNTs in the cell division process. To further elucidate this aspect, studying the impact of different SWCNT wrapping molecules on cell division is required. Extending the use of SWCNTs for the long-term monitoring of cell differentiation processes is one potential downstream application of our technique, and could be used to obtain valuable information on local variations of membrane structure within specific cell compartments.

The successful characterization of SWCNT translocation across a variety of cell architectures creates a more complete understanding of nanoparticle delivery. This is needed to expand SWCNT applicability and the use of this technology into an even broader range of living systems. **Chapter 5** shows the potential applications of the findings presented in this thesis in two possible domains, BPVs and gene-delivery. Preliminary studies on BPV fabrication and performance show improved bioelectricity generation from cells of unicellular cyanobacteria treated with SWCNTs. Future research on the integration of SWCNTs into BPVs will focus on exploring alternative electrode configurations to further improve the optical transparency and increase long-term stability of generated photo-currents in these systems. Promising approaches for this include the use of indium-tin-oxide electrode substrates for the immobilization of SWCNT-treated photosynthetic cells, as well as the use of purified metallic SWCNTs, which would offer greater electrical conductivity.

Based on the findings presented through *Chapter 2* and *Chapter 3*, future research on the SWCNT-complexes developed in these thesis could expand the capabilities of these hybrids for biomolecule translocation to transport larger biomolecules, such as plasmid DNA. The preliminary studies shown in *Chapter 5* indicated that electrostatic grafting of DNA on the surface of these positively-charged SWCNT complexes is a promising method for obtaining stable vectors for gene delivery applications. These applications are particularly advantageous for cyanobacteria cells, as the majority strains are not readily capable of active DNA uptake and require tedious, specialized procedures for DNA transformation. The diverse membrane archi-

---

texture of these species will undoubtedly require an equally diverse set of SWCNT-wrappings to preserve long-term cell viability while simultaneously facilitating maximised uptake efficiencies. In conclusion, the work reported in this thesis expanded the current knowledge of SWCNT interaction with cells of photosynthetic microbes, and further demonstrated the application of non-covalently functionalized SWCNTs for long-term imaging, biomolecule delivery and improved bioelectricity generation in prokaryotic systems.







## Appendix



# A Interaction of SWCNTs with Unicellular Cyanobacteria

**Uptake of SWCNTs by isolated plant chloroplasts.** Chloroplasts were isolated from commercially available spinach leaves as described by Giebel et al.[192] with modifications. Briefly, 15 g of spinach leaves were ground in the presence of 30 mL of chilled chloroplast isolation buffer (0.05 M sodium-phosphate buffer (pH 7.3) made with 0.4 M sucrose and 0.01 M KCl). After centrifuging at 200 x g for 1 minute at 4°C to pellet unbroken cells and fragments, the supernatant was collected and transferred to a 50 mL tube. The solution was centrifuged three times at 1500 x g for 10 minutes at 4°C, and pellets containing chloroplasts were stored in the dark at 4°C. Freshly isolated chloroplasts were immobilized onto poly-lysine coated glass-bottom Petri dishes and imaged in the near-infrared using the custom-built confocal microscope described previously.

## Appendix A. Interaction of SWCNTs with Unicellular Cyanobacteria

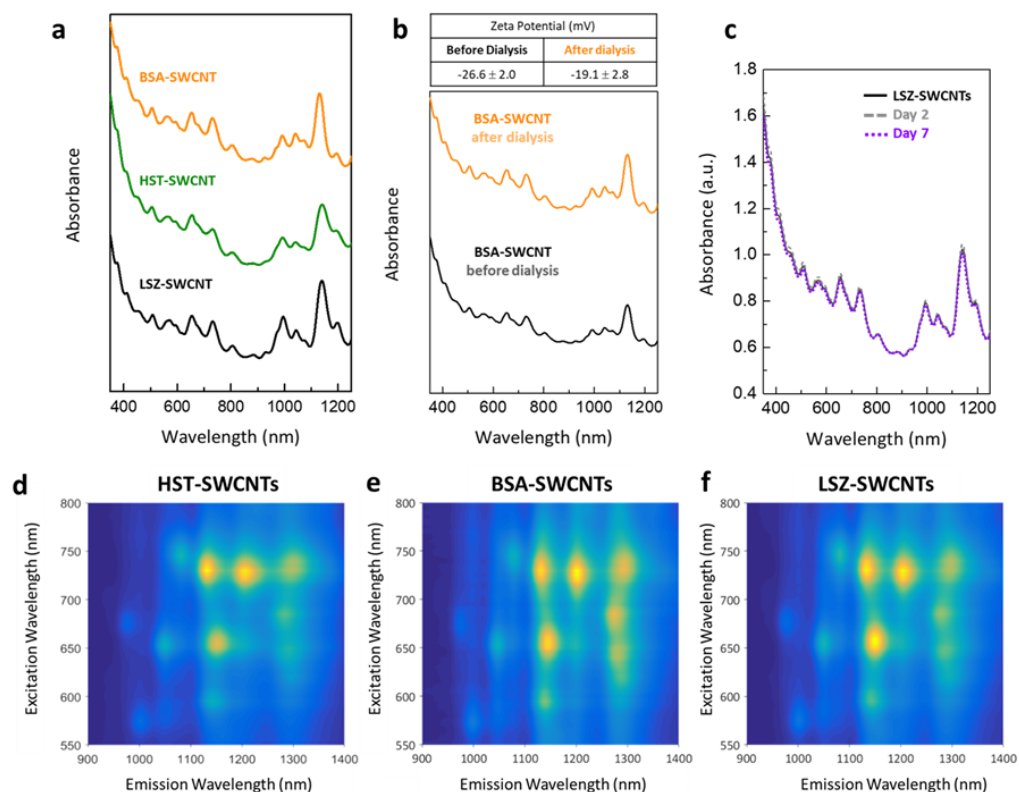


**Figure A.1 – Optical Characterization of SWCNT Solutions.** (a) Absorption spectra of SWCNTs functionalized with LSZ (black), HST (green), and BSA (orange). (b) Stability of BSA-SWCNT suspension after removal of excess protein molecules via dialysis with 300 kDa cut-off membrane. The zeta-potential (mV) of the BSA-SWCNT solution slightly increases after dialysis. Absorption spectra of BSA-SWCNTs before (black) and after (orange) dialysis show sharp van Hove peaks that are indicative of individually dispersed SWCNTs. (c) Long-term stability of LSZ-SWCNT suspensions. Absorbance spectra of LSZ-SWCNTs in 1 mM HEPES buffer after dialysis (dark grey, solid line) and after 2 (grey, dashed line) or 7 days (purple, dotted line) all show distinct van Hove peaks. All absorption spectra are normalized to absorbance at 930 nm. Photoluminescence plots of (d) HST-SWCNTs, (e) BSA-SWCNTs, and (f) LSZ-SWCNTs.

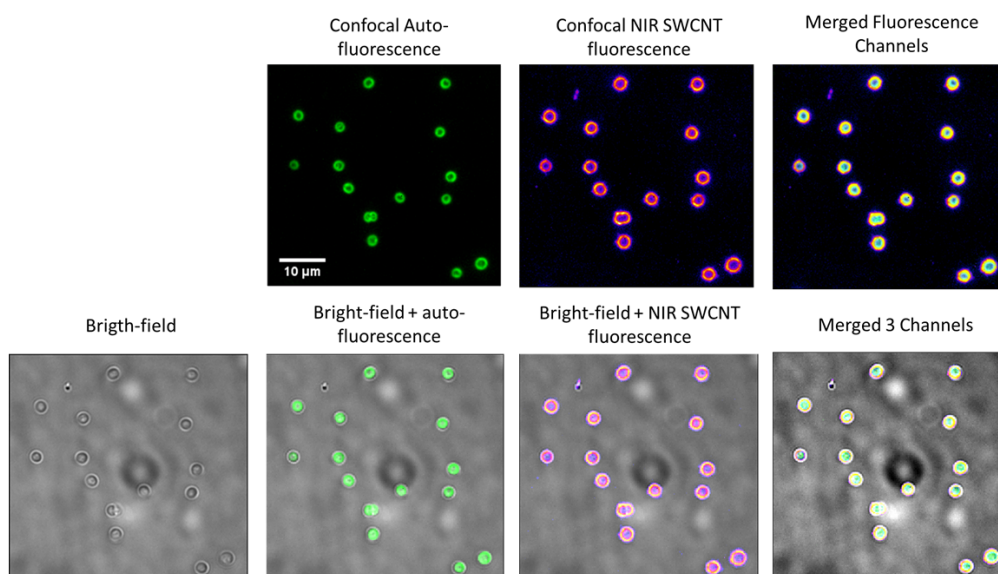


**Figure A.2 – NIR Confocal and Bright-field Imaging.** Representative NIR fluorescence (top), bright-field (bottom), and merged images of *Synechocystis* cells treated with 2 mg/L LSZ-SWCNTs. The overlay of the confocal SWCNT fluorescence and the bright-field images shows enhanced SWCNT fluorescence overlapping with the peripheral regions of the cells, suggesting that the majority of the nanoparticles lie within the periplasmic region.

## Appendix A. Interaction of SWCNTs with Unicellular Cyanobacteria

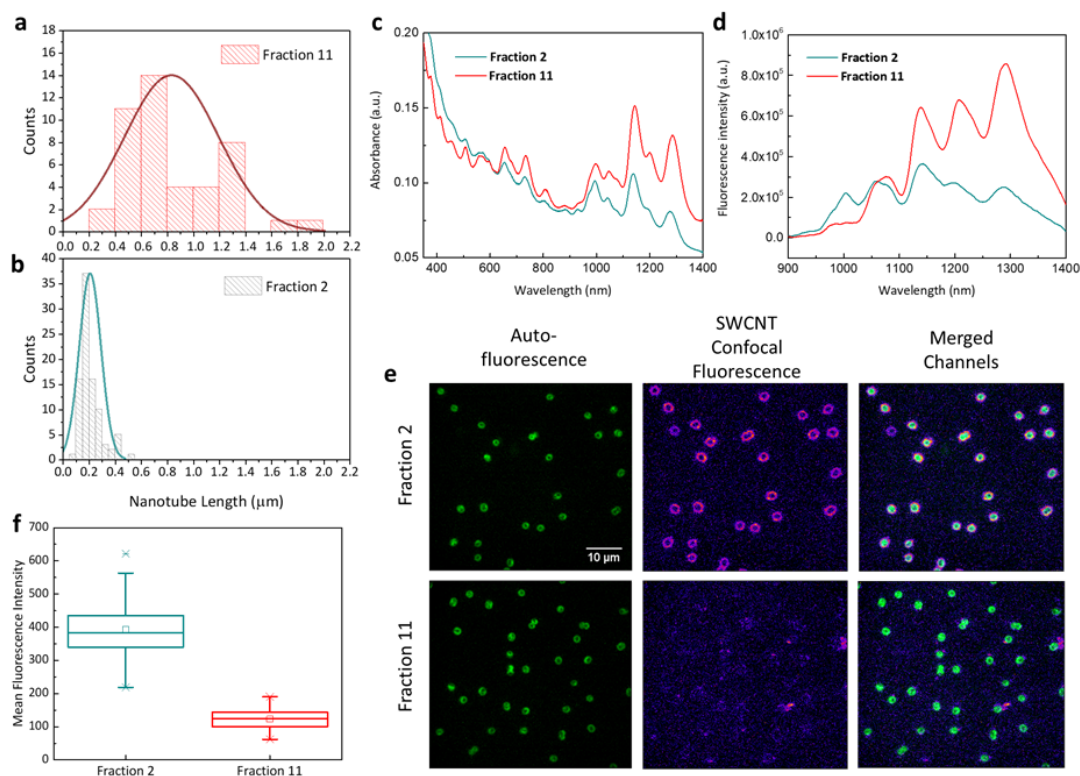


**Figure A.3 – Effect of SWCNT-Length on Nanoparticle Internalization.** (a,b) Length distribution of SWCNT fractions 11 and 2, containing preferentially long-SWCNTs and short-SWCNTs respectively. From this point forward, data that are referred to fractions 11 and 2 will be depicted in red and dark-cyan colors respectively. (c) Absorption spectra of length sorted SWCNTs from fractions 11 and 2, after resuspension with LSZ proteins. The solutions were adjusted to obtain the same SWCNT concentration (same absorbance at 632 nm). (d) Fluorescence spectra of length sorted-SWCNTs suspended with LSZ proteins. SWCNT fluorescence was excited at 780 nm. At the same SWCNT concentration, the short-SWCNT fraction 2 shows lower fluorescence levels above 1100 nm. (e) Confocal fluorescence images of wild-type *Synechocystis* cells incubated with LSZ-SWCNTs from fraction 2 and fraction 11 at the same concentration. (f) The analysis of mean SWCNT-fluorescence intensity shows that higher fluorescence levels are detected within the cells incubated with short-SWCNTs of fraction 2 than in those that interact with longer SWCNTs from fraction 11.

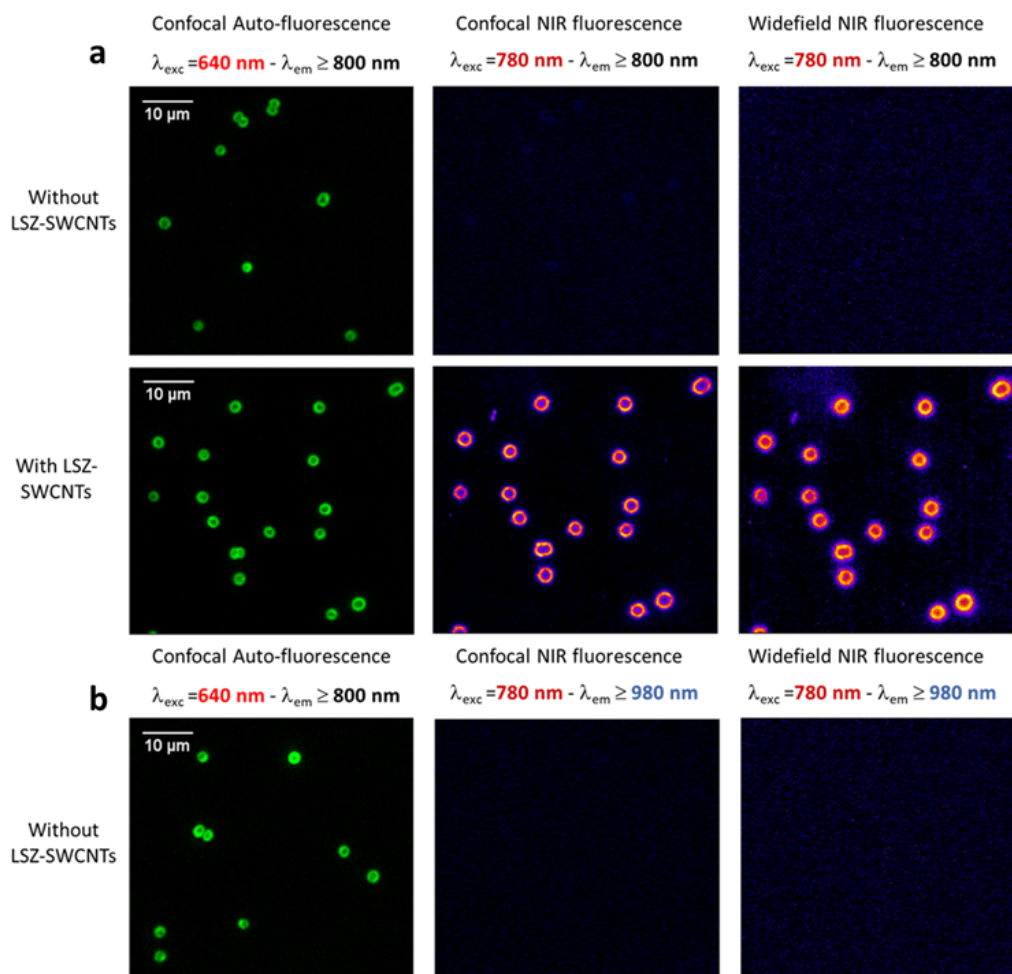


**Figure A.4 – NIR Imaging of Control *Synechocystis* cells.** (a) Representative NIR images of *Synechocystis* cells treated without or with LSZ-SWCNTs (top and bottom respectively). The first column shows autofluorescence of *Synechocystis* cells excited with a 640 nm laser in confocal mode. In contrast to cells treated with LSZ-SWCNTs, control cells without SWCNTs do not show any significant autofluorescence above 800 nm when excited with a 780 nm laser, neither in confocal (3.7 mW/cm<sup>2</sup> laser power) or in widefield mode (1.8 mW/cm<sup>2</sup> laser power). (b) Representative NIR images of control *Synechocystis* cells without LSZ-SWCNTs, imaged in confocal and in widefield mode, with a 780 nm laser excitation. No autofluorescence is observed above 980 nm.

## Appendix A. Interaction of SWCNTs with Unicellular Cyanobacteria

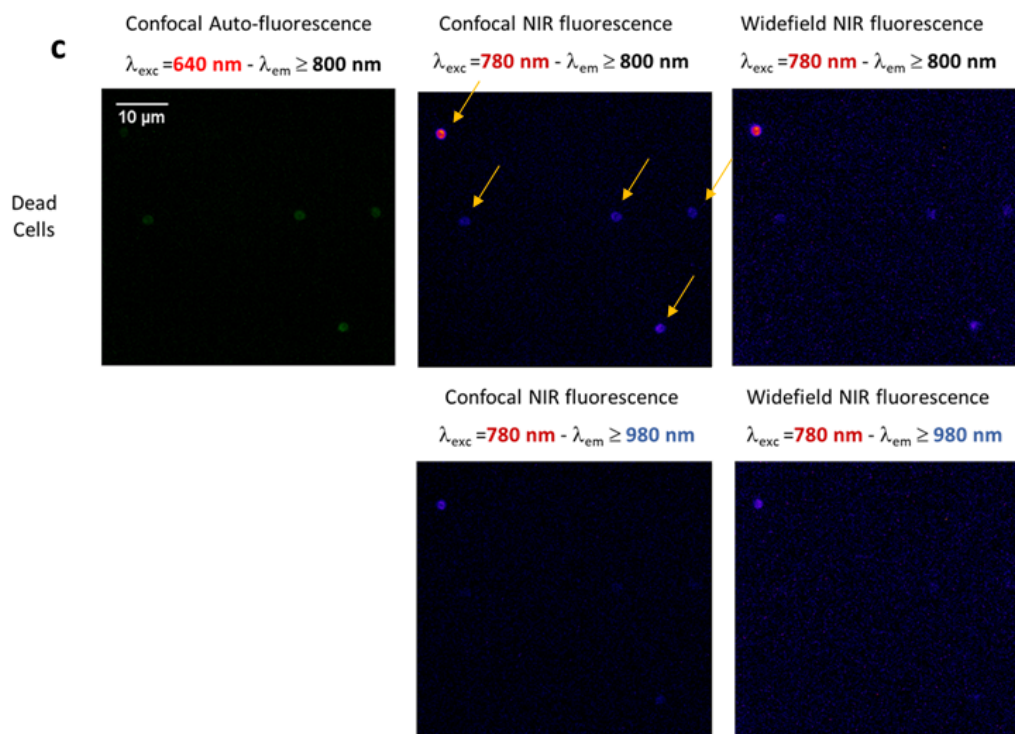


**Figure A.5 – NIR Imaging of Dead *Synechocystis* cells.** NIR images of *Synechocystis* cells suspended in 100% ethanol for 30 minutes. In contrast to living cells, ethanol-killed cells do not exhibit any autofluorescence above 800 nm when excited at 640 nm. On the other hand, dead cells shows significant levels of autofluorescence above 800 or 980 nm when excited with 780 nm laser.



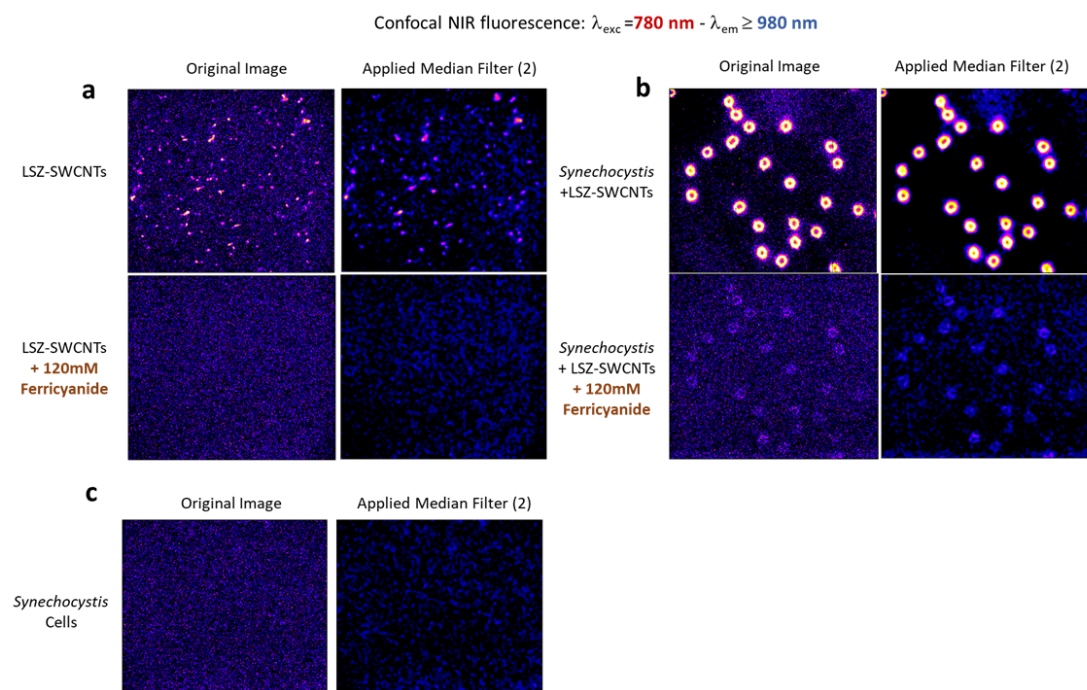


**Figure A.6 – Confocal NIR Fluorescence Imaging of *Synechocystis* after ferricyanide addition.** Confocal NIR fluorescence images of (a) individual LSZ-SWCNTs immobilized onto poly-lysine coated glass-slides, (b) *Synechocystis* cells treated with 2 mg/L LSZ-SWCNTs, and (c) control *Synechocystis* cells before and after addition of 120 mM ferricyanide solution. Background-corrected images are compared to images to which a median filter (size = 2) was applied for noise removal. While not significant NIR signal is detected for individual LSZ-SWCNTs, *Synechocystis* cells retain substantial NIR fluorescence after addition of ferricyanide. By contrast, control *Synechocystis* cells do not show any appreciable NIR auto-fluorescence in absence of LSZ-SWCNTs. All images are acquired under 780 nm excitation, using a 980 nm long-pass emission filter, at 3.7 mW/cm<sup>2</sup>.

## Appendix A. Interaction of SWCNTs with Unicellular Cyanobacteria

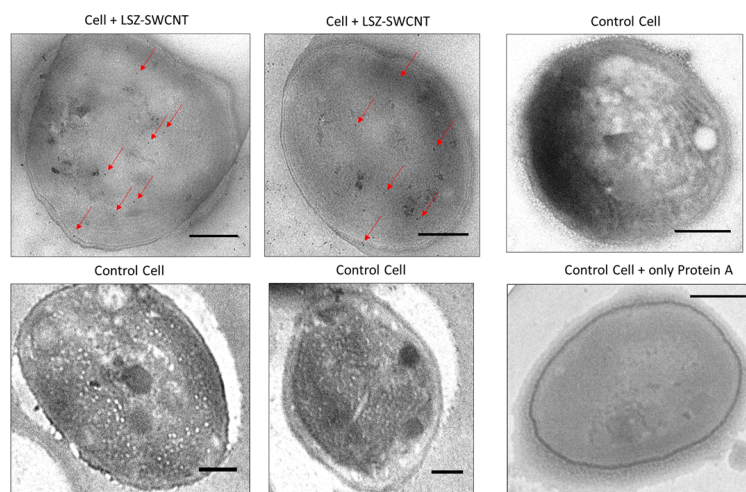


**Figure A.7 – Transmission electron microscopy (TEM) immunogold labeling of *Synechocystis* cells.** TEM sections of *Synechocystis* cells treated with LSZ-SWCNTs (Cell + LSZ-SWCNTs) or with LSZ alone (Control cells), labeled with anti-lysozyme antibody and 10 nm gold-labeled secondary antibody. *Synechocystis* cells stained with only 10 nm gold-labeled secondary antibody do not show any unspecific labeling (bottom right). Gold nanoparticles inside *Synechocystis* cells are indicated with red arrows. Scale bars on the images correspond to 500 nm.

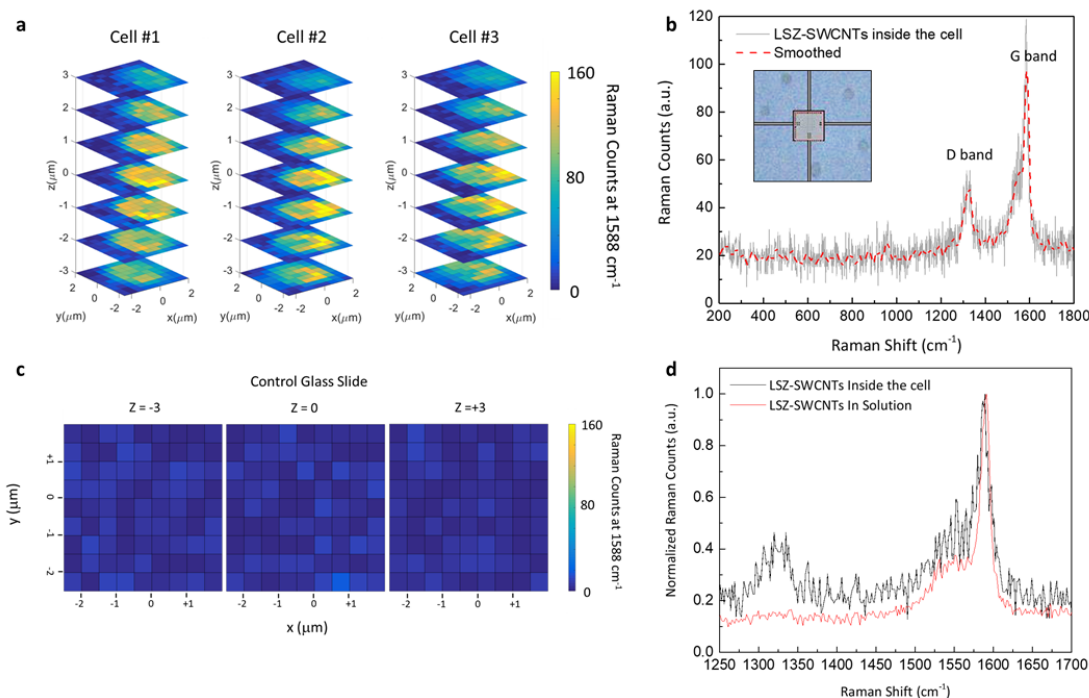


**Figure A.8 – Confocal Raman Characterization of SWCNT Internalization in *Synechocystis*.** (a) Representative confocal 3D Raman mapping of the characteristic SWCNT G'-band used to explore the spatial distribution of LSZ-SWCNTs within cells of wild type *Synechocystis* that are immobilized onto a poly-lysine coated glass-slide. Values correspond to SWCNT intensity at 1580 cm<sup>-1</sup> under a green laser excitation of 532 nm. (b) Typical Raman spectrum corresponding to a central point of the scanning grid (x,y = 0) for a cell containing SWCNTs. The inset shows a representative brightfield image with a 9 x 9 mapping grid centered on a *Synechocystis* cell. (c) Confocal Raman z-stacks acquired for background glass slide show no contaminating signal at 1580 cm<sup>-1</sup> under excitation with 532 nm laser. (d) Comparison of Raman spectra of LSZ-SWCNTs inside the cell (black) and in solution (red).

**Imaging cell interaction with poly-arginine functionalized SWCNTs.** Poly-arginine SWCNTs were prepared by suspending 0.5 mg of HiPco nanotubes and 20 mg of poly-L-arginine (>70000 MW, Sigma Aldrich) in 1 mL of 1 mM HEPES buffer (pH 7.4) and sonicating for 90 minutes at 1% amplitude on ice. The sonicated SWCNT suspension was centrifuged (Eppendorf Centrifuge 5424 R) for 180 min at 16500 x g to pellet SWCNT aggregates. Cells were immobilized onto poly-lysine coated glass bottom Petri dishes and treated with poly-arginine/SWCNTs at a final concentration of 2 mg/L. Treated cells were imaged by NIR widefield microscopy (**Figure A.9**).

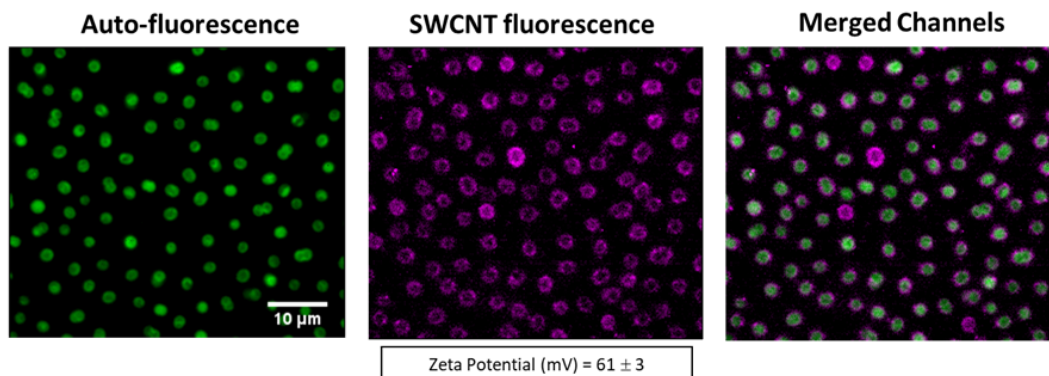


**Figure A.9 – Interaction of *Synechocystis* with poly-arginine/SWCNTs.** Representative widefield fluorescence image of *Synechocystis* cells after incubation with SWCNTs functionalized with poly-arginine. Fluorescence intensity was recorded for cell autofluorescence (excitation at 640 nm, emission above 800 nm) and SWCNT fluorescence (excitation at 780 nm, emission above 800 nm).

**Cell viability measurements.** To assess the effect of SWCNT interaction on cell viability, suspensions of *Synechocystis* cells, previously incubated for 1 hour with LSZ-SWCNTs, were washed two times with 1 mM HEPES buffer (pH 7.5) and plated in duplicate on BG-11 agar plates supplemented with sodium thiosulfate (0.15%). Plates were incubated for 10 days at 30°C under constant illumination of  $25 \mu\text{mol photons m}^{-2} \text{s}^{-1}$  (**Figure A.10**). Alternatively, 5  $\mu\text{L}$  volumes of serially diluted ( $10^0$ ,  $10^{-1}$ ,  $10^{-2}$ ,  $10^{-3}$  and  $10^{-4}$ ) *Synechocystis* cells suspensions treated for 1 hour with LSZ-SWCNTs, DNA-SWCNTs (at 2 mg/L concentration), LSZ alone (5 mg/mL concentration) or HEPES only as control, were spotted on BG-11 agar plates. Plates were incubated for 7 days at 30°C under constant illumination of  $25 \mu\text{mol photons m}^{-2} \text{s}^{-1}$ . After 7 days pictures of the plates were acquired with a gel imager (**Figure A.11**). Colonies were counted for the  $10^{-4}$  diluted spot using the ImageJ software. We counted  $25.7 \pm 0.4$  colonies for the control,  $18.6 \pm 2.3$  colonies for LSZ treated cells,  $27.3 \pm 2.4$  colonies for the DNA-SWCNT treated cells, and  $19.3 \pm 5$  colonies for the LSZ-SWCNT treated cells.

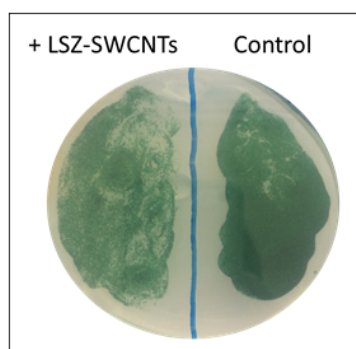


**Figure A.10 – Cell Growth on Agar.** *Synechocystis* cell growth after 10 days under illumination (ca.  $25 \mu\text{mol photons m}^{-2} \text{s}^{-1}$ ) on a BG-11 agar in the absence (right) and presence (left) of LSZ-SWCNTs.

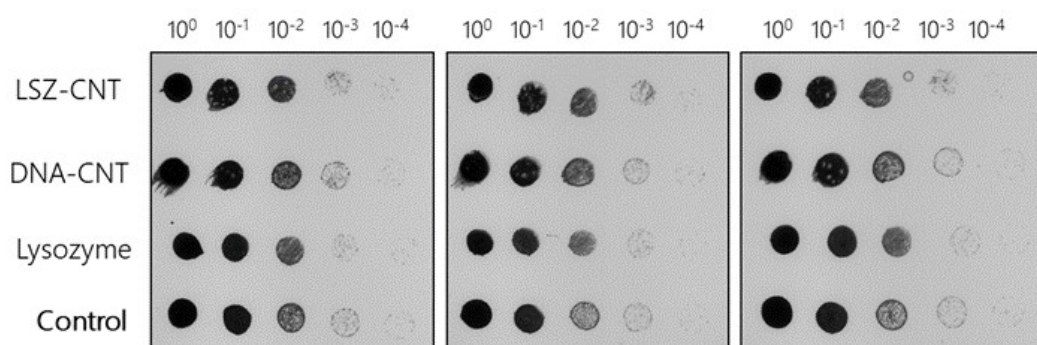


**Figure A.11 – Serial dilutions on agar plate.** Triplicates of *Synechocystis* growth after treatment with LSZ-SWCNTs, DNA-SWCNTs, lysozyme (5 mg/mL) or buffer only as control, following 7 days of incubation on BG-11 agar plate. 5  $\mu$ L aliquots of cells from a dilution series representing 100,  $10^{-1}$ ,  $10^{-2}$ ,  $10^{-3}$  and  $10^{-4}$  of the original cell suspensions were spotted on the agar plates.

Summary				
Groups	Count	Sum	Average	Variance
- LSZ-SWCNTs	3	494.64	164.88	36.4608
+ LSZ-SWCNTs	3	480.48	160.16	106.0608
Anova				
Source of variation	SS	F	P-value	F crit
Between Groups	33.4176	0.47	0.53	7.70
Within Groups	285.0432			

**Table A.1 – One-way Anova analysis of the rates of the oxygen production under illumination with (+ LSZ-SWCNTs) and without (- LSZ-SWCNTs) SWCNTs.**

## Appendix A. Interaction of SWCNTs with Unicellular Cyanobacteria

**Computational Modeling.** A dynamic nonlinear least squares (DNLS) problem to determine the unknown parameters of the proposed kinetic model was solved in Matlab by using a free Toolbox for optimization called “OPTI Toolbox”<sup>2</sup>. The problem is setup as a standard Nonlinear Least Squares problem, where the nonlinear experimental functions to be fitted involve solving a system of ordinary differential equations (ODEs) using a numerical integration scheme. The ODE is written in the form:

%ODE system

$$\begin{aligned} ode = & @(t, p, z)[(-p(1) * z(1)) * (p(2) - z(2))); \\ & (p(1) * z(1)) * (p(2) - s(2)) - p(3) * z(2) - \\ & p(3) * z(2)] \end{aligned} \quad (A.1)$$

where  $z$  is the vector of the observations of the system and  $p$  is the vector of the parameters, namely the kads of nanotube adsorption onto the cell wall,  $[SWCNT]_{max}$ , the maximum binding sites, and the kin of nanotube internalization. Since the set of experimental data is represented by the time-traces of SWCNT fluorescence variation at the periphery and at the center of the cell, all SWCNT concentrations reported in the model have been expressed in terms of fluorescence counts. Therefore a direct correlation between the varying amount of carbon nanotubes bound to or penetrated into the cell, and the observed NIR-fluorescence accumulation over time has been assumed. OPTI introduces additional arguments to the OPTI constructor: “ode” for supplying the ODE function, the vector  $z0$  for supplying the initial state vector and  $\theta_0$  for the starting guess of the parameters. The initial state vector  $z0$  contains the values of initial SWCNT concentration expressed in terms of initial fluorescence counts at the moment of addition of the carbon nanotubes. The inherent function *optidynset* of the OPTI toolbox has been used to fit the solution of the system of differential equations only to output states where experimental data have been obtained, namely the time traces of  $[SWCNT]$  at the periphery and at the center of the cell.

OPTI Fit Statistics	
$R^2$	0.973659
Adjusted $R^2$	0.973628
RMSE	105.156
SSE	1.87651 e+07
Model Form	Zero (No Intercept)

---

Nonlinear Least-Squares Confidence Interval and Coefficient Statistics				
Parameter	Estimate (95% CI)	Std. Error	<i>t</i> Value	<i>p</i> Value
$k_{ads}$	$9e-08 \pm (3e-09)$	1.6 e-09	57.2748	0
$SWCNT_{max}$	$3220 \pm 48$	44.4291	131.848	0
$k_{in}$	$0.00015 \pm (2e-06)$	1.1 e-06	138.775	0

**Table A.2** – Goodness of fit for curve fitting and parameter estimation problems calculated with Matlab OPTI Toolbox.





## B Interaction of SWCNTs with Filamentous Cyanobacteria

**Cell treatment with LSZ-SWCNTs in solution.** Cells were harvested during the late exponential growth phase ( $OD_{750nm}$  between 1-1.5) by centrifugation, washed twice with 1 mM HEPES buffer (pH 7.4), and re-suspended in the same buffer to an  $OD_{750nm} = 0.9$ . LSZ-SWCNTs were added to the cell suspension to desired final concentration of 2 mg/L. Cells and SWCNTs were allowed to interact at room temperature, in the dark, for 10 minutes under mixing.

**Isolation of heterocysts.** Heterocysts of *Nostoc* sp. were isolated following a modified protocol from Ermakova et al. [193] Briefly, cells were cultivated in BG11<sub>0</sub> (without addition of combined nitrogen) supplemented with 10 mM TES buffer (pH 8.0) at 30°C under 50  $\mu\text{mol photons m}^{-2} \text{ s}^{-1}$  of white light with constant shaking. Filaments (20 mL) were harvested during the logarithmic growth phase ( $OD_{750nm}$  between 1-1.5) by centrifugation at 5000 rpm, at room temperature for 5 minutes. After discarding the growth medium, pellets were resuspended in 20 mL of extraction buffer containing 50 mM HEPES-NaOH (pH 7.2), 0.4 M sucrose, 10 mM NaCl and 10 mM EDTA (all reagents were from Sigma Aldrich). Fresh lysozyme was added to the suspension to a final concentration of 1 mg/mL, following incubation for 1 hour at 30°C with continuous mixing on orbital shaker (180 rpm). Cells were sonicated for 1 min in water bath (37 kHz at 40% power) filled with cold water. Following digestion of vegetative cells, the cell suspension was centrifuged at 1000 x g for 5 min at 4°C, and the blue supernatant was discarded. The pellet containing heterocysts was resuspended in 10 mL of cold extraction buffer, then vortexed and centrifuged at 250 x g for 3 min at 4°C. These last steps were repeated twice until a colorless supernatant was obtained. The residual pellet is finally washed with 1 mM HEPES buffer (pH 7.4).

**Spheroplast induction in *Nostoc*.** Filaments of *Nostoc* sp. were harvested during the logarithmic growth phase ( $OD_{750nm}$  between 1-1.5) by centrifugation at 5000 rpm, at room temperature for 5 minutes. Pellets were resuspended into a spheroplast-induction solution containing 0.5 M mannitol, 1 mM EDTA, 10 mM TES and 1 mg/mL lysozyme. Cells were incubated at 30°C for 4 hours under shaking conditions, followed by centrifugation at 5000 rpm for 5 min. The sedimented spheroplasts were resuspended in 1 mM HEPES buffer (pH 7.4).

## Appendix B. Interaction of SWCNTs with Filamentous Cyanobacteria

**Alcian Blue staining.** The polysaccharide layer of heterocysts was stained with Alcian blue. Specifically, 2  $\mu\text{L}$  of Alcian blue solution (1% in 3% acetic acid) was added to 1 mL of a culture containing *Nostoc* filaments and incubated for 10-15 minutes.

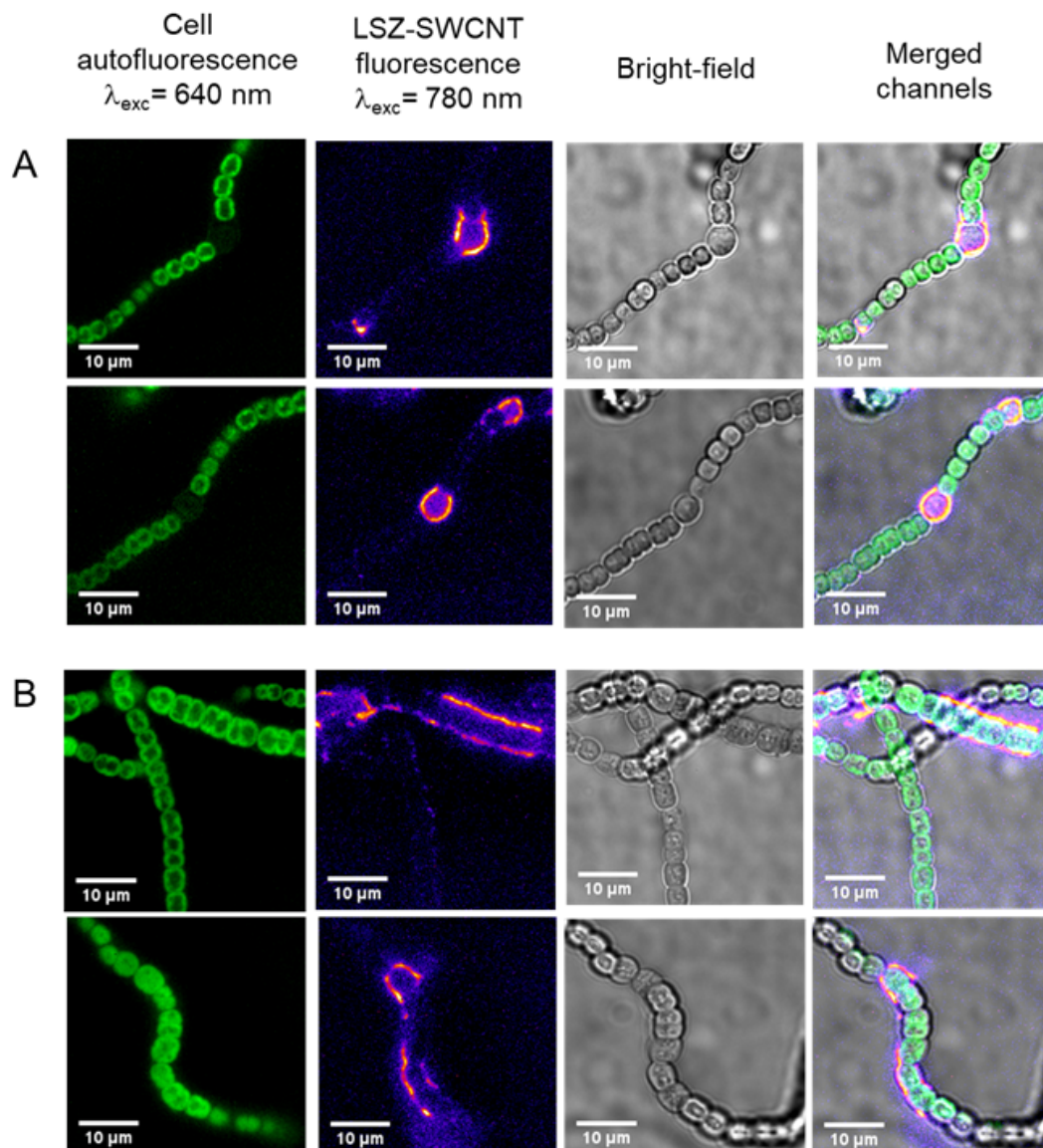


**Figure B.1 – NIR Imaging of LSZ-SWCNT Interaction with *Nostoc* and *Nostoc*-Het cells.** Representative images of (a) *Nostoc*-Het cells and (b) *Nostoc* cells immobilized onto poly-lysine coated glass slides, after incubation with LSZ-wrapped SWCNTs. Fluorescence intensity was recorded for cell autofluorescence (excitation at 640 nm, emission above 800 nm), and SWCNTs in confocal mode (excitation at 780 nm, emission above 980 nm, at 3.7 mW/cm<sup>2</sup>).

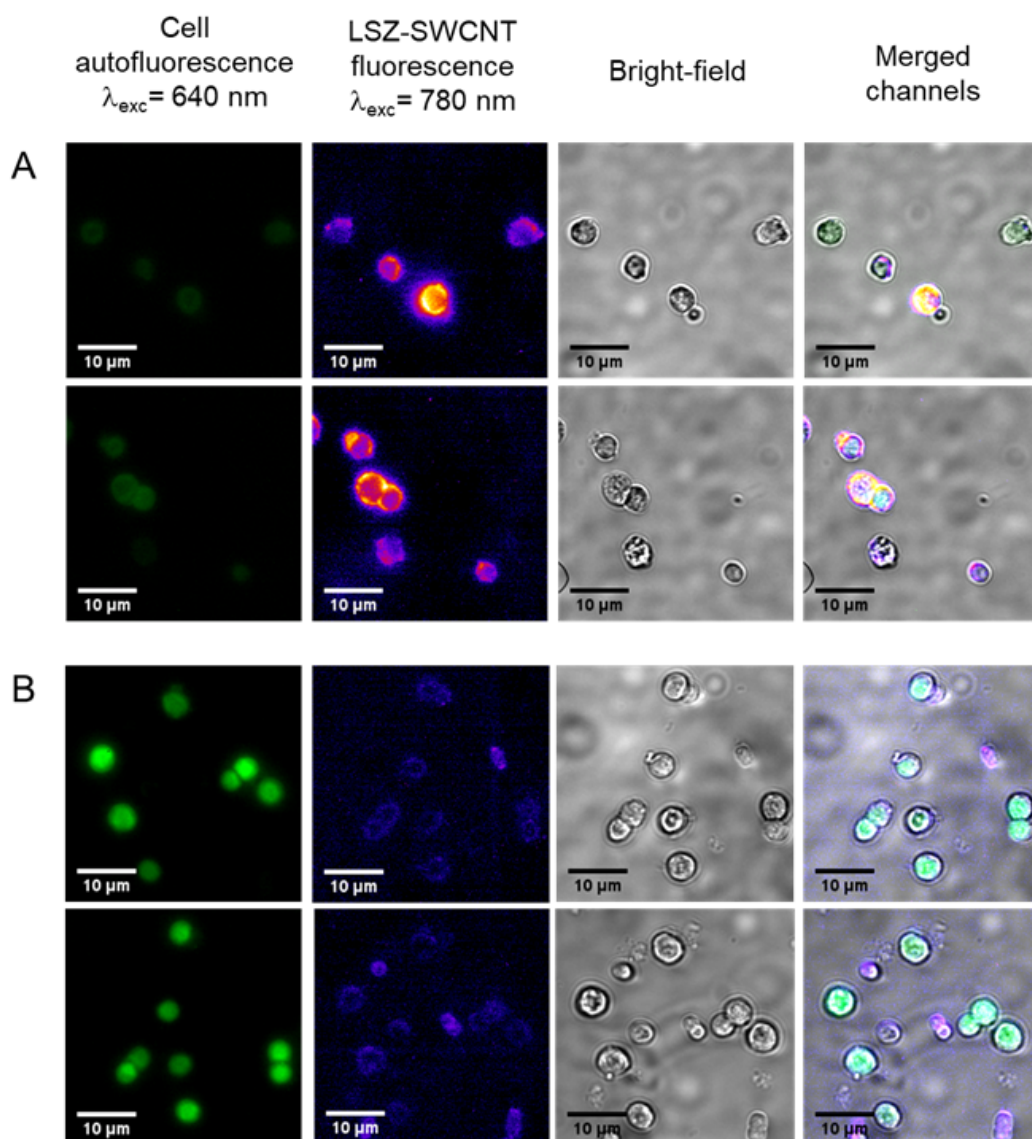


**Figure B.2 – NIR Imaging of SWCNT Interaction with isolated *Nostoc* heterocysts and spheroplasts.** Representative images of isolated (a) *Nostoc* heterocysts and (b) *Nostoc* spheroplasts after incubation with LSZ-wrapped SWCNTs. Fluorescence intensity was recorded for cell autofluorescence (excitation at 640 nm, emission above 800 nm), and SWCNTs in confocal mode (excitation at 780 nm, emission above 980 nm, at  $3.7 \text{ mW/cm}^2$ ). Due to diminished pigmentation, isolated heterocysts displayed reduced cell autofluorescence compared to spheroplasts of vegetative cells. On the contrary, heterocysts exhibited stronger SWCNT intensity levels under excitation at 780 nm.

## Appendix B. Interaction of SWCNTs with Filamentous Cyanobacteria

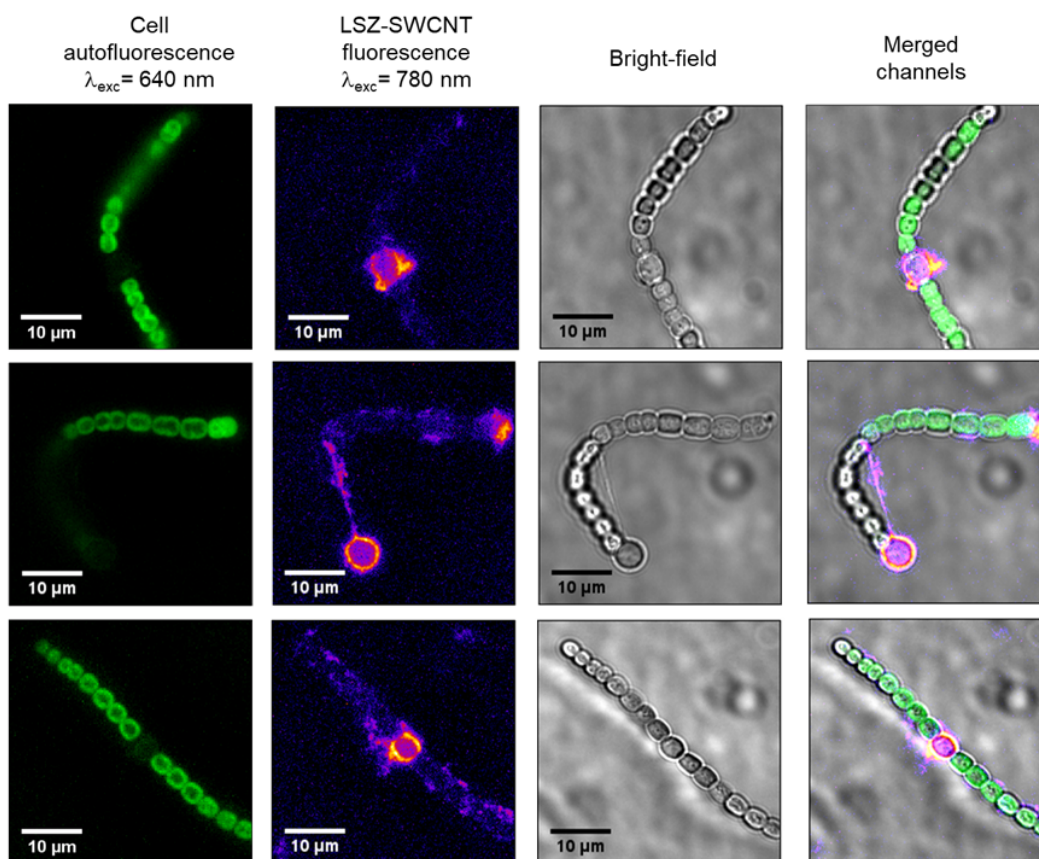


**Figure B.3 – NIR Imaging of SWCNT Interaction with *Nostoc-Het* cells in solution under mixing.** Representative images of *Nostoc-Het* cells after incubation with LSZ-wrapped SWCNTs in solution of 1 mM HEPES buffer, under shaking. Fluorescence intensity was recorded for cell autofluorescence (excitation at 640 nm, emission above 800 nm), and SWCNTs in confocal mode (excitation at 780 nm, emission above 980 nm, at 3.7 mW/cm<sup>2</sup>).

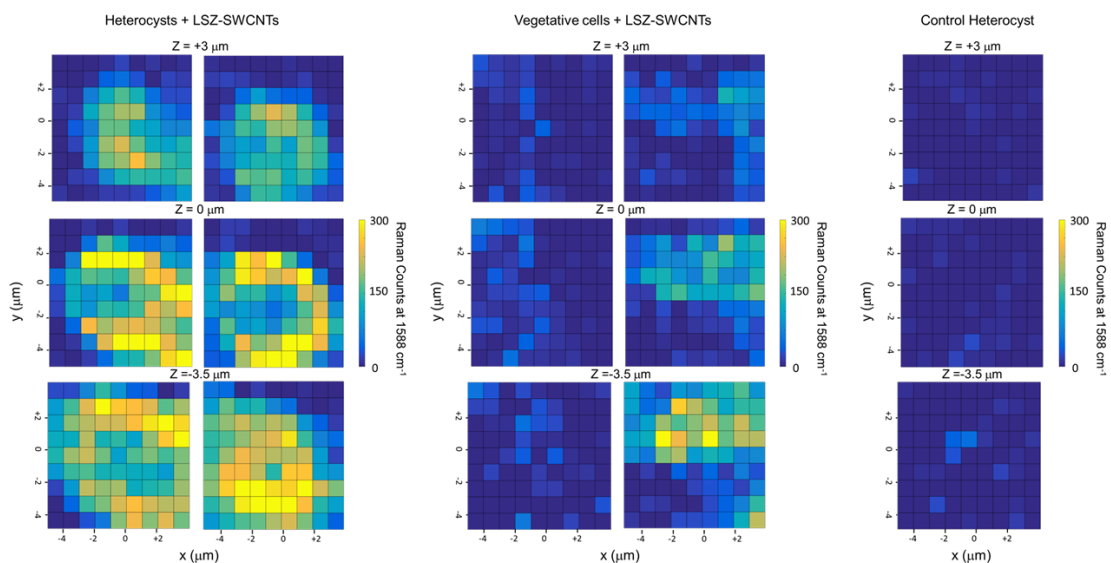


**Figure B.4 – Confocal Raman Characterization of SWCNT Distribution in *Nostoc* heterocysts.** Representative confocal 3D Raman mapping of the characteristic SWCNT G'-band used to explore the spatial distribution of LSZ-SWCNTs within heterocysts (**left**) or vegetative cells (**center**) of *Nostoc* filaments that are immobilized onto a poly-lysine coated glass-slide. Values correspond to SWCNT intensity at  $1580\text{ cm}^{-1}$  under a green laser excitation of  $532\text{ nm}$ . Confocal Raman z-stacks acquired for *Nostoc* heterocyst without LSZ-SWCNTs (**right**) shows no contaminating signal at  $1580\text{ cm}^{-1}$  under excitation with  $532\text{ nm}$  laser.



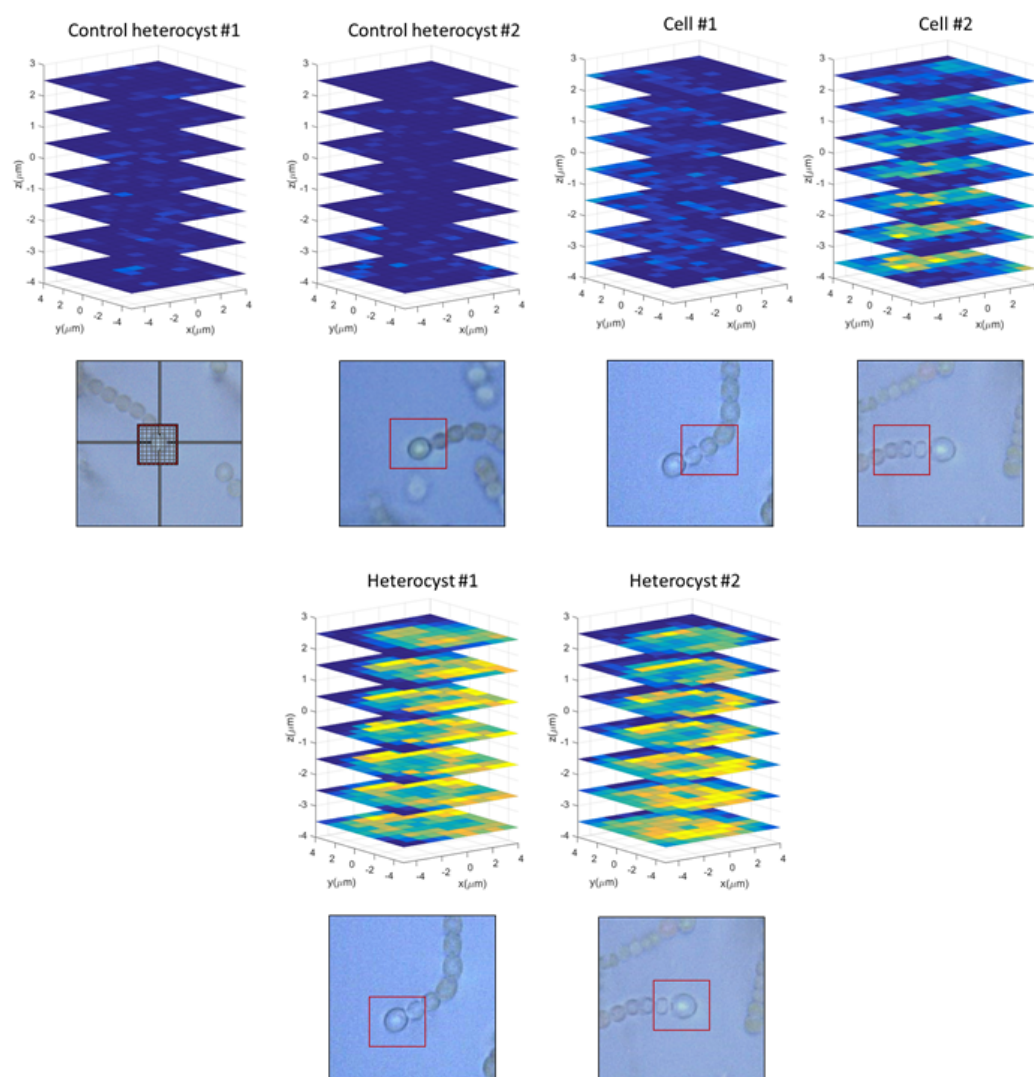


**Figure B.5 – 3D Confocal Raman maps of SWCNT Distribution in *Nostoc* heterocysts.** Full confocal Raman 3D maps of the characteristic SWCNT G'-band used to explore the spatial distribution of LSZ-SWCNTs within heterocysts (Heterocyst #1 and #2) or vegetative cells (Cell #1 and #2) of *Nostoc* filaments. Control 3D Raman maps of G'-band distribution in control heterocysts in absence of LSZ-SWCNTs is shown as control (Control heterocyst #1 and #2). The images below each Raman map show the corresponding brightfield images of analyzed *Nostoc* cells. The first image shows a 9 x 9 mapping grid centered on a *Nostoc* heterocyst.

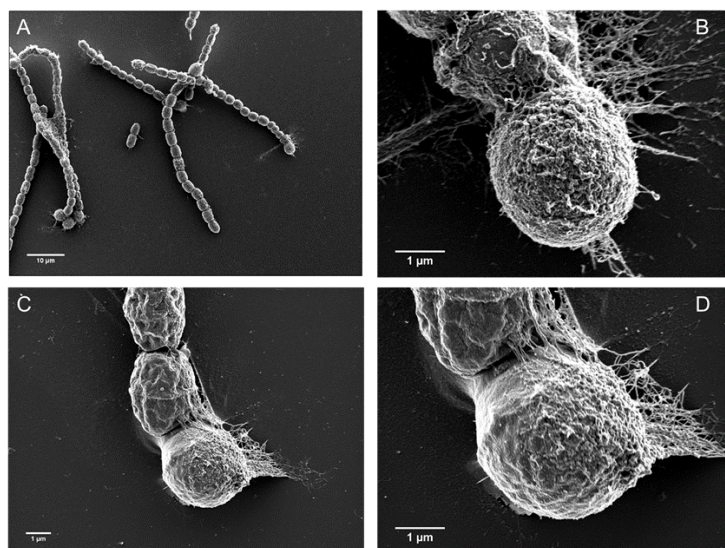


**Figure B.6 – Scanning electron microscopy (SEM) of *Nostoc*-Het cells with LSZ-SWCNTs.** (a-d) SEM images of *Nostoc*-Het cells treated with LSZ-SWCNTs: (a,c) low magnification and (b,d) high magnification.

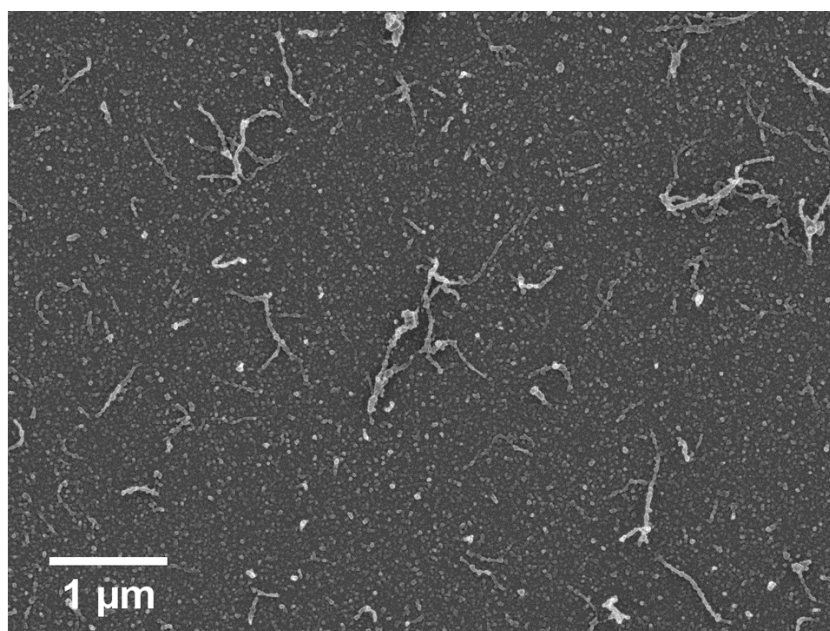


**Figure B.7 – Scanning electron microscopy (SEM) of LSZ-SWCNTs.** Representative SEM image of LSZ-SWCNTs immobilized onto poly-lysine coated glass slide.

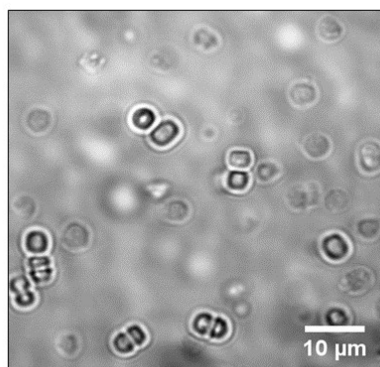


**Figure B.8 – Loss of viability of *Nostoc* after long incubation with LSZ-SWCNTs.** Representative bright-field image of *Nostoc* cells after prolonged incubation with LSZ-SWCNTs at 2 mg/L concentration. Almost complete rupture of the filaments is observed.

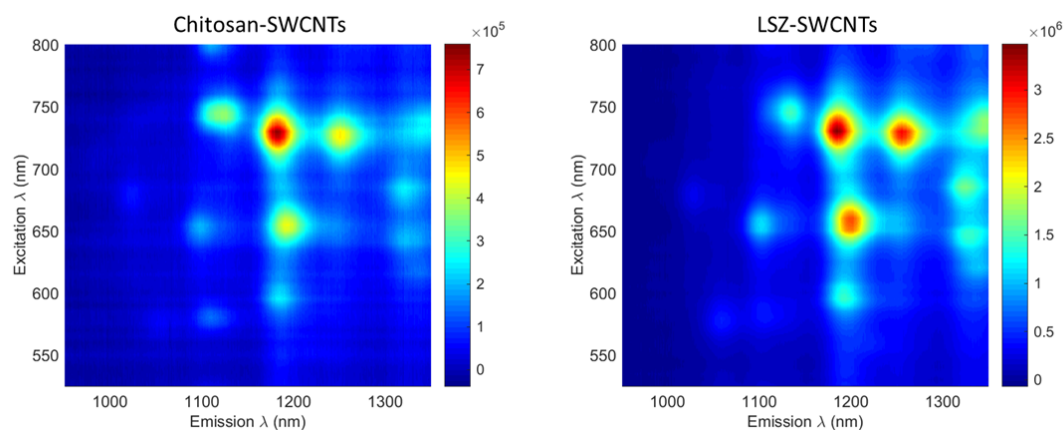


**Figure B.9 – Optical characterization of chitosan-SWCNTs and LSZ-SWCNTs suspensions.** Photoluminescence plots of chitosan-SWCNTs and LSZ-SWCNTs respectively, at the same SWCNT concentration measured from absorbance at 632 nm.



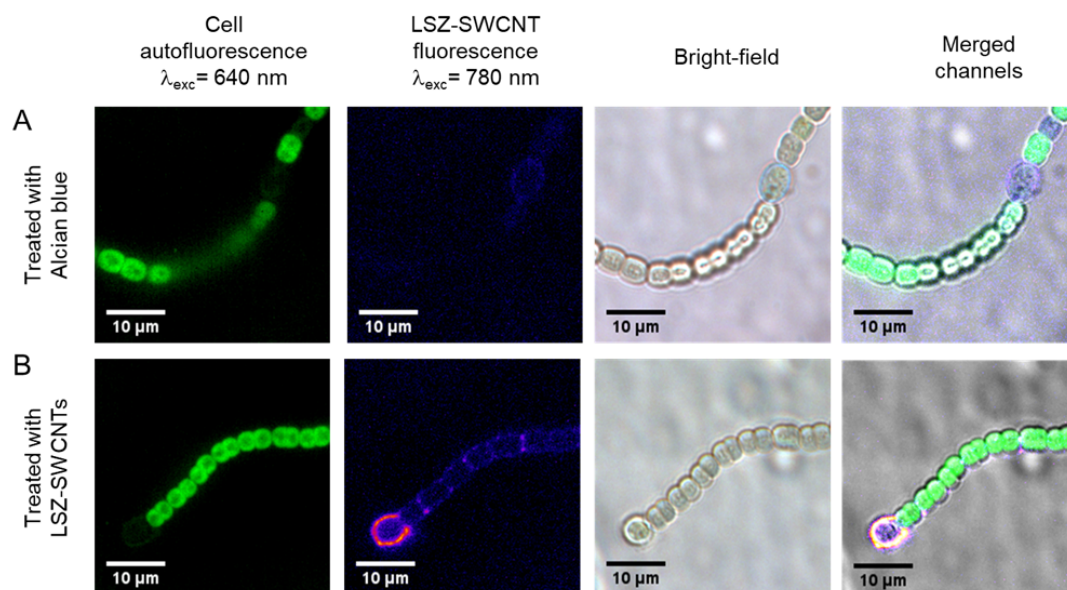


**Figure B.10 – NIR imaging of stained heterocysts.** Representative images of *Nostoc*-Het cells stained with (a) Alcian Blue and (b) with LSZ-wrapped SWCNTs. Fluorescence intensity was recorded for cell autofluorescence (excitation at 640 nm, emission above 800 nm), and SWCNTs in confocal mode (excitation at 780 nm, emission above 980 nm, at 3.7 mW/cm<sup>2</sup>).

## Appendix B. Interaction of SWCNTs with Filamentous Cyanobacteria

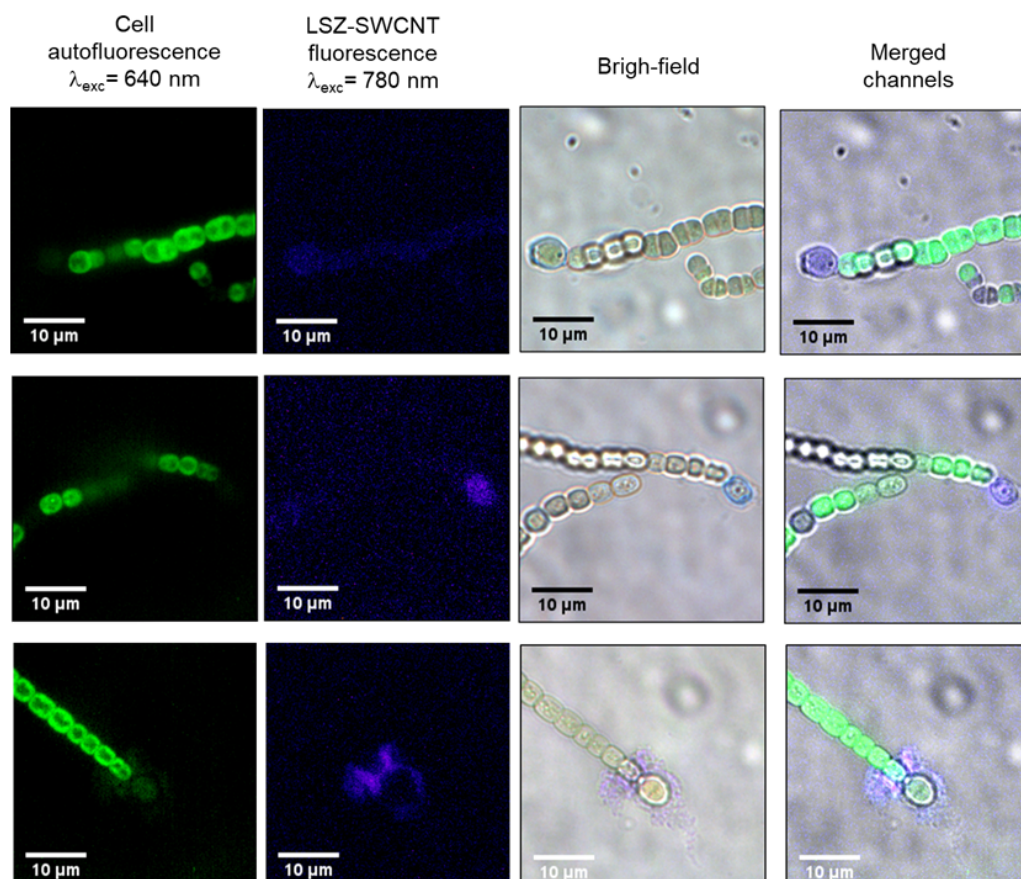


**Figure B.11 – Staining of *Nostoc* heterocysts with Alcian blue.** Representative images of *Nostoc*-Het cells immobilized onto poly-lysine coated glass slides, after incubation with Alcian blue. Fluorescence intensity was recorded for cell autofluorescence (excitation at 640 nm, emission above 800 nm), and SWCNTs in confocal mode (excitation at 780 nm, emission above 980 nm, at 3.7 mW/cm<sup>2</sup>). Alcian blue stains exo-polysaccharide in blue.

## **C Real-time monitoring of bacterial growth in the presence of SWCNTs**

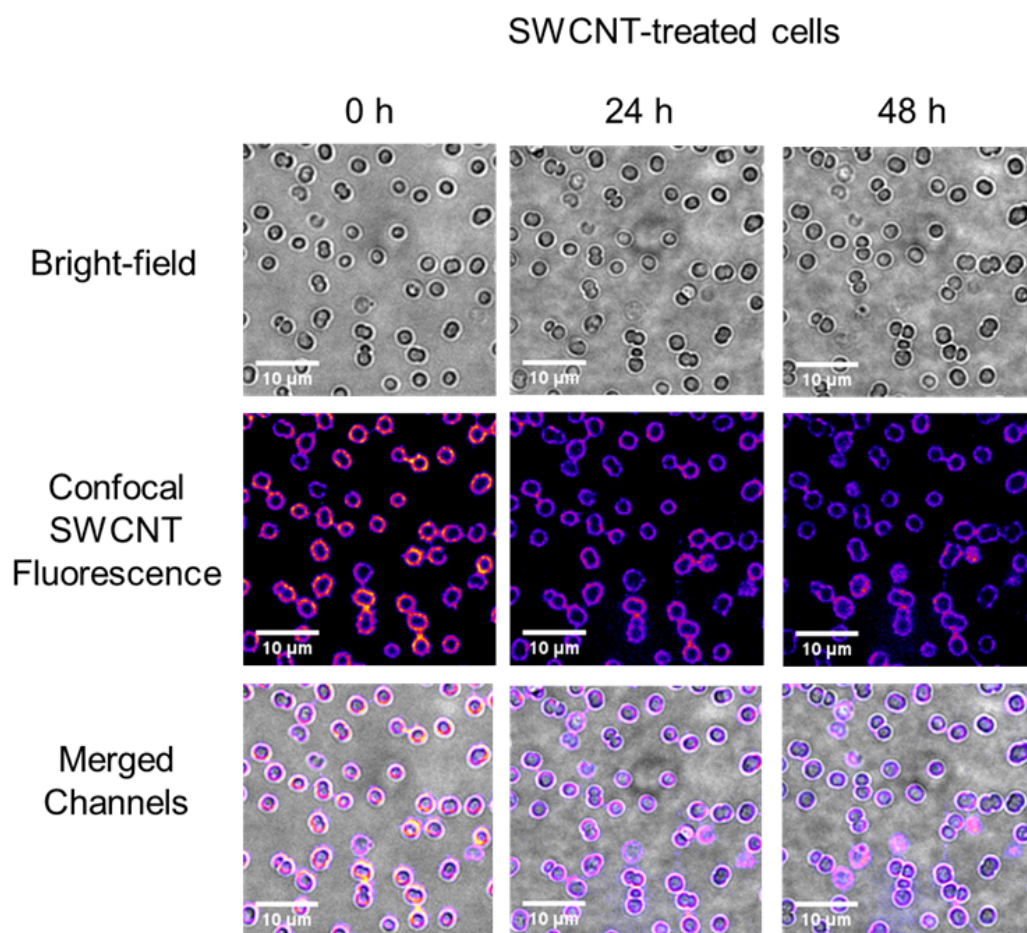


**Figure C.1 – NIR Imaging of *Synechocystis* cells growth in the presence of LSZ-SWCNTs.** NIR confocal fluorescence and bright-field images of *Synechocystis* cells treated with LSZ-SWCNTs (2 mg/L) and grown on 1% agar in BG11. Fluorescence intensity was recorded every 24 hours for SWCNTs in confocal mode (excitation at 780 nm, emission above 980 nm, at 2.5 mW/cm<sup>2</sup>). Cell growth is monitored for 48 hours.

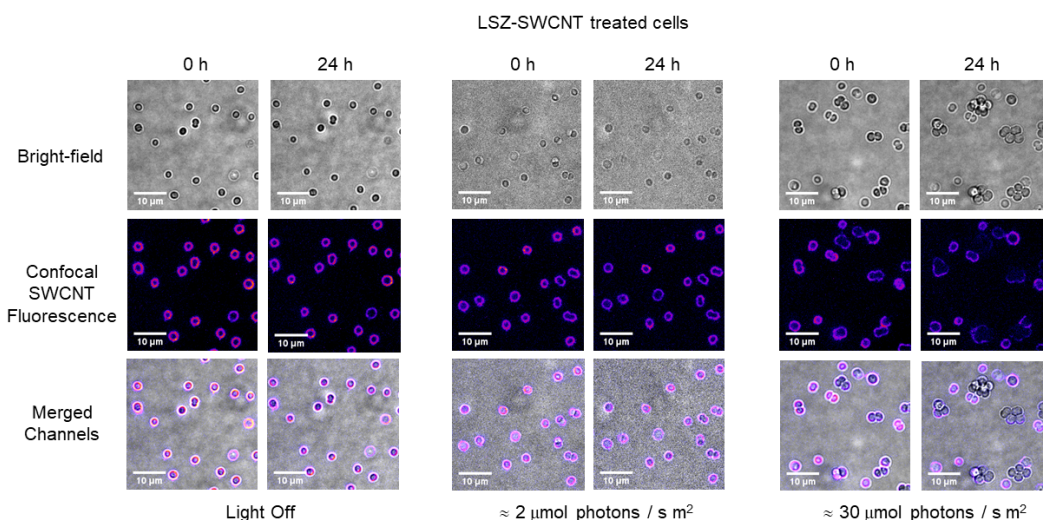


**Figure C.2 – NIR Imaging of SWCNT-treated *Synechocystis* cells growth at different light intensities.** NIR confocal fluorescence and bright-field images of *Synechocystis* cells treated with LSZ-SWCNTs (2 mg/L) and grown on 1% agar in BG11. Fluorescence intensity was recorded every 24 hours for SWCNTs in confocal mode (excitation at 780 nm, emission above 980 nm, at 2.5 mW/cm<sup>2</sup>). Cell growth is monitored for 24 hours at increasing light intensities of 0, 2 and 30  $\mu\text{mol photons m}^{-2} \text{s}^{-1}$  respectively.

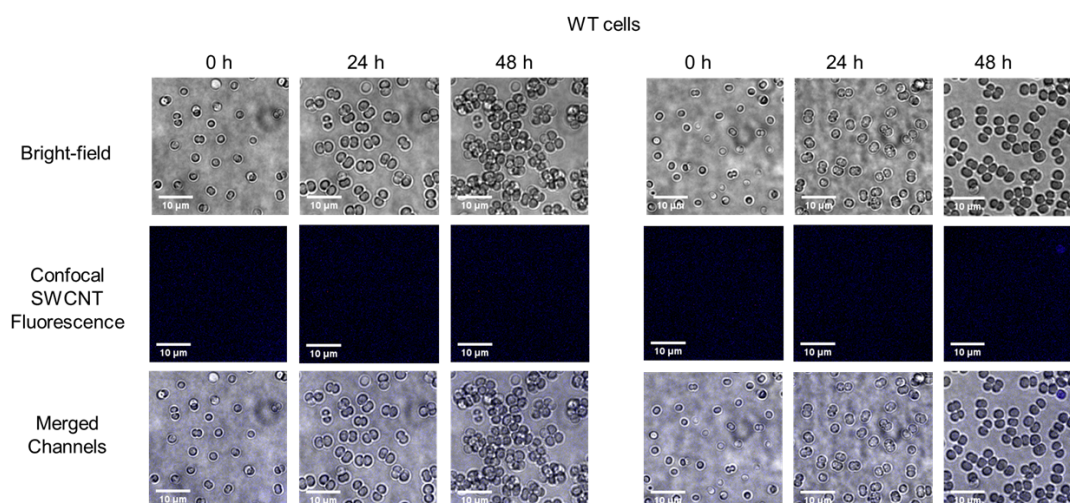


**Figure C.3 – NIR Imaging of control *Synechocystis* cells growth in absence of LSZ-SWCNTs.** NIR confocal fluorescence and bright-field images of *Synechocystis* cells treated with 1 mM HEPES buffer and grown on 1% agar in BG11. Fluorescence intensity was recorded every 24 hours for SWCNTs in confocal mode (excitation at 780 nm, emission above 980 nm, at 2.5 mW/cm<sup>2</sup>). Cell growth is monitored for 48 hours.



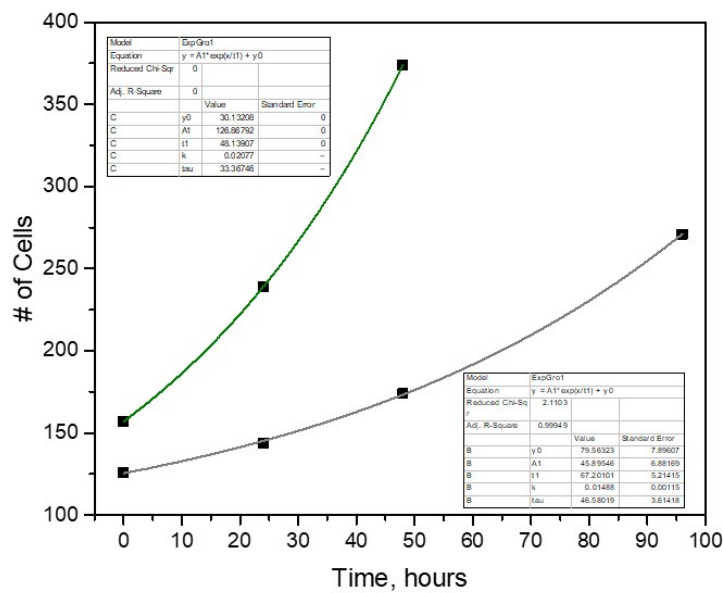


**Figure C.4 – Exponential growth of wild-type and SWCNT-treated *Synechocystis* cells.** The scatter plots show exponential growth of wild-type *Synechocystis* cells (green) and cells treated with LSZ-SWCNTs (gray). The two insets report the parameters obtained from exponential fitting.

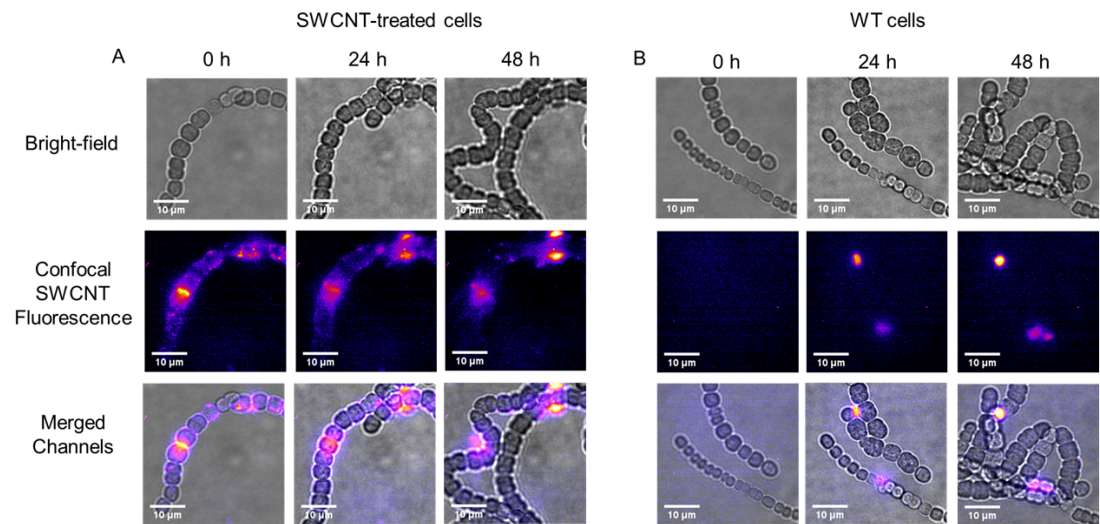


**Figure C.5 – NIR Imaging *Nostoc* cells growth with or without LSZ-SWCNTs.** Representative NIR confocal fluorescence and bright-field images of *Nostoc* cells treated with LSZ-SWCNTs (a) or with 1 mM HEPES buffer (b) and grown on 1% agar in BG11. Fluorescence intensity was recorded every 24 hours for SWCNTs in confocal mode (excitation at 780 nm, emission above 980 nm, at 2.5 mW/cm<sup>2</sup>). Cell growth is monitored for 48 hours.

## D Outlook on Potential Applications of SWCNT-treated Photosynthetic Microbes

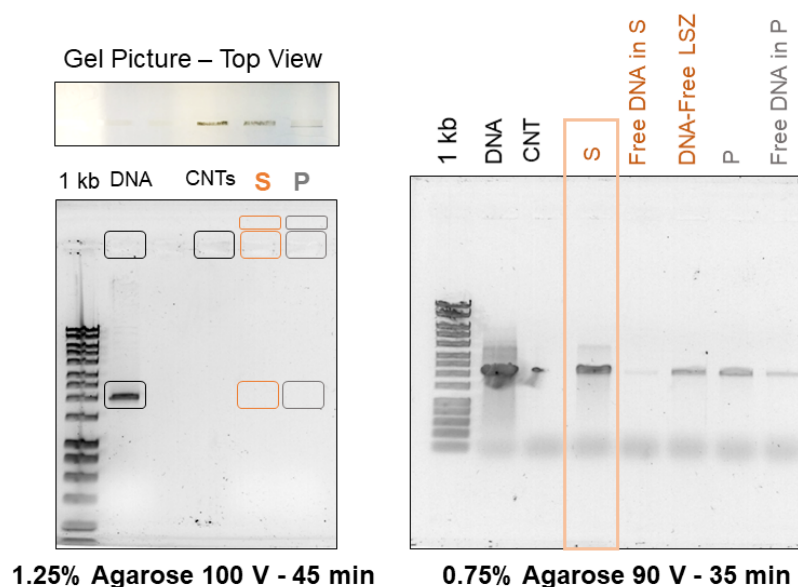


**Figure D.1 – Electrophoretic mobility of DNA-LSZ-SWCNTs complexes.** Agarose gel electrophoresis of linear DNA vectors after incubation with LSZ-SWCNTs (a,b). (a) Top view of 1.25% agarose gel in (b). 1 kb: DNA ladder; pDNA: control linear DNA vector at 1.4 mg/L; CNTs: control LSZ-SWCNTs at 20 mg/L; S: DNA-LSZ-SWCNT supernatant after incubation; P: DNA-LSZ-SWCNT pellet after incubation. (c) 0.75% agarose gel electrophoresis of linear DNA vectors following DNA recovery from the SWCNT surface and PCR amplification. The orange box indicates the presence of a strong DNA band in the lane corresponding to the original DNA-LSZ-SWCNT supernatant fraction, suggesting the formation of stable complexes.





## Bibliography

- [1] E. Roduner, "Size matters: Why nanomaterials are different," *Chemical Society Reviews*, vol. 35, no. 7, pp. 583–592, 2006.
- [2] L. S. Li and X. Yan, "Colloidal graphene quantum dots," *Journal of Physical Chemistry Letters*, vol. 1, no. 17, pp. 2572–2576, 2010.
- [3] J. Peng, W. Gao, B. K. Gupta, Z. Liu, R. Romero-Aburto, L. Ge, L. Song, L. B. Alemany, X. Zhan, G. Gao, S. A. Vithayathil, B. A. Kaiparettu, A. A. Marti, T. Hayashi, J. J. Zhu, and P. M. Ajayan, "Graphene quantum dots derived from carbon fibers," *Nano Letters*, vol. 12, no. 2, pp. 844–849, 2012.
- [4] Y. P. Sun, B. Zhou, Y. Lin, W. Wang, K. A. Fernando, P. Pathak, M. J. Meziani, B. a. Harruff, X. Wang, H. Wang, P. G. Luo, H. Yang, M. E. Kose, B. Chen, L. M. Veca, and S. Y. Xie, "Quantum-sized carbon dots for bright and colorful photoluminescence," *Journal of the American Chemical Society*, vol. 128, no. 24, pp. 7756–7757, 2006.
- [5] J. Wang, Y. Chen, and W. J. Blau, "Carbon nanotubes and nanotube composites for nonlinear optical devices," *Journal of Materials Chemistry*, vol. 19, no. 40, pp. 7425–7443, 2009.
- [6] P. Avouris, M. Freitag, and V. Perebeinos, "Carbon-nanotube photonics and optoelectronics," *Nature Photonics*, vol. 2, pp. 341–350, 2008.
- [7] A. D. Franklin, "The road to carbon nanotube transistors," *Nature*, pp. 0–1, 2013.
- [8] R. J. Chen, S. Bangsaruntip, K. A. Drouvalakis, N. W. S. Kam, M. Shim, Y. Li, W. Kim, P. J. Utz, and H. Dai, "Noncovalent functionalization of carbon nanotubes for highly specific electronic biosensors," *Proceedings of the National Academy of Sciences of the United States of America*, vol. 100, no. 9, pp. 4984–4989, 2003.
- [9] J. Qian, D. Wang, F.-H. Cai, W. Xi, L. Peng, Z.-F. Zhu, H. He, M.-L. Hu, and S. He, "Observation of Multiphoton-Induced Fluorescence from Graphene Oxide Nanoparticles and Applications in In Vivo Functional Bioimaging," *Angewandte Chemie International Edition*, vol. 51, no. 42, pp. 10570–10575, 2012.

## Bibliography

---

- [10] P. W. Barone, S. Baik, D. A. Heller, and M. S. Strano, "Near-infrared optical sensors based on single-walled carbon nanotubes.," *Nature materials*, vol. 4, no. 1, pp. 86–92, 2005.
- [11] D. A. Heller, H. Jin, B. M. Martinez, D. Patel, B. M. Miller, T.-K. Yeung, P. V. Jena, C. Höbartner, T. Ha, S. K. Silverman, and M. S. Strano, "Multimodal optical sensing and analyte specificity using single-walled carbon nanotubes.," *Nature nanotechnology*, vol. 4, no. 2, pp. 114–120, 2009.
- [12] M. S. Mauter and M. Elimelech, "Environmental Applications of Carbon-Based Nanomaterials," *American Chemical Society*, pp. 5843–5859, 2008.
- [13] S. Kruss, A. J. Hilmer, J. Zhang, N. F. Reuel, B. Mu, and M. S. Strano, "Carbon nanotubes as optical biomedical sensors," *Advanced Drug Delivery Reviews*, vol. 65, no. 15, pp. 1933–1950, 2013.
- [14] S. F. Oliveira, G. Bisker, N. A. Bakh, S. L. Gibbs, M. P. Landry, and M. S. Strano, "Protein Functionalized Carbon Nanomaterials for Biomedical Applications," *Carbon*, vol. 95, pp. 767–779, 2015.
- [15] D. Maiti, X. Tong, X. Mou, and K. Yang, "Carbon-Based Nanomaterials for Biomedical Applications: A Recent Study," *Frontiers in Pharmacology*, vol. 9, no. March, pp. 1–16, 2019.
- [16] B. Lambert, A. J. Gillen, N. Schuergers, S. J. Wu, and A. A. Boghossian, "Directed evolution of the optoelectronic properties of synthetic nanomaterials," *Chemical Communications*, vol. 55, no. 22, pp. 3239–3242, 2019.
- [17] F. J. Cunningham, N. S. Goh, G. S. Demirer, J. L. Matos, and M. P. Landry, "Nanoparticle-Mediated Delivery towards Advancing Plant Genetic Engineering," *Trends in Biotechnology*, vol. 36, no. 9, pp. 882–897, 2018.
- [18] K. Bates and K. Kostarelos, "Carbon nanotubes as vectors for gene therapy: Past achievements, present challenges and future goals," *Advanced Drug Delivery Reviews*, vol. 65, no. 15, pp. 2023–2033, 2013.
- [19] P. D. Boyer, H. Shams, S. L. Baker, M. R. K. Mofrad, M. F. Islam, and K. N. Dahl, "Enhanced intracellular delivery of small molecules and drugs via non-covalent ternary dispersions of single-wall carbon nanotubes," *Journal of Materials Chemistry B*, vol. 4, no. 7, pp. 1324–1330, 2016.
- [20] G. Hong, S. Diao, A. L. Antaris, and H. Dai, "Carbon Nanomaterials for Biological Imaging and Nanomedicinal Therapy," *Chemical Reviews*, vol. 115, no. 19, pp. 10816–10906, 2015.
- [21] M. S. Strano, A. A. Boghossian, W.-J. Kim, P. W. Barone, E. S. Jeng, D. A. Heller, N. Nair, H. Jin, R. Sharma, and C. Y. Lee, "The Chemistry of Single-Walled Nanotubes," *MRS Bulletin*, vol. 34, no. 12, pp. 950–961, 2009.

- [22] V. Zubkovs, A. Antonucci, N. Schuergers, B. Lambert, A. Latini, R. Ceccarelli, A. Santinelli, A. Rogov, D. Ciepielewski, and A. A. Boghossian, "Spinning-disc confocal microscopy in the second near-infrared window (NIR-II)," *Scientific Reports*, vol. 8, no. 1, pp. 1–10, 2018.
- [23] S. Kruss, D. P. Salem, L. Vuković, B. Lima, E. Vander Ende, E. S. Boyden, and M. S. Strano, "High-resolution imaging of cellular dopamine efflux using a fluorescent nanosensor array," *Proceedings of the National Academy of Sciences*, vol. 114, no. 8, pp. 1789–1794, 2017.
- [24] L. Chio, J. T. Del Bonis-O'Donnell, M. P. Landry, G. F. Dorlhiac, and I. R. McFarlane, "Advances in nanomaterials for brain microscopy," *Nano Research*, vol. 11, no. 10, pp. 5144–5172, 2018.
- [25] M. H. Wong, R. P. Misra, J. P. Giraldo, S. Y. Kwak, Y. Son, M. P. Landry, J. W. Swan, D. Blankschtein, and M. S. Strano, "Lipid Exchange Envelope Penetration (LEEP) of Nanoparticles for Plant Engineering: A Universal Localization Mechanism," *Nano Letters*, vol. 16, no. 2, pp. 1161–1172, 2016.
- [26] V. Zubkovs, N. Schuergers, B. Lambert, E. Ahunbay, and A. A. Boghossian, "Mediatorless, Reversible Optical Nanosensor Enabled through Enzymatic Pocket Doping," *Small*, vol. 13, no. 42, pp. 1–10, 2017.
- [27] A. J. Gillen, J. Kupis-Rozmyslowicz, C. Gigli, N. Schürgers, and A. A. Boghossian, "Xeno Nucleic Acid Nanosensors for Enhanced Stability Against Ion-induced Perturbations," *The Journal of Physical Chemistry Letters*, pp. 4336–4343, 2018.
- [28] A. J. Gillen and A. A. Boghossian, "Non-covalent Methods of Engineering Optical Sensors Based on Single-Walled Carbon Nanotubes," vol. 7, no. September, pp. 1–13, 2019.
- [29] A. J. Gillen, D. J. Siefman, S.-j. Wu, C. Bourmaud, B. Lambert, and A. A. Boghossian, "Templating colloidal sieves for tuning nanotube surface interactions and optical sensor responses," *Journal of Colloid And Interface Science*, vol. 565, pp. 55–62, 2020.
- [30] A. Antonucci, J. Kupis-Rozmysłowicz, and A. A. Boghossian, "Noncovalent Protein and Peptide Functionalization of Single-Walled Carbon Nanotubes for Biodelivery and Optical Sensing Applications," 2017.
- [31] P. Boyer, S. Ganesh, Z. Qin, B. D. Holt, M. J. Buehler, M. F. Islam, and K. N. Dahl, "Delivering Single-Walled Carbon Nanotubes to the Nucleus Using Engineered Nuclear Protein Domains," *ACS Applied Materials & Interfaces*, vol. 8, no. 5, pp. 3524–3534, 2016.
- [32] G. S. Demirer, H. Zhang, J. L. Matos, N. S. Goh, F. J. Cunningham, Y. Sung, R. Chang, A. J. Aditham, L. Chio, M.-J. Cho, B. Staskawicz, and M. P. Landry, "High aspect ratio nanomaterials enable delivery of functional genetic material without DNA integration in mature plants," *Nature Nanotechnology*, vol. 14, pp. 456–464, 2019.

## Bibliography

---

- [33] J. P. Giraldo, M. P. Landry, S. M. Faltermeier, T. P. McNicholas, N. M. Iverson, A. A. Boghossian, N. F. Reuel, A. J. Hilmer, F. Sen, J. a. Brew, and M. S. Strano, "Plant nanobionics approach to augment photosynthesis and biochemical sensing.," *Nature materials*, vol. 13, no. 4, pp. 400–8, 2014.
- [34] G. D. Scholes and E. H. Sargent, "Bioinspired materials: Boosting plant biology," *Nature materials*, vol. 13, no. 4, pp. 329–31, 2014.
- [35] V. B. Koman, T. T. Lew, M. H. Wong, S. Y. Kwak, J. P. Giraldo, and M. S. Strano, "Persistent drought monitoring using a microfluidic-printed electro-mechanical sensor of stomata: In planta," *Lab on a Chip*, vol. 17, no. 23, pp. 4015–4024, 2017.
- [36] M. H. Wong, J. P. Giraldo, S.-Y. Kwak, V. B. Koman, R. Sinclair, T. T. S. Lew, G. Bisker, P. Liu, and M. S. Strano, "Nitroaromatic detection and infrared communication from wild-type plants using plant nanobionics," *Nature Materials*, vol. 16, pp. 1–8, 2016.
- [37] K. Lee, J. Park, M. S. Lee, J. Kim, B. G. Hyun, D. J. Kang, K. Na, C. Y. Lee, F. Bien, and J. U. Park, "In-situ synthesis of carbon nanotube-graphite electronic devices and their integrations onto surfaces of live plants and insects," *Nano Letters*, vol. 14, no. 5, pp. 2647–2654, 2014.
- [38] H. Zhang, G. S. Demirel, H. Zhang, T. Ye, N. S. Goh, A. J. Aditham, F. J. Cunningham, C. Fan, and M. P. Landry, "DNA nanostructures coordinate gene silencing in mature plants," *Proceedings of the National Academy of Sciences*, vol. 116, no. 15, pp. 7543–7548, 2019.
- [39] S.-Y. Kwak, T. T. S. Lew, C. J. Sweeney, V. B. Koman, M. H. Wong, K. Bohmert-Tatarev, K. D. Snell, J. S. Seo, N.-H. Chua, and M. S. Strano, "Chloroplast-selective gene delivery and expression in planta using chitosan-complexed single-walled carbon nanotube carriers," *Nature Nanotechnology*, vol. 14, pp. 447–455, 2019.
- [40] A. Beloqui, P. Dominguez de Maria, P. N. Golyshin, and M. Ferrer, "Recent trends in industrial microbiology," *Current Opinion in Microbiology*, vol. 11, 2008.
- [41] A. Perez-Garcia, D. Romero, and A. de Vicente, "Plant protection and growth stimulation by microorganisms : biotechnological applications of Bacilli in agriculture," *Current Opinion in Biotechnology*, vol. 22, pp. 187–193, 2011.
- [42] M. Mouhib, A. Antonucci, M. Reggente, A. Amirjani, A. J. Gillen, and A. A. Boghossian, "Enhancing bioelectricity generation in microbial fuel cells and biophotovoltaics using nanomaterials," *Nano Research*, vol. 12, no. 1, 2019.
- [43] N. M. Bardhan, D. Ghosh, and A. M. Belcher, "Carbon nanotubes as in vivo bacterial probes," *Nature Communications*, 2014.
- [44] M. P. Landry, H. Ando, A. Chen, J. Cao, V. Isaac, L. Chio, D. Yang, J. Dong, T. Lu, and M. Strano, "Single-Molecule Detection of Protein Efflux from Microorganisms using

- Fluorescence Single Walled Carbon Nanotube Sensor Arrays,” *Nature Nanotechnology*, vol. 12, no. 4, pp. 368–377, 2017.
- [45] J. Rojas-Chapana, J. Troszczyńska, I. Firkowska, C. Morsczech, and M. Giersig, “Multi-walled carbon nanotubes for plasmid delivery into *Escherichia coli* cells,” *Lab on a Chip*, vol. 5, no. 5, pp. 536–539, 2005.
- [46] H. Chen, B. Wang, D. Gao, M. Guan, L. Zheng, H. Ouyang, Z. Chai, Y. Zhao, and W. Feng, “Broad-spectrum antibacterial activity of carbon nanotubes to human gut bacteria,” *Small*, vol. 9, no. 16, pp. 2735–2746, 2013.
- [47] S. Kang, M. Herzberg, D. F. Rodrigues, and M. Elimelech, “Antibacterial Effects of Carbon Nanotubes : Size Does Matter !,” no. 15, pp. 6409–6413, 2008.
- [48] A. Battigelli, C. Ménard-Moyon, T. Da Ros, M. Prato, and A. Bianco, “Endowing carbon nanotubes with biological and biomedical properties by chemical modifications,” *Advanced Drug Delivery Reviews*, vol. 65, no. 15, pp. 1899–1920, 2013.
- [49] L. Lacerda, H. Ali-Boucetta, M. A. Herrero, G. Pastorin, A. Bianco, M. Prato, and K. Kostarelos, “Tissue histology and physiology following intravenous administration of different types of functionalized multiwalled carbon nanotubes,” *Nanomedicine*, vol. 3, no. 2, pp. 149–161, 2008.
- [50] P. Wu, X. Chen, N. Hu, U. C. Tam, O. Blixt, A. Zettl, and C. R. Bertozzi, “Biocompatible carbon nanotubes generated by functionalization with glycodendrimers,” *Angewandte Chemie - International Edition*, vol. 47, no. 27, pp. 5022–5025, 2008.
- [51] K. E. Sapsford, W. R. Algar, L. Berti, K. B. Gemmill, B. J. Casey, E. Oh, M. H. Stewart, and I. L. Medintz, “Functionalizing nanoparticles with biological molecules: Developing chemistries that facilitate nanotechnology,” *Chemical Reviews*, vol. 113, no. 3, pp. 1904–2074, 2013.
- [52] T. Fujigaya and N. Nakashima, “Non-covalent polymer wrapping of carbon nanotubes and the role of wrapped polymers as functional dispersants,” *Science and Technology of Advanced Materials*, vol. 16, no. 2, p. 024802, 2015.
- [53] M. Zheng, A. Jagota, E. D. Semke, B. A. Diner, R. S. Mclean, S. R. Lustig, R. E. Richardson, and N. G. Tassi, “DNA-assisted dispersion and separation of carbon nanotubes,” *Nature Materials*, vol. 2, no. 5, pp. 338–342, 2003.
- [54] G. Sánchez-Pomales, C. R. Cabrera, C. Pagan-Miranda, and L. Santiago-Rodriguez, “DNA-wrapped carbon nanotubes: from synthesis to applications,” in *Carbon Nanotubes*, pp. 721–749, 2010.
- [55] J. Kupis-Rozmysłowicz, A. Antonucci, and A. A. Boghossian, “Review—Engineering the Selectivity of the DNA-SWCNT Sensor,” *ECS Journal of Solid State Science and Technology*, vol. 5, no. 8, pp. M3067–M3074, 2016.

- [56] M. P. Landry, L. Vuković, S. Kruss, G. Bisker, A. M. Landry, S. Islam, R. Jain, K. Schulten, and M. S. Strano, "Comparative Dynamics and Sequence Dependence of DNA and RNA Binding to Single Walled Carbon Nanotubes," *The Journal of Physical Chemistry C*, vol. 119, no. 18, pp. 10048–10058, 2015.
- [57] A. Hirano, T. Tanaka, H. Kataura, and T. Kameda, "Arginine side chains as a dispersant for individual single-wall carbon nanotubes," *Chemistry - A European Journal*, vol. 20, pp. 4922–4930, 2014.
- [58] D. R. Samarajeewa, G. R. Dieckmann, S. O. Nielsen, and I. H. Musselman, "Modifying the electronic properties of single-walled carbon nanotubes using designed surfactant peptides," *Nanoscale*, vol. 4, no. 15, p. 4544, 2012.
- [59] D. Nepal and K. E. Geckeler, "Proteins and carbon nanotubes: Close encounter in water," *Small*, vol. 3, no. 7, pp. 1259–1265, 2007.
- [60] M. Calvaresi and F. Zerbetto, "The devil and holy water: protein and carbon nanotube hybrids," *Accounts of chemical research*, vol. 46, no. 11, pp. 2454–63, 2013.
- [61] D. Tuncel, "Non-covalent interactions between carbon nanotubes and conjugated polymers," *Nanoscale*, vol. 3, no. 9, pp. 3545–3554, 2011.
- [62] S. Marchesan and M. Prato, "Under the lens: carbon nanotube and protein interaction at the nanoscale," *Chem. Commun.*, vol. 51, no. 21, pp. 4347–4359, 2015.
- [63] W. Feng and P. Ji, "Enzymes immobilized on carbon nanotubes," *Biotechnology Advances*, vol. 29, no. 6, pp. 889–895, 2011.
- [64] T. W. Tsai, G. Heckert, L. F. Neves, Y. Tan, D. Y. Kao, R. G. Harrison, D. E. Resasco, and D. W. Schmidtke, "Adsorption of glucose oxidase onto single-walled carbon nanotubes and its application in layer-by-layer biosensors," *Analytical Chemistry*, vol. 81, no. 19, pp. 7917–7925, 2009.
- [65] U. Hanefeld, L. Gardossi, and E. Magner, "Understanding enzyme immobilisation," *Chemical Society reviews*, vol. 38, no. 2, pp. 453–468, 2009.
- [66] S. S. Karajanagi, A. A. Vertegel, R. S. Kane, and J. S. Dordick, "Structure and Function of Enzymes Adsorbed on Single-Walled Carbon Nanotubes," *Langmuir*, vol. 20, no. 10, p. 11594, 2004.
- [67] J. H. Kim, J. H. Ahn, P. W. Barone, H. Jin, J. Zhang, D. A. Heller, and M. S. Strano, "A luciferase/single-walled carbon nanotube conjugate for nearInfrared fluorescent detection of cellular ATP," *Angewandte Chemie - International Edition*, vol. 49, no. 8, pp. 1456–1459, 2010.
- [68] H. Yoon, J. H. Ahn, P. W. Barone, K. Yum, R. Sharma, A. A. Boghossian, J. H. Han, and M. S. Strano, "Periplasmic binding proteins as optical modulators of single-walled

- carbon nanotube fluorescence: Amplifying a nanoscale actuator," *Angewandte Chemie - International Edition*, vol. 50, no. 8, pp. 1828–1831, 2011.
- [69] K. Besteman, J.-O. Lee, F. G. M. Wiertz, H. A. Heering, and C. Dekker, "Enzyme-Coated Carbon Nanotubes as Single-Molecule Biosensors," *Nano Letters*, vol. 3, no. 6, pp. 727–730, 2003.
- [70] H. L. Pang, J. Liu, D. Hu, X. H. Zhang, and J. H. Chen, "Immobilization of laccase onto 1-aminopyrene functionalized carbon nanotubes and their electrocatalytic activity for oxygen reduction," *Electrochimica Acta*, vol. 55, no. 22, pp. 6611–6616, 2010.
- [71] C. Wang, S. Li, R. Zhang, and Z. Lin, "Adsorption and properties of aromatic amino acids on single-walled carbon nanotubes," *Nanoscale*, vol. 4, no. 4, p. 1146, 2012.
- [72] V. Sanz, H. M. Coley, S. R. P. Silva, and J. McFadden, "Modeling the binding of peptides on carbon nanotubes and their use as protein and DNA carriers," *Journal of Nanoparticle Research*, vol. 14, no. 2, 2012.
- [73] K. Kostarelos, L. Lacerda, G. Pastorin, W. Wu, S. Wieckowski, J. Luangsivilay, S. Godefroy, D. Pantarotto, J. P. Briand, S. Muller, M. Prato, and A. Bianco, "Cellular uptake of functionalized carbon nanotubes is independent of functional group and cell type," *Nature Nanotechnology*, vol. 2, no. 2, pp. 108–113, 2007.
- [74] S. Pogodin, N. K. H. Slater, and V. A. Baulin, "Surface patterning of carbon nanotubes can enhance their penetration through a phospholipid bilayer," *ACS Nano*, vol. 5, no. 2, pp. 1141–1146, 2011.
- [75] D. Pantarotto, R. Singh, D. McCarthy, M. Erhardt, J. P. Briand, M. Prato, K. Kostarelos, and A. Bianco, "Functionalized carbon nanotubes for plasmid DNA gene delivery," *Angewandte Chemie - International Edition*, vol. 43, no. 39, pp. 5242–5246, 2004.
- [76] C. F. Lopez, S. O. Nielsen, P. B. Moore, and M. L. Klein, "Understanding nature's design for a nanosyringe," *Proceedings of the National Academy of Sciences of the United States of America*, vol. 101, no. 13, pp. 4431–4434, 2004.
- [77] S. Kraszewski, A. Bianco, M. Tarek, and C. Ramseyer, "Insertion of short amino-functionalized single-walled carbon nanotubes into phospholipid bilayer occurs by passive diffusion," *PLoS ONE*, vol. 7, no. 7, pp. 1–11, 2012.
- [78] A. Antonelli, S. Serafini, M. Menotta, C. Sfara, F. Pierigé, L. Giorgi, G. Ambrosi, L. Rossi, and M. Magnani, "Improved cellular uptake of functionalized single-walled carbon nanotubes," *Nanotechnology*, vol. 21, no. 42, 2010.
- [79] M. L. Becker, J. A. Fagan, N. D. Gallant, B. J. Bauer, V. Bajpai, E. K. Hobbie, S. H. Lacerda, K. B. Migler, and J. P. Jakupciak, "Length-dependent uptake of DNA-wrapped single-walled carbon nanotubes," *Advanced Materials*, vol. 19, no. 7, pp. 939–945, 2007.

- [80] B. Kang, S. Chang, Y. Dai, D. Yu, and D. Chen, "Cell response to carbon nanotubes: Size-dependent intracellular uptake mechanism and subcellular fate," *Small*, vol. 6, no. 21, pp. 2362–2366, 2010.
- [81] F. Zhou, D. Xing, B. Wu, S. Wu, Z. Ou, and W. R. Chen, "New insights of transmembranal mechanism and subcellular localization of noncovalently modified single-walled carbon nanotubes," *Nano Letters*, vol. 10, no. 5, pp. 1677–1681, 2010.
- [82] M. Zheng, A. Jagota, M. S. Strano, A. P. Santos, P. Barone, S. G. Chou, B. a. Diner, M. S. Dresselhaus, R. S. McLean, G. B. Onoa, G. G. Samsonidze, E. D. Semke, M. Usrey, and D. J. Walls, "Structure-based carbon nanotube sorting by sequence-dependent DNA assembly," *Science (New York, N.Y.)*, vol. 302, no. 5650, pp. 1545–1548, 2003.
- [83] L. Lacerda, H. Ali-Boucetta, S. Kraszewski, M. Tarek, M. Prato, C. Ramseyer, K. Kostarelos, and A. Bianco, "How do functionalized carbon nanotubes land on, bind to and pierce through model and plasma membranes," *Nanoscale*, vol. 5, no. 21, pp. 10242–10250, 2013.
- [84] L. Gao, L. Nie, T. Wang, Y. Qin, Z. Guo, D. Yang, and X. Yan, "Carbon nanotube delivery of the GFP gene into mammalian cells," *ChemBioChem*, vol. 7, no. 2, pp. 239–242, 2006.
- [85] Z. Zhang, X. Yang, Y. Zhang, B. Zeng, S. Wang, T. Zhu, R. B. Roden, Y. Chen, and R. Yang, "Delivery of telomerase reverse transcriptase small interfering RNA in complex with positively charged single-walled carbon nanotubes suppresses tumor growth," *Clinical Cancer Research*, vol. 12, no. 16, pp. 4933–4939, 2006.
- [86] T. T. S. Lew, M. H. Wong, S. Y. Kwak, R. Sinclair, V. B. Koman, and M. S. Strano, "Rational Design Principles for the Transport and Subcellular Distribution of Nanomaterials into Plant Protoplasts," *Small*, vol. 14, no. 44, pp. 1–13, 2018.
- [87] L. Fan, R. Li, J. Pan, Z. Ding, and J. Lin, "Endocytosis and its regulation in plants," *Trends in Plant Science*, vol. 20, no. 6, pp. 388–397, 2015.
- [88] S. Jin, P. Wijesekara, P. D. Boyer, K. N. Dahl, and M. F. Islam, "Length-dependent intracellular bundling of single-walled carbon nanotubes influences retention," *Journal of Materials Chemistry B*, vol. 5, no. 32, pp. 6657–6665, 2017.
- [89] P. D. Boyer, B. D. Holt, M. F. Islam, and K. N. Dahl, "Decoding membrane- versus receptor-mediated delivery of single-walled carbon nanotubes into macrophages using modifications of nanotube surface coatings and cell activity," *Soft Matter*, vol. 9, no. 3, pp. 758–764, 2013.
- [90] A. E. Porter, M. Gass, K. Muller, J. N. Skepper, P. A. Midgley, and M. Welland, "Direct imaging of single-walled carbon nanotubes in cells," *Nature Nanotechnology*, vol. 2, no. 11, pp. 713–717, 2007.



- [91] P. Cherukuri, S. M. Bachilo, S. H. Litovsky, and R. B. Weisman, "Near-infrared fluorescence microscopy of single-walled carbon nanotubes in phagocytic cells," *Journal of the American Chemical Society*, vol. 126, no. 48, pp. 15638–15639, 2004.
- [92] X. Cui, B. Wan, Y. Yang, X. Ren, and L. H. Guo, "Length effects on the dynamic process of cellular uptake and exocytosis of single-walled carbon nanotubes in murine macrophage cells," *Scientific Reports*, vol. 7, no. 1, pp. 1–13, 2017.
- [93] D. Zhao, D. Alizadeh, L. Zhang, W. Liu, O. Farrukh, E. Manuel, D. J. Diamond, and B. Badie, "Carbon nanotubes enhance CpG uptake and potentiate antiglioma immunity," *Clinical Cancer Research*, vol. 17, no. 4, pp. 771–782, 2011.
- [94] K. Das, S. Nimushakavi, A. Chaudhuri, and P. K. Das, "An Integrin-Targeting RGDK-Tagged Nanocarrier: Anticancer Efficacy of Loaded Curcumin," *ChemMedChem*, vol. 12, no. 10, pp. 738–750, 2017.
- [95] N. W. S. Kam, Z. Liu, and H. Dai, "Carbon nanotubes as intracellular transporters for proteins and DNA: An investigation of the uptake mechanism and pathway," *Angewandte Chemie - International Edition*, vol. 45, no. 4, pp. 577–581, 2006.
- [96] Q. Liu, B. Chen, Q. Wang, X. Shi, Z. Xiao, J. Lin, and X. Fang, "Carbon Nanotubes as Molecular Transporters for Walled Plant Cells," *Nano Letters*, vol. 9, no. 3, pp. 1007–1010, 2009.
- [97] J. Budhathoki-Uprety, J. D. Harvey, E. Isaac, R. M. Williams, T. V. Galassi, R. E. Langenbacher, and D. a. Heller, "Polymer cloaking modulates the carbon nanotube protein corona and delivery into cancer cells," *Journal of Materials Chemistry B*, vol. 5, no. 32, pp. 6637–6644, 2017.
- [98] M. F. Serag, N. Kaji, S. Habuchi, A. Bianco, and Y. Baba, "Nanobiotechnology meets plant cell biology: carbon nanotubes as organelle targeting nanocarriers," *RSC Advances*, vol. 3, no. 15, p. 4856, 2013.
- [99] S. Meiners, P. K. Gharyal, and M. Schindler, "Permeabilization of the plasmalemma and wall of soybean root cells to macromolecules," *Planta*, vol. 184, no. 4, pp. 443–447, 1991.
- [100] M. F. Serag, K. Braeckmans, S. Habuchi, N. Kaji, A. Bianco, and Y. Baba, "Spatiotemporal visualization of subcellular dynamics of carbon nanotubes," *Nano Letters*, vol. 12, no. 12, pp. 6145–6151, 2012.
- [101] M. F. Serag, N. Kaji, M. Tokeshi, and Y. Baba, "Introducing carbon nanotubes into living walled plant cells through cellulase-induced nanoholes," *RSC Advances*, vol. 2, no. 2, pp. 398–400, 2012.
- [102] E. Hoiczyk and A. Hansel, "Cyanobacterial cell walls: News from an unusual prokaryotic envelope," *Journal of Bacteriology*, vol. 182, no. 5, pp. 1191–1199, 2000.

## Bibliography

---

- [103] Y. N. Slavin, J. Asnis, U. O. Häfeli, and H. Bach, "Metal nanoparticles: Understanding the mechanisms behind antibacterial activity," *Journal of Nanobiotechnology*, vol. 15, no. 1, pp. 1–20, 2017.
- [104] Y. H. Lee, B. Wu, W. Q. Zhuang, D. R. Chen, and Y. J. Tang, "Nanoparticles facilitate gene delivery to microorganisms via an electrospray process," *Journal of Microbiological Methods*, vol. 84, no. 2, pp. 228–233, 2011.
- [105] M. Kumari, S. Pandey, A. Mishra, and C. S. Nautiyal, "Finding a facile way for the bacterial DNA transformation by biosynthesized gold nanoparticles," *FEMS Microbiology Letters*, vol. 364, no. 12, pp. 1–5, 2017.
- [106] J. Gao, H. Li, P. Torab, K. E. Mach, D. W. Craft, N. J. Thomas, C. M. Puleo, J. C. Liao, T. H. Wang, and P. K. Wong, "Nanotube assisted microwave electroporation for single cell pathogen identification and antimicrobial susceptibility testing," *Nanomedicine: Nanotechnology, Biology, and Medicine*, vol. 17, pp. 246–253, 2019.
- [107] X. Wang and Z. Liu, "Carbon nanotubes in biology and medicine: An overview," *Chinese Science Bulletin*, vol. 57, no. 2-3, pp. 167–180, 2012.
- [108] Y. Hashida, H. Tanaka, S. Zhou, S. Kawakami, F. Yamashita, T. Murakami, T. Umeyama, H. Imahori, and M. Hashida, "Photothermal ablation of tumor cells using a single-walled carbon nanotube-peptide composite," *Journal of Controlled Release*, vol. 173, no. 1, pp. 58–66, 2014.
- [109] P. V. Jena, Y. Shamay, J. Shah, D. Roxbury, N. Paknejad, and D. A. Heller, "Photoluminescent carbon nanotubes interrogate the permeability of multicellular tumor spheroids," *Carbon*, vol. 97, pp. 99–109, 2016.
- [110] S. M. Bachilo, M. S. Strano, C. Kittrell, R. H. Hauge, R. E. Smalley, and R. B. Weisman, "Structure-assigned optical spectra of single-walled carbon nanotubes," *Science*, vol. 298, no. 5602, pp. 2361–6, 2002.
- [111] B. D. Holt, K. N. Dahl, M. F. Islam, and H. E. T. Al, "Cells Take up and Recover from Nanotubes with Two Distinct Rates," *ACS Nano*, vol. 6, no. 4, pp. 3481–3490, 2012.
- [112] S. Pogodin and V. A. Baulin, "Can a carbon nanotube pierce through a phospholipid bilayer?," *ACS Nano*, vol. 4, no. 9, pp. 5293–5300, 2010.
- [113] L. Lacerda, J. Russier, G. Pastorin, M. A. Herrero, E. Venturelli, H. Dumortier, K. T. Al-Jamal, M. Prato, K. Kostarelos, and A. Bianco, "Translocation mechanisms of chemically functionalised carbon nanotubes across plasma membranes," *Biomaterials*, vol. 33, no. 11, pp. 3334–3343, 2012.
- [114] Z. W. Ulissi, F. Sen, X. Gong, S. Sen, N. Iverson, A. A. Boghossian, L. C. Godoy, G. N. Wogan, D. Mukhopadhyay, and M. S. Strano, "Spatiotemporal intracellular nitric oxide signaling captured using internalized, near-infrared fluorescent carbon nanotube nanosensors," *Nano Letters*, vol. 14, no. 8, pp. 4887–4894, 2014.

- 
- [115] B. D. Holt, K. N. Dahl, and M. F. Islam, "Quantification of uptake and localization of bovine serum albumin-stabilized single-wall carbon nanotubes in different human cell types," *Small*, vol. 7, no. 16, pp. 2348–2355, 2011.
- [116] U. B. Sleytr, B. Schuster, E. M. Egelseer, and D. Pum, "S-layers: Principles and applications," *FEMS Microbiology Reviews*, vol. 38, no. 5, pp. 823–864, 2014.
- [117] A. Vioque, "Transformation of cyanobacteria," *Advances in Experimental Medicine and Biology*, vol. 616, pp. 12–22, 2007.
- [118] E. Stavriniidou, R. Gabrielsson, E. Gomez, X. Crispin, O. Nilsson, D. T. Simon, and M. Berggren, "Electronic plants," *Science Advances*, vol. 1, no. 10, p. e1501136, 2015.
- [119] N. F. Reuel, J.-h. Ahn, J.-h. Kim, J. Zhang, A. A. Boghossian, L. K. Mahal, and M. S. Strano, "Transduction of Glycan-Lectin Binding Using Near-Infrared Fluorescent Single-Walled Carbon Nanotubes for Glycan Profiling," *Journal of the American Chemical Society*, vol. 133, pp. 17923–17933, 2011.
- [120] L. Xie, S. G. Chou, A. Pande, J. Pande, J. Zhang, M. S. Dresselhaus, J. Kong, and Z. Liu, "Single-walled carbon nanotubes probing the denaturation of lysozyme," *Journal of Physical Chemistry C*, vol. 114, no. 17, pp. 7717–7720, 2010.
- [121] R. Rippka, J. Deruelles, J. B. Waterbury, M. Herdman, and R. Y. Stanier, "Generic Assignments, Strain Histories and Properties of Pure Cultures of Cyanobacteria," *Journal of General Microbiology*, vol. 111, no. 1, pp. 1–61, 1979.
- [122] N. Schuergers, D. J. Nürnberg, T. Wallner, C. W. Mullineaux, and A. Wilde, "PilB localization correlates with the direction of twitching motility in the cyanobacterium *Synechocystis* sp. PCC 6803," *Microbiology (Reading, England)*, vol. 161, no. 2015, pp. 960–966, 2015.
- [123] Z. Gao, L. Oudjedi, R. Faes, F. Moroté, C. Jaillet, P. Poulin, B. Lounis, and L. Cognet, "Optical detection of individual ultra-short carbon nanotubes enables their length characterization down to 10 nm," *Scientific Reports*, vol. 5, pp. 1–10, 2015.
- [124] H. Jin, D. a. Heller, R. Sharma, and M. S. Strano, "Size-dependent cellular uptake and expulsion of single-walled carbon nanotubes: Single particle tracking and a generic uptake model for nanoparticles," *ACS Nano*, vol. 3, no. 1, pp. 149–158, 2009.
- [125] R. J. Ritchie, "Consistent sets of spectrophotometric chlorophyll equations for acetone, methanol and ethanol solvents," *Photosynthesis Research*, vol. 89, no. 1, pp. 27–41, 2006.
- [126] J. Currie and D. I. Wilson, "OPTI, Lowering the Barrier Between Open Source Optimizers and the Industrial MATLAB User," *Foundations of Computer-Aided Process Operations*, 2012.

## Bibliography

---

- [127] F. Bomboi, a. Bonincontro, C. La Mesa, and F. Tardani, "Interactions between single-walled carbon nanotubes and lysozyme," *Journal of Colloid and Interface Science*, vol. 355, no. 2, pp. 342–347, 2011.
- [128] D. Nepal and K. E. Geckeler, "PH-sensitive dispersion and debundling of single-walled carbon nanotubes: Lysozyme as a tool," *Small*, vol. 2, no. 3, pp. 406–412, 2006.
- [129] D. W. Horn, K. Tracy, C. J. Easley, and V. A. Davis, "Lysozyme dispersed single-walled carbon nanotubes: Interaction and activity," *Journal of Physical Chemistry C*, vol. 116, no. 18, pp. 10341–10348, 2012.
- [130] D. W. Horn, G. Ao, M. Maugey, C. Zakri, P. Poulin, and V. A. Davis, "Dispersion state and fiber toughness: Antibacterial lysozyme-single walled carbon nanotubes," *Advanced Functional Materials*, vol. 23, no. 48, pp. 6082–6090, 2013.
- [131] D. Nepal, M. L. Minus, and S. Kumar, "Lysozyme coated DNA and DNA/SWNT fibers by solution spinning," *Macromolecular Bioscience*, vol. 11, no. 7, pp. 875–881, 2011.
- [132] A. G. Nyankima, D. W. Horn, and V. A. Davis, "Free-Standing Films from Aqueous Dispersions of Lysozyme, Single- Walled Carbon Nanotubes, and Polyvinyl Alcohol," *ACS Macro letters*, vol. 3, pp. 77–79, 2014.
- [133] Y. Lee and K. E. Geckeler, "Cytotoxicity and cellular uptake of lysozyme-stabilized gold nanoparticles," *Journal of Biomedical Materials Research - Part A*, vol. 100 A, no. 4, pp. 848–855, 2012.
- [134] B. D. Holt, M. C. McCorry, P. D. Boyer, K. N. Dahl, and M. F. Islam, "Not all protein-mediated single-wall carbon nanotube dispersions are equally bioactive," *Nanoscale*, pp. 7425–7434, 2012.
- [135] D. A. Heller, R. M. Mayrhofer, S. Baik, Y. V. Grinkova, M. L. Usrey, and M. S. Strano, "Concomitant length and diameter separation of single-walled carbon nanotubes," *Journal of the American Chemical Society*, vol. 126, no. 44, pp. 14567–14573, 2004.
- [136] A. Rajan, M. S. Strano, D. A. Heller, T. Hertel, and K. Schulten, "Length-dependent optical effects in single walled carbon nanotubes," *Journal of Physical Chemistry B*, vol. 112, no. 19, pp. 6211–6213, 2008.
- [137] P. D. Boyer and N. Dahl, "Length-dependent intracellular bundling of single-walled carbon nanotubes influences," *Journal of Materials Chemistry B*, vol. 5, pp. 6657–6665, 2017.
- [138] P. W. Barone, R. S. Parker, and M. S. Strano, "In vivo fluorescence detection of glucose using a single-walled carbon nanotube optical sensor: design, fluorophore properties, advantages, and disadvantages," *Anal Chem*, vol. 77, no. 23, pp. 7556–7562, 2005.

- [139] S. J. Robinson, C. S. Deroo, and C. F. Yocum, "Photosynthetic Electron Transfer in Preparations of the Cyanobacterium *Spirulina platensis*," *Plant physiology*, vol. 70, no. 1, pp. 154–161, 1982.
- [140] M. G. Clark, E. J. Patrick, G. S. Pattern, F. L. Crane, H. Low, and C. Grebing, "Evidence for the extracellular reduction of ferricyanide by rat liver. A transplasma membrane redox system," *Biochemical Journal*, vol. 200, pp. 565–572, 1996.
- [141] K. K. Mehta, N. H. Evitt, and J. R. Swartz, "Chemical lysis of cyanobacteria," *Journal of Biological Engineering*, vol. 9, no. 1, pp. 1–8, 2015.
- [142] J. G. Williams, "Construction of Specific Mutations in Photosystem II Photosynthetic Reaction Center by Genetic Engineering Methods in *Synechocystis* 6803," *Methods in Enzymology*, vol. 167, pp. 766–778, 1988.
- [143] C. Trautner and W. F. J. Vermaas, "The *sll1951* Gene encodes the surface layer protein of *synechocystis* sp. strain PCC 6803," *Journal of Bacteriology*, vol. 195, no. 23, pp. 5370–5380, 2013.
- [144] V. Neves, E. Heister, S. Costa, C. Tilmaciu, E. Borowiak-Palen, C. E. Giusca, E. Flahaut, B. Soula, H. M. Coley, J. McFadden, and S. R. P. Silva, "Uptake and release of double-walled carbon nanotubes by mammalian cells," *Advanced Functional Materials*, vol. 20, no. 19, pp. 3272–3279, 2010.
- [145] H. R. Ibrahim, "On the novel catalytically-independent antimicrobial function of hen egg-white lysozyme: a conformation-dependent activity," *Die Nahrung*, vol. 42, no. 3-4, pp. 187–193, 1998.
- [146] S. T. Henriques, M. N. Melo, and M. A. R. B. Castanho, "Cell-penetrating peptides and antimicrobial peptides: how different are they?," *The Biochemical journal*, vol. 399, pp. 1–7, Oct. 2006.
- [147] K. H. Jacobson, I. L. Gunsolus, T. R. Kuech, J. M. Troiano, E. S. Melby, S. E. Lohse, D. Hu, W. B. Chrisler, C. J. Murphy, G. Orr, F. M. Geiger, C. L. Haynes, and J. A. Pedersen, "Lipopolysaccharide Density and Structure Govern the Extent and Distance of Nanoparticle Interaction with Actual and Model Bacterial Outer Membranes," *Environmental Science and Technology*, vol. 49, no. 17, pp. 10642–10650, 2015.
- [148] L. Shang, K. Nienhaus, X. Jiang, L. Yang, K. Landfester, V. Mailänder, T. Simmet, and G. U. Nienhaus, "Nanoparticle interactions with live cells: Quantitative fluorescence microscopy of nanoparticle size effects," *Beilstein Journal of Nanotechnology*, vol. 5, no. 1, pp. 2388–2397, 2014.
- [149] N. Schuergers and A. Wilde, "Appendages of the Cyanobacterial Cell," *Life*, vol. 5, no. 1, pp. 700–715, 2015.

## Bibliography

---

- [150] D. Dienst, U. Dühring, H. J. Mollenkopf, J. Vogel, J. Golecki, W. R. Hess, and A. Wilde, "The cyanobacterial homologue of the RNA chaperone Hfq is essential for motility of *Synechocystis* sp. PCC 6803," *Microbiology*, vol. 154, no. 10, pp. 3134–3143, 2008.
- [151] Y. Gao, M. Li, B. Chen, Z. Shen, P. Guo, M. G. Wientjes, and J. L.-S. Au, "Predictive Models of Diffusive Nanoparticle Transport in 3-Dimensional Tumor Cell Spheroids," *The AAPS Journal*, vol. 15, no. 3, pp. 816–831, 2013.
- [152] G. S. Demirer, H. Zhang, J. L. Matos, N. S. Goh, F. J. Cunningham, Y. Sung, R. Chang, A. J. Aditham, L. Chio, M.-J. Cho, B. Staskawicz, and M. P. Landry, "High aspect ratio nanomaterials enable delivery of functional genetic material without DNA integration in mature plants," *Nature Nanotechnology*, pp. 1–31, 2019.
- [153] H. Jin, D. a. Heller, and M. S. Strano, "Single-particle tracking of endocytosis and exocytosis of single-walled carbon nanotubes in NIH-3T3 cells," *Nano Letters*, vol. 8, no. 6, pp. 1577–1585, 2008.
- [154] D. A. Donkor and X. S. Tang, "Tube length and cell type-dependent cellular responses to ultra-short single-walled carbon nanotube," *Biomaterials*, vol. 35, no. 9, pp. 3121–3131, 2014.
- [155] C. Contini, M. Schneemilch, S. Gaisford, and N. Quirke, "Nanoparticle–membrane interactions," *Journal of Experimental Nanoscience*, vol. 13, no. 1, pp. 62–81, 2018.
- [156] D. Roxbury, P. V. Jena, Y. Shamay, C. P. Horoszkó, and D. A. Heller, "Cell Membrane Proteins Modulate the Carbon Nanotube Optical Bandgap via Surface Charge Accumulation," *ACS Nano*, p. acsnano.5b05438, 2015.
- [157] H. H. Tuson and D. B. Weibel, "Bacteria-surface interactions," *Soft Matter*, vol. 9, no. 17, pp. 4368–4380, 2013.
- [158] K. Nicolaisen, A. Hahn, and E. Schleiff, "The cell wall in heterocyst formation by *Anabaena* sp. PCC 7120," *Journal of Basic Microbiology*, vol. 49, no. 1, pp. 5–24, 2009.
- [159] J. C. Meeks, E. L. Campbell, M. L. Summers, and F. C. Wong, "Cellular differentiation in the cyanobacterium *Nostoc punctiforme*," *Archives of Microbiology*, vol. 178, no. 6, pp. 395–403, 2002.
- [160] A. Herrero, J. Stavans, and E. Flores, "The multicellular nature of filamentous heterocyst-forming cyanobacteria," *FEMS Microbiology Reviews*, vol. 40, no. 6, pp. 831–854, 2016.
- [161] J. Šmarda, D. Šmajs, J. Komrska, and V. Krzyžánek, "S-layers on cell walls of cyanobacteria," *Micron*, vol. 33, no. 3, pp. 257–277, 2002.
- [162] Y. Zhang, M. Yang, N. G. Portney, D. Cui, G. Budak, E. Ozbay, M. Ozkan, and C. S. Ozkan, "Zeta potential: A surface electrical characteristic to probe the interaction of nanoparticles with normal and cancer human breast epithelial cells," *Biomedical Microdevices*, vol. 10, no. 2, pp. 321–328, 2008.

- [163] Y. Zhang, M. Yang, J.-H. Park, J. Singelyn, H. Ma, M. J. Sailor, E. Ruoslahti, M. Ozkan, and C. Ozkan, "A Surface-Charge Study on Cellular-Uptake Behavior of F3-Peptide-Conjugated Iron Oxide Nanoparticles," *Small*, vol. 17, no. 5, pp. 1990–1996, 2009.
- [164] T. Jittawuttipoka, M. Planchon, O. Spalla, K. Benzerara, F. Guyot, C. Cassier-Chauvat, and F. Chauvat, "Multidisciplinary Evidences that Synechocystis PCC6803 Exopolysaccharides Operate in Cell Sedimentation and Protection against Salt and Metal Stresses," *PLoS ONE*, vol. 8, no. 2, 2013.
- [165] A. Ivask, E. Suarez, T. Patel, D. Boren, Z. Ji, P. Holden, D. Telesca, R. Damoiseaux, K. a. Bradley, and H. Godwin, "Genome-wide bacterial toxicity screening uncovers the mechanisms of toxicity of a cationic polystyrene nanomaterial," *Environmental Science and Technology*, vol. 46, no. 4, pp. 2398–2405, 2012.
- [166] H. Jin, D. a. Heller, and M. S. Strano, "Single-particle tracking of endocytosis and exocytosis of single-walled carbon nanotubes in NIH-3T3 cells," *Nano Letters*, vol. 8, no. 6, pp. 1577–1585, 2008.
- [167] T. Ignatova, S. Chandrasekar, M. Pirbhai, S. S. Jedlicka, and S. V. Rotkin, "Micro-Raman spectroscopy as an enabling tool for long-term intracellular studies of nanomaterials at nanomolar concentration levels," *Journal of Materials Chemistry B*, vol. 5, no. 32, pp. 6536–6545, 2017.
- [168] M. Pirbhai, S. Chandrasekar, M. Zheng, T. Ignatova, S. V. Rotkin, and S. S. Jedlicka, "Augmentation of C17.2 Neural Stem Cell Differentiation via Uptake of Low Concentrations of ssDNA-Wrapped Single-Walled Carbon Nanotubes," *Advanced Biosystems*, vol. 3, no. 4, pp. 1–10, 2019.
- [169] J. Cheng, K. A. S. Fernando, L. M. Veca, Y. P. Sun, A. I. Lamond, Y. W. Lam, and S. H. Cheng, "Reversible accumulation of PEGylated single-walled carbon nanotubes in the mammalian nucleus," *ACS Nano*, vol. 2, no. 10, pp. 2085–2094, 2008.
- [170] N. F. Reuel, A. Dupont, O. Thouvenin, D. C. Lamb, and M. S. Strano, "Three-dimensional tracking of carbon nanotubes within living cells," *ACS Nano*, vol. 6, no. 6, pp. 5420–5428, 2012.
- [171] Q. Tong, W. Qingzhi, D. Honglian, W. Xinyu, W. Youfa, L. Shipu, and L. Junli, "A comparative study on the effects of pristine and functionalized single-walled carbon nanotubes on osteoblasts: Ultrastructural and biochemical properties," *Journal of Materials Science: Materials in Medicine*, vol. 25, no. 8, pp. 1915–1923, 2014.
- [172] D. Cui, F. Tian, C. S. Ozkan, M. Wang, and H. Gao, "Effect of single wall carbon nanotubes on human HEK293 cells," *Toxicology Letters*, vol. 155, no. 1, pp. 73–85, 2005.
- [173] J. P. Kaiser, P. Wick, P. Manser, P. Spohn, and A. Bruinink, "Single walled carbon nanotubes (SWCNT) affect cell physiology and cell architecture," *Journal of Materials Science: Materials in Medicine*, vol. 19, no. 4, pp. 1523–1527, 2008.

## Bibliography

---

- [174] Y. Liu, C. Chipot, X. Shao, and W. Cai, "Free-energy landscape of the helical wrapping of a carbon nanotube by a polysaccharide," *Journal of Physical Chemistry C*, vol. 115, no. 5, pp. 1851–1856, 2011.
- [175] B. D. Holt, P. a. Short, A. D. Rape, Y. L. Wang, M. F. Islam, and K. N. Dahl, "Carbon nanotubes reorganize actin structures in cells and ex Vivo," *ACS Nano*, vol. 4, no. 8, pp. 4872–4878, 2010.
- [176] S. A. Angermayr, M. Paszota, and K. J. Hellingwerf, "Engineering a cyanobacterial cell factory for production of lactic acid," *Applied and Environmental Microbiology*, vol. 78, no. 19, pp. 7098–7106, 2012.
- [177] N. Sekar, Y. Umasankar, and R. P. Ramasamy, "Photocurrent generation by immobilized cyanobacteria via direct electron transport in photo-bioelectrochemical cells," *Physical chemistry chemical physics : PCCP*, vol. 16, no. 17, pp. 7862–71, 2014.
- [178] M. Sawa, A. Fantuzzi, P. Bombelli, C. J. Howe, K. Hellgardt, and P. J. Nixon, "Electricity generation from digitally printed cyanobacteria," *Nature Communications*, vol. 8, no. 1, pp. 1–9, 2017.
- [179] X. Jiang, J. Hu, A. M. Lieber, C. S. Jackan, J. C. Biffinger, L. A. Fitzgerald, B. R. Ringeisen, and C. M. Lieber, "Nanoparticle facilitated extracellular electron transfer in microbial fuel cells," *Nano Letters*, vol. 14, no. 11, pp. 6737–6742, 2014.
- [180] R. Wu, L. Cui, L. Chen, C. Wang, C. Cao, G. Sheng, H. Yu, and F. Zhao, "Effects of Bio-Au Nanoparticles on Electrochemical Activity of *Shewanella oneidensis* Wild Type and  $\Delta$ omcA/mtrC Mutant," *Scientific Reports*, vol. 3, pp. 1–7, 2013.
- [181] T. Kou, Y. Yang, B. Yao, and Y. Li, "Interpenetrated Bacteria-Carbon Nanotubes Film for Microbial Fuel Cells," *Small Methods*, vol. 2, no. 10, p. 1800152, 2018.
- [182] J. M. Pisciotta, Y. Zou, and I. V. Baskakov, "Light-dependent electrogenic activity of cyanobacteria," *PLoS ONE*, vol. 5, no. 5, 2010.
- [183] Y. Yang, M. Xu, J. Guo, and G. Sun, "Bacterial extracellular electron transfer in bioelectrochemical systems," *Process Biochemistry*, vol. 47, no. 12, pp. 1707–1714, 2012.
- [184] K. Hasan, H. Bekir Yildiz, E. Sperling, P. Ó Conghaile, M. A. Packer, D. Leech, C. Hägerhäll, and L. Gorton, "Photo-electrochemical communication between cyanobacteria (*Leptolyngbia* sp.) and osmium redox polymer modified electrodes," *Phys. Chem. Chem. Phys.*, vol. 16, no. 45, pp. 24676–24680, 2014.
- [185] K. Stucken, R. Koch, and T. Dagan, "Cyanobacterial defense mechanisms against foreign DNA transfer and their impact on genetic engineering," *Biological Research*, vol. 46, no. 4, pp. 373–382, 2013.
- [186] K. E. Wendt and H. B. Pakrasi, "Genomics approaches to deciphering natural transformation in cyanobacteria," *Frontiers in Microbiology*, vol. 10, no. JUN, pp. 1–7, 2019.



- 
- [187] A. Vasilescu, Q. Wang, M. Li, R. Boukherroub, and S. Szunerits, "Aptamer-based electrochemical sensing of lysozyme," *Chemosensors*, vol. 4, no. 2, pp. 1–20, 2016.
- [188] H. M. Jensen, A. E. Albers, K. R. Malley, Y. Y. Londer, B. E. Cohen, B. A. Helms, P. Weigle, J. T. Groves, and C. M. Ajo-Franklin, "Engineering of a synthetic electron conduit in living cells," *Proceedings of the National Academy of Sciences of the United States of America*, vol. 107, no. 45, pp. 19213–19218, 2010.
- [189] H. M. Jensen, M. A. TerAvest, M. G. Kokish, and C. M. Ajo-Franklin, "CymA and Exogenous Flavins Improve Extracellular Electron Transfer and Couple It to Cell Growth in Mtr-Expressing *Escherichia coli*," *ACS Synthetic Biology*, vol. 5, no. 7, pp. 679–688, 2016.
- [190] S. J. Wu, N. Schuergers, K. H. Lin, A. J. Gillen, C. Corminboeuf, and A. A. Boghossian, "Restriction Enzyme Analysis of Double-Stranded DNA on Pristine Single-Walled Carbon Nanotubes," *ACS Applied Materials and Interfaces*, vol. 10, no. 43, pp. 37386–37395, 2018.
- [191] R. Singh, D. Pantarotto, D. McCarthy, O. Chaloin, J. Hoebeke, C. D. Partidos, J. P. Briand, M. Prato, A. Bianco, and K. Kostarelos, "Binding and condensation of plasmid DNA onto functionalized carbon nanotubes: Toward the construction of nanotube-based gene delivery vectors," *Journal of the American Chemical Society*, vol. 127, no. 12, pp. 4388–4396, 2005.
- [192] P. E. Giebel and W. F. Street, "Extraction of Chloroplasts from Plant Tissue and Their Use in Demonstrating the Hill Reaction," pp. 31–47, 2006.
- [193] M. Ermakova, N. Battchikova, P. Richaud, H. Leino, S. Kosourov, J. Isojarvi, G. Peltier, E. Flores, L. Cournac, Y. Allahverdiyeva, and E. M. Aro, "Heterocyst-specific flavodiiron protein Flv3B enables oxic diazotrophic growth of the filamentous cyanobacterium *Anabaena* sp. PCC 7120," *Proceedings of the National Academy of Sciences of the United States of America*, vol. 111, no. 30, pp. 11205–11210, 2014.





## **Curriculum Vitae**



# Alessandra Antonucci

## Personal Information

<i>Date of birth</i>	September 27th, 1989
<i>Contacts</i>	phone: +39 349 3262227, mail: antonucci.alee@gmail.com

## Education

<i>2015 – Exp. 2019</i>	<b>PhD in Chemistry and Chemical Engineering</b> <i>École Polytechnique Fédérale de Lausanne, Switzerland</i> Thesis title: Interaction of Fluorescent Single-Walled Carbon Nanotubes (SWCNTs) with Photosynthetic Microbes.
<i>2014</i>	<b>M.Sc. in Chemistry</b> <i>University of Bari, Aldo Moro, Italy.</i> Grade: 110/110 cum laude. GPA: 30/30 Thesis title: Bioconjugation of photosynthetic proteins with organic substrates for energy conversion.
<i>2008 – 2012</i>	<b>B.Sc. in Chemistry</b> <i>University of Bari, Aldo Moro, Italy.</i> Grade: 110/110 cum laude. Thesis title: Use of derivative Vis-NIR spectroscopy for the analysis of multi-peak optical spectra in the presence of particulate.

## Work Experience

<i>2015 – today</i>	<b>Doctoral Assistant, École Polytechnique Fédérale de Lausanne, Switzerland</b> PhD student in the Laboratory of Nanobiotechnology (LNB) led by Prof. Ardemis Boghossian. Currently investigating the interaction of photosynthetic organisms with single-walled carbon nanotubes for biomolecule delivery and energy applications.
<i>2013 – 2015</i>	<b>Research Assistant, National Research Council – Institute for Chemical-Physical Processes (CNR-IPCF), Bari, Italy</b> Research assistant in the Physical Chemistry group in University of Bari under the supervision of Prof. Angela Agostiano and Dr. Massimo Trotta. Projects focused on developing hybrid organic-biological systems based on bacterial reaction centers for artificial photosynthesis and bioelectronics.
<i>2012</i>	<b>Research Assistant, National Research Council – Institute for Chemical-Physical Processes (CNR-IPCF), Bari, Italy</b> Undertook a 6 month project in the group of Dr. Massimo Trotta applying derivative UV-Vis spectroscopy for the analysis of multi-peak optical spectra.

## Teaching

<i>2015 – 2018</i>	Teaching assistant for the courses entitled "Photomedicine", "Bio-oriented chemistry", "Organic Chemistry I" and "Chemical Engineering of heterogeneous reactions". Supervised students in 2 internship projects.
--------------------	---

## Courses and Trainings

<i>2019</i>	<b>Management of Innovation and Technology Transfer (MINTT)</b> Organized by the Technology Transfer Office (TTO) at EPFL Analysis of patent application process, examples of technologies commercialization and case studies on EPFL start-ups
<i>2017</i>	<b>Photomedicine</b> Taught by Prof. Georges Wagnieres at EPFL Lectures on photometry, general and tissue optics, and light-tissues interactions
<i>2017</i>	<b>Advanced Light Microscopy for Life Science</b> Organized by the BioImaging and Optics Platform (BIOP) at EPFL Theoretical and practical courses in light microscopy and live cell analysis
<i>2017</i>	<b>Image processing for Life Science</b> Organized by the BioImaging and Optics Platform (BIOP) at EPFL Lectures and exercises on digital image analysis using ImageJ software

## Conferences and Workshops

<i>July 2019</i>	NT19: International Conference on the Science and Application of Nanotubes and Low-Dimensional Materials in Wurzburg, Germany (oral and poster presentation)
<i>September 2018</i>	Swiss Chemical Society Fall Meeting in Lausanne, Switzerland (poster)
<i>November 2017</i>	AIChE Annual Meeting in Minneapolis, USA (two oral presentations)
<i>May 2017</i>	230 <sup>th</sup> Electro Chemical Society Meeting in New Orleans, USA (oral presentation)
<i>September 2016</i>	Trends in NanoTechnology (TNT) Conference in Fribourg, Switzerland (poster)
<i>July 2016</i>	Workshop on Bio-inspired nanosystems for energy conversion in Berlin, Germany (poster)

## Awards

<i>2019</i>	ElectroChemical Society (ECS) Travel Grant
<i>2017</i>	SCS/SCNAT 2017 Chemistry Travel Award recipient
<i>2017</i>	ElectroChemical Society (ECS) Travel Grant
<i>2016</i>	Trends in Nanotechnology International Conference (TNT2016) Travel Award

## Key Skills

<i>Mastered Techniques</i>	UV-vis-NIR Spectroscopy, Light Microscopy, Fourier-Transform Infrared (FTIR) and Raman Spectroscopy, Cell Culture, Dynamic Light Scattering (DLS), Protein Bioconjugation Techniques, Functionalization of nanomaterials, Gel Electrophoresis, Polymerase Chain Reaction (PCR).
<i>IT Knowledge</i>	MATLAB, Microsoft Office (Word, Power Point, Excel), ImageJ, OriginLab, Adobe (Illustrator), L <sup>A</sup> T <sub>E</sub> X.
<i>Languages</i>	Italian: mother tongue, English: fluent, French: basic.

## Additional Information

<i>Volunteering</i>	Bookcity Festival in Milan (Edition 2016 and 2018) My role as volunteer: coordinating a group of volunteers, set-up the rooms, meet and greet the audience, introduce the speakers.
<i>Memberships</i>	Swiss Chemical Society (SCS), Electro Chemical Society (ECS)

## Publications

- 2019 | **Inherited Nanobionics Enable Cross-generational Tracking of Bacteria Using Near-infrared Confocal Microscopy**  
**A. Antonucci**, N. Schuergers, V. Zubkovs, M. Reggente, A. J. Gillen, B. Lambert, E. Carata, L. Dini and A. A. Boghossian  
*Submitted*
- 2019 | **Biotechnology applications of nanocarbons in plant and algal systems**  
**A. Antonucci**, A. J. Gillen and A. A. Boghossian  
*Submitted*
- 2019 | **Design of optimized PEDOT-based electrodes for enhancing performance of living photovoltaics based on phototropic bacteria**  
M. Reggente, S. Politi, **A. Antonucci**, E. Tamburri, A. A. Boghossian  
*Submitted*
- 2019 | **Enhancing bioelectricity generation in microbial fuel cells and biophotovoltaics using nanomaterials**  
M. Mouhib, **A. Antonucci**, M. Reggente, A.A. Amirjani, A. Gillen and A. A. Boghossian  
*NanoResearch*
- 2018 | **Spinning-disc confocal microscopy in the second near-infrared window (NIR-II)**  
V. Zubkovs, **A. Antonucci**, N. Schuergers, A. A. Boghossian et al.  
*Scientific Reports*
- 2017 | **Noncovalent Protein and Peptide Functionalization of Single-Walled Carbon Nanotubes for Biodelivery and Optical Sensing Applications**  
**A. Antonucci\***, J. Kupis-Rozmyslowicz\*, A. A. Boghossian  
*ACS Applied Materials and Interfaces*
- 2016 | **Review-Engineering the selectivity of the DNA-SWCNT sensor**  
J. Kupis-Rozmyslowicz\*, **A. Antonucci\***, A. Boghossian  
*ECS Journal of Solid State Science and Technology*
- 2015 | **Semiquinone oscillations as tool for investigating the ubiquinone binding to photosynthetic reaction centers**  
F. Ciriaco, R.R. Tangorra, **A. Antonucci**, L. Giotto, A. Agostiano, M. Trotta, F. Milano  
*European Biophysics Journal*
- 2015 | **Garnishing the photosynthetic reaction center for bioelectronics**  
A. Operamolla, **A. Antonucci**, M. Trotta, G.M. Farinola et al.  
*Journal of Material Chemistry C*
- 2015 | **Photoactive film by covalent immobilization of a bacterial photosynthetic protein on reduced graphene oxide surface**  
R.R. Tangorra, **A. Antonucci**, F. Milano, M. Maggini, A. Agostiano, M. Trotta, G.M. Farinola et al.  
*MRS Proceedings*